**KU Leuven**
**Group Biomedical Sciences**
**Faculty of Pharmaceutical Sciences**
**Pharmaceutical Analysis**

# Evaluation of new trends in hydrophilic interaction liquid chromatography

Huiying Song

Jury:

| | |
|---|---|
| Promoter: | Prof. Dr. Deirdre Cabooter |
| Co-promoter: | Prof. Dr. Erwin Adams |
| Chair: | Prof. Dr. Ann Van Schepdael |
| Jury members: | Prof. Dr. Guy Bormans |
| | Prof. Dr. Patrick Augustijns |
| | Prof. Dr. Ken Broeckhoven |
| | Prof. Dr. Yvan Vander Heyden |

Leuven, September 2016

Doctoral Thesis in Pharmaceutical Science

“The best way to predict the future is to create it.”

*Abraham Lincoln*

## Table of Contents

# Chapter 1

# General Introduction

Parts of this chapter have been published in:

- **Huiying Song,** Deirdre Cabooter, Relevance and assessment of molecular diffusion coefficients in liquid chromatography, *Chromatographia*, submitted.
- Getu Kahsay, **Huiying Song**, Ann Van Schepdael, Deirdre Cabooter, Erwin Adams, Hydrophilic interaction chromatography (HILIC) in the analysis of antibiotics, *Journal of Pharmaceutical and Biomedical Analysis*, 87 (2014) 142-154.

## 1.1. Basic principles of chromatography

Chromatography is a separation method wherein different components are distributed between two immiscible phases, called the stationary and the mobile phase. The stationary phase is normally fixed in the system and can be a solid or a liquid immobilized on a solid. The mobile phase passes through the chromatographic system and can be a gas, liquid or supercritical fluid. The chromatographic separation process occurs as a result of the different affinity of the analytes for the stationary and mobile phase which causes the analytes to migrate through the column at different velocities, leading to their separation.

Nowadays, chromatography as an analytical separation tool is extensively used for component analysis in many fields, such as pharmaceutical [1-2] and food industries [3-4], clinical [5] and environmental chemistry [6-7] and synthetic polymer analysis [8].

Based on the physical state of the mobile phase, the chromatographic technique is generally classified into gas chromatography (GC), liquid chromatography (LC) and supercritical fluid chromatography (SFC). Liquid chromatography is the focus of the current thesis. Pressure driven LC is currently the most widely used separation technique and comprises all liquid chromatographic techniques that require elevated pressures to force the liquid through the chromatographic system.

One of the most essential parts for separation is the chromatographic column which can either be an open-tubular capillary or a packed bed column with an inner diameter between 10 μm and 4.6 mm. In the former case, the stationary phase is bonded onto the inner wall of the capillary, while a packed bed column is either filled with beads (packed particulate column) or a continuous skeleton with large through pores (monolithic column). For particulate columns, the particles can be solid (non-porous particles), partially porous (porous-shell particles) or fully porous. Complex mixtures and matrices that are separated in a column, can subsequently be detected or quantitated by various detection modes, such as ultra-violet (UV), fluorescence, refractive index, electrochemical and mass spectrometry detection. This will result in a chromatogram displaying the detection signal as a function of the elution time (example shown in Fig. 1.1).

## 1.2. Thermodynamics of chromatography

Once the sample components are introduced on the chromatographic column via the mobile phase, the partitioning of a component between the stationary and the mobile phase will start. The extent of this partitioning is expressed by the equilibrium constant ($K$), which is the ratio of the concentration of the component in the stationary phase ($C_s$) to that in the mobile phase ($C_m$):

$$K = \frac{C_s}{C_m} \tag{1.1}$$

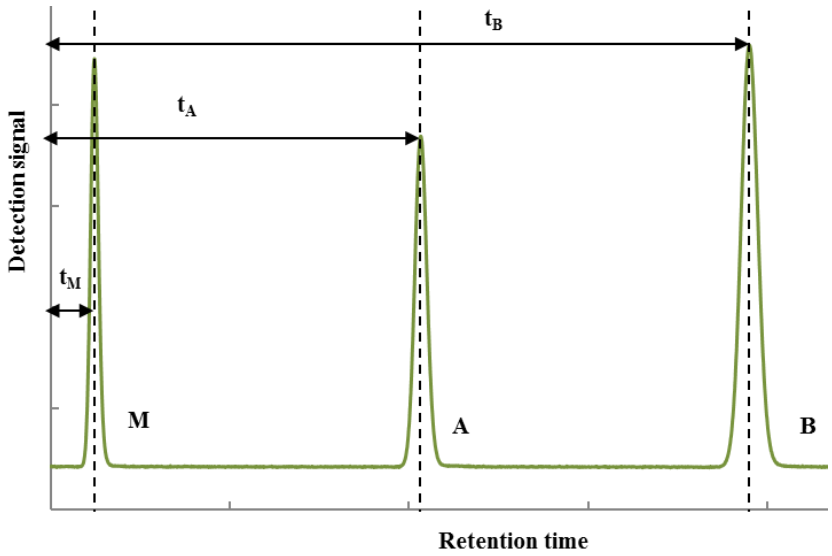


**Figure 1.1:** A simple chromatogram showing the retention time as a function of the observed signal. M is an unretained compound, A and B are two retained compounds. ($t_M$, $t_A$, $t_B$ are the elution times of compounds M, A and B, respectively)

The higher the affinity of a component for the stationary phase, the larger the equilibrium constant will be. The phase retention factor (k′) can also be used to define this partition equilibrium. It is defined as the ratio of the number of molecules in the stationary phase ($N_s$) to those in the mobile phase ($N_m$):

$$k' = \frac{N_s}{N_m} \tag{1.2}$$

Since the number of molecules in the stationary and mobile phase is proportional to their respective concentrations in both phases, the equilibrium constant can be related to the retention factor as:

$$k' = \frac{N_s}{N_m} = \frac{C_s \cdot V_s}{C_m \cdot V_m} = K\beta \tag{1.3}$$

Where β is the phase ratio factor, which is the ratio of the volume of the stationary phase ($V_s$) relative to the volume of the mobile phase ($V_m$).

The phase retention factor can also be written as a function of the residence time, since the number of molecules in the mobile and stationary phases is proportional to the time spent by the molecules in each phase ($t_m$, $t_s$). As shown in Fig 1.1, component M has no affinity for the stationary phase, therefore it migrates through the column with the same speed as the mobile phase. The elution time of compound M ($t_M$) hence corresponds to the time needed for the mobile phase to pass through the column and is also referred to as the column dead time ($t_0$). A component eluting at the $t_0$-time is considered to be unretained. Compound A on the other hand, partitions to a certain extent, its elution time ($t_A$) is the sum of the time the mobile phase needs to pass through the column and the time compound A interacts with the stationary phase. The phase retention factor characterizes the chromatographic behavior of a compound and is independent of column dimensions, mobile phase composition, flow rate and stationary phase. Moreover, it has the advantage of being dimensionless in contrast to the retention time:

$$k' = \frac{N_S}{N_m} = \frac{t_S}{t_m} = \frac{t_A - t_M}{t_M} \qquad (1.4)$$

Chromatographic retention can also be defined by the zone retention factor (k") [9], which is based on the partitioning of a solute between the stationary zone and the mobile zone, and is defined as the ratio of the number of solute molecules in the stationary zone ($N_{s,zone}$) relative to that in the mobile zone ($N_{m,zone}$). Since the amount of solute in both zones is proportional to the time the solute spends in each individual zone, the zone retention factor is presented as:

$$k'' = \frac{N_{S,zone}}{N_{m,zone}} = \frac{t_S + t_{ms}}{t_{me}} \qquad (1.5)$$

Where $t_s$ is the time spent in the stationary phase, $t_{ms}$ is the time spent in the stagnant liquid of the particle pores, $t_s + t_{ms}$ is the time spent in the stationary zone and $t_{me}$ is the time spent in the mobile zone.

For open-tubular columns, there is no difference between mobile phase and mobile zone, stationary phase and stationary zone. However, for packed bed columns, as illustrated in Fig.1.2, the mobile phase includes both the flowing liquid outside the particles and the stagnant liquid inside the particle pores, while the mobile zone is limited to the flowing liquid outside the particles. The stationary zone includes both the stationary phase and the stagnant liquid inside the particles.

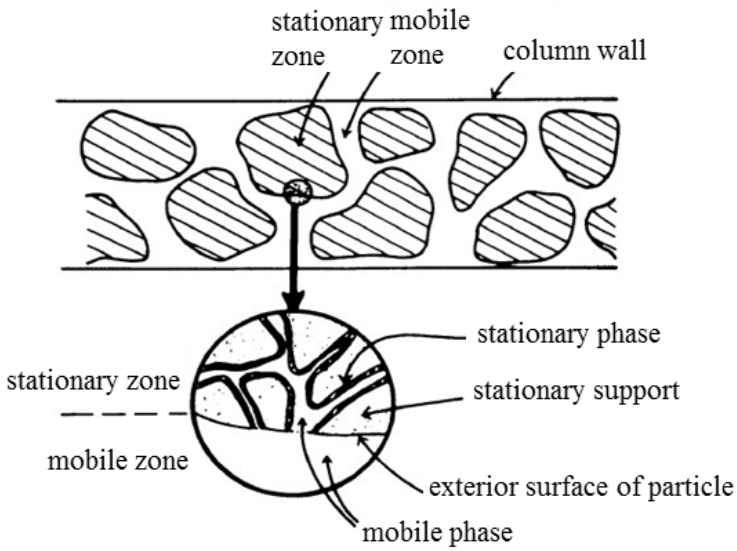


**Figure 1.2:** Schematic representation of the structure of a packed liquid chromatographic column. (Figure reprinted with permission from [9])

## 1.3. Definitions in chromatography

### 1.3.1. Height equivalent to a theoretical plate (HETP) and plate count

When a small volume of sample is injected onto a chromatographic column, the distance between the centers of the different peaks increases proportionally to the distance they have travelled in the column due to their different affinities for the stationary phase. Meanwhile, the peaks broaden due to dispersion, which is in direct proportion with the square root of the length the peaks have travelled. Sample separation and peak broadening occur simultaneously, but since the distance between the peaks increases faster than the rate at which the peaks broaden, the peaks will eventually become separated. The farther apart the bands move, the better separated the peaks will be.

In 1941, Martin and Synge introduced the concept of the height equivalent to a theoretical plate (abbreviated as plate height, H) to quantify the performance of a chromatographic separation. The term can be traced back to the distillation theory, where the plate height is the "height" of each hypothetical stage of the multistage distillation tower in which two phases, such as the liquid and vapor phases of a substance, reach equilibrium with each other. The number of stages in the tower (column) corresponds to the column plate count (N), which is a measure for the separation quality. The better the distillation efficiency is, the smaller the plate height will be and the larger the number of plates that can be placed in the distillation tower.

Analogous to the distillation theory, the plate height concept is also applied to chromatographic separations, where a chromatographic column is treated as consisting of a number of plates. The mixed compounds in the mobile phase are transported stepwise from plate to plate, where a new equilibrium sets in at each plate. The more frequently equilibrium is established, the better the separation will be. The relationship between H, N and the column length (L) can be defined as:

$$H = \frac{L}{N} \tag{1.6}$$

The chromatographic band is actually a statistical distribution of molecules. The peak variance ($\sigma_x^2$) or the second moment is used to define this distribution. The peak width (w) is always proportional to the square root of the peak variance, and is independent of the shape of the distribution. Since the peak width increases with the square root of the length it has traveled, the peak variance increases proportionally to the distance it has traveled. The relation between peak variance, the length traveled by the peak (L) and the plate height can be expressed as:

$$H = \frac{d\sigma_x^2}{dL} \tag{1.7}$$

Where $\sigma_x^2$ is the spatial variance of a peak ($m^2$). Since peak widths and variances are normally detected in time units at the detector, the spatial and time based variances and widths can be converted into each other by introducing the velocity ($u_e$) at the elution point:

$$\sigma_x^2 = \sigma_t^2 \cdot u_e^2 \tag{1.8}$$

$$w_x = w_t \cdot u_e \tag{1.9}$$

Where $\sigma_t^2$ is the time based variance, $w_x$ is the spatial based peak width and $w_t$ is the time based peak width. For Gaussian peaks, the peak width relates to its standard deviation ($\sigma$) with a factor *f* that depends on how the peak width is measured, as shown in Fig.1.3.

$$w_t^2 = f \cdot \sigma^2 \tag{1.10}$$

The plate count can be expressed for isocratic elution as:

$$N = f \frac{t_R^2}{w_t^2} \tag{1.11}$$

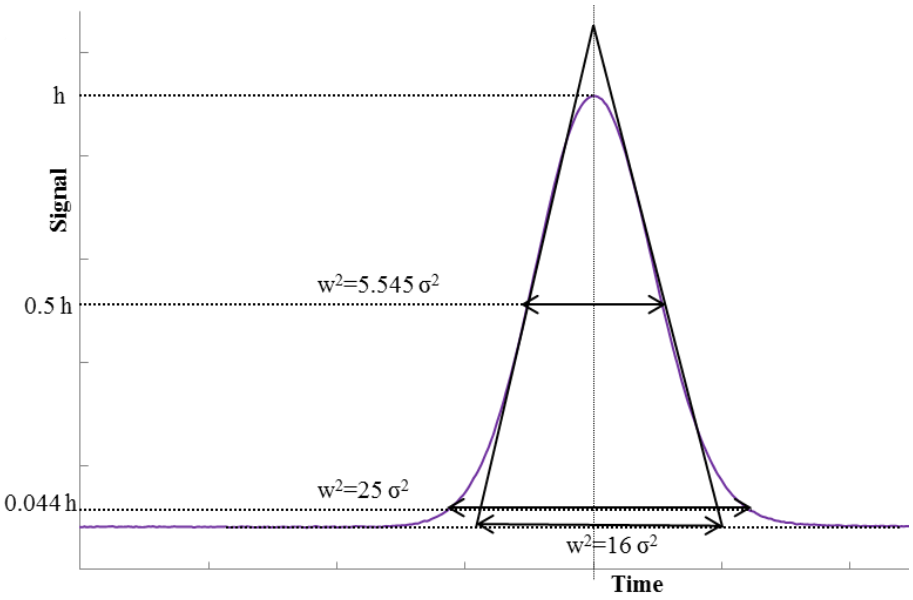


**Figure 1.3:** A Gaussian peak with the different procedures to estimate the variance of a peak, their relation to the peak variance, peak width and peak height.

### 1.3.2. Resolution

The separation quality between two consecutively eluting peaks can be measured by the resolution ($R_s$), which is the ratio of the distances between the two peaks ($t_{R,B}$-$t_{R,A}$) and the average of their respective peak widths ($w_A$, $w_B$):

$$R_s = \frac{t_{R,B} - t_{R,A}}{\frac{1}{2}(w_A + w_B)} \qquad (1.12)$$

Where $t_{R,i}$ is the time needed for component *i* to migrate through the column and $w_i$ is the peak width of this compound in time units measured at baseline using the tangent method, as indicated in Fig. 1.3. Resolution is dimensionless. For Gaussian and equally high peaks, a resolution of 1.5 results in the baseline separation of two peaks (with 0.3% overlap between the two peaks), whereas a resolution of 1.0 gives a peak overlap of around 4%. Since the distance between two peaks increases with the length they have migrated through the column, and the peak width is only proportional with the square root of this distance, the resolution increases with the square root of the distance migrated by the peaks. Therefore, the longer the column is, the higher the resolution will be. Resolution can also be expressed as a function of the phase retention factor, the plate count and the selectivity factor ($\alpha = k_2'/k_1'$), for Gaussian peaks under isocratic elution:

$$R_s = \frac{\sqrt{N}}{4}\left(\frac{\alpha - 1}{\alpha}\right)\left(\frac{k_2'}{1 + k_2'}\right) \qquad (1.13)$$

As can be derived from Eq. (1.13), the selectivity factor has a large influence on resolution. Therefore, an adequate selection of the mobile and stationary phase is critical for sample separation. Resolution moreover increases proportionally to the square root of the plate count, which is increased by increasing the column length, be it at the cost of an increased elution time. Increasing the retention factor has a positive influence on the resolution, at least to a certain extent, but will also lead to longer analysis times.

### 1.3.3. Porosity

Porosity is defined as the fraction of non-solid space in a certain volume element. In liquid chromatography, porosity is used to quantify the space in the column that is available for or accessible to the mobile phase. Customarily, three types of porosities are defined to study porous materials: the total porosity ($\varepsilon_T$), external porosity ($\varepsilon_e$), and internal porosity ($\varepsilon_{int}$) [10].

Considering a porous particulate liquid chromatographic column for instance, as shown in Fig. 1.4, the external porosity is the column volume that is not occupied by the particles, relative to the column geometrical volume:

$$\varepsilon_e = \frac{V_{flowing\ mobile\ phase}}{V_{column}} = \frac{V_{flowing\ mobile\ phase}}{\pi r^2 L} \qquad (1.14)$$

Where r is the column radius and L is the column length. $\varepsilon_e$ can be determined experimentally by the total pore blocking method [11-12] or inverse size-exclusion chromatography (ISEC) [13]. A precise knowledge of the external porosity is essential to understand column performance.

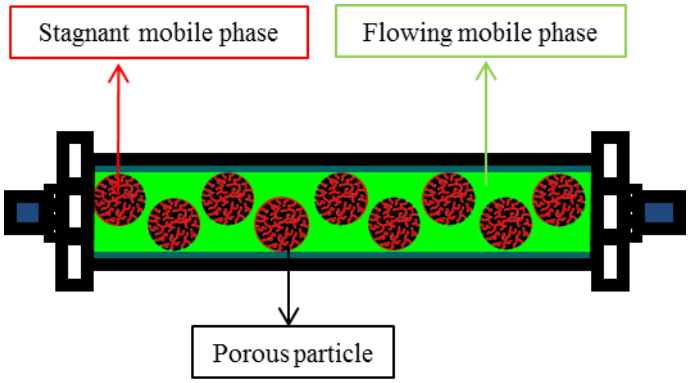


**Figure 1.4:** Schematic illustration of the external porosity (green), internal porosity (red) and the total porosity (red and green) in a packed column.

The internal porosity is the volumetric fraction of the pores in the particles, corresponding to the ratio of the volume of stagnant mobile phase inside the particle pores ($v_{stagnant\ mobile\ phase}$) to the geometrical volume of the particle ($v_{particle}$) [14]:

$$\varepsilon_{int} = \frac{V_{stagnant\ mobile\ phase}}{V_{particle}} = \frac{V_{stagnant\ mobile\ phase}}{V_{column} \cdot (1-\varepsilon_e)} \tag{1.15}$$

The total porosity is determined by dividing the total volume of mobile phase in the column ($v_{total\ mobile\ phase}$) by the geometrical volume of the column:

$$\varepsilon_T = \frac{V_{total\ mobile\ phase}}{V_{column}} = \frac{V_{flowing\ mobile\ phase} + V_{stagnant\ mobile\ phase}}{\pi r^2 L} \tag{1.16}$$

$\varepsilon_T$ can be determined via pycnometry experiments [10].

### 1.3.4. Velocity

Conceptually, flow velocity is merely a way to normalize the flow rate by the cross section of the column. There are, in general, three definitions for the velocity: linear velocity ($u_0$), interstitial velocity ($u_i$) and superficial velocity ($u_s$).

The linear velocity is based on the column dead time ($t_0$), which is the time needed for the molecules to migrate through both the mobile zone outside the particles and the liquid stagnant area inside the particles.

$$u_0 = \frac{L}{t_0} \tag{1.17}$$

The superficial velocity ($u_s$), commonly used for open tubular columns, is calculated based on the volumetric flow rate (F) and the column cross section (A′):

$$u_s = \frac{F}{A'} = \frac{F}{\pi r^2} \tag{1.18}$$

The interstitial velocity ($u_i$) is the velocity of the liquid in the mobile zone of the column:

$$u_i = \frac{F}{\varepsilon_e \pi r^2} \tag{1.19}$$

These three velocities are related to each other as follows:

$$u_0 = \frac{u_s}{\varepsilon_T} = u_i \frac{\varepsilon_e}{\varepsilon_T} = u_i \cdot \frac{1}{1+(1-\varepsilon_e)\cdot \varepsilon_{int}/\varepsilon_e} \tag{1.20}$$

### 1.3.5. Permeability and pressure

Permeability ($K_v$) combines all parameters influencing the column pressure drop (ΔP). It is defined as:

$$K_V = \frac{F\eta L}{\pi r^2 \Delta P} = \frac{u\eta L}{\Delta P} \quad (1.21)$$

Where η is the dynamic viscosity of the mobile phase. Longer columns, higher flow rates, or more viscous mobile phases require higher operating pressures. Since velocity can be expressed in different ways, as mentioned in 1.3.4, the bed permeability can be expressed in terms of the superficial velocity ($K_{vs}$), the interstitial velocity ($K_{vi}$) and the unretained $t_0$-marker velocity ($K_{v0}$). The relation between these expressions can be written as [10]:

$$K_{vs} = K_{vi} \cdot \varepsilon_e = K_{v0} \cdot \varepsilon_T \quad (1.22)$$

The flow resistance (ϕ), as another measure of column permeability, is a dimensionless quantity:

$$\phi = \frac{d_p^2}{K_v} \quad (1.23)$$

Similar to Eq. (1.22), a similar relation holds for the different forms of flow resistances:

$$\phi_s = \frac{\phi_i}{\varepsilon_e} = \frac{\phi_0}{\varepsilon_T} \quad (1.24)$$

### 1.3.6. Molecular diffusion coefficient

Molecular diffusion is a process wherein molecules move down a concentration gradient, from a region of high concentration to a region of low concentration, eventually resulting in complete mixing [15]. It is the thermal motion of all molecules at temperatures above absolute zero. The rate of this movement is a function of many physical parameters such as temperature, viscosity, size and mass of the molecule. Molecular diffusion can occur in a gas, liquid or even solid, where the former two cases are most frequently studied [16-17]. The molecular diffusion coefficient ($D_m$), also called the molecular diffusivity, is a parameter to quantify the speed and amount of this process, commonly defined as [18]:

$$D_m = \frac{dQ}{A_{molecule} \cdot dt \cdot \frac{dc}{dx}} \quad (1.25)$$

Where *dQ* is the amount of molecules that pass through a plane of area $A_{molecule}$ in time *dt* under a concentration gradient *dc/dx*. Eq. (1.25) is only applicable to infinitely dilute solutions;

e.g., for a binary mixture of solute A and solvent B, the environment of each molecule A is essentially pure B. Accurate values of the molecular diffusivity of the solutes involved are critical for the kinetic study of mass transfer phenomena [19]. Several empirical correlations are available to estimate this parameter in solution, such as the Wilke-Chang [20], the Scheibel [21] and the Hayduk-Laudie equation [22]. The Wilke-Chang equation (Eq. (1.26)) is the most popular and therefore the most frequently used one:

$$D_m(cm^2/s) = 7.4 \times 10^{-8} \frac{\sqrt{\varphi_B MW_B}}{\eta_B V_A^{0.6}} T \qquad (1.26)$$

A and B refer to the solute and the solvent, respectively. $\varphi_B$ is the solvent-solvent interaction or association factor [17]. $V_A$ is the molar volume of the solute at normal boiling point and can be calculated by a group contribution method [20]. $\eta_B$ is the solvent viscosity (cP), T is the temperature, $MW_B$ refers to the molecular weight of the solvent (g/mol).

Some efforts have been undertaken in literature to compare the accuracy of the most commonly used correlations to estimate molecular diffusion [17]. Li and Carr, for example, evaluated the accuracy of the Wilke-Chang, Scheibel, Lusis-Ratcliff and Hayduk-Laudie correlations for the diffusion coefficients of alkylbenzenes and alkylphenones in ACN/water and MeOH/water mixtures within a specific range of temperatures (30 to 60°C) [17]. The estimated values were compared to values obtained via the Taylor-Aris method. The authors demonstrated that the errors of the estimated $D_m$-values using the Wilke-Chang, Scheibel, and Lusis-Ratcliff correlations are generally less than 20% in MeOH/water mixtures, while those using the Wilke-Chang, Scheibel, and Hayduk-Laudie correlations are generally less than 20% in ACN/water mixtures. Moreover, the Scheibel correlation offers a higher accuracy than the Wilke-Chang correlation in all ACN/water mixture conditions, especially in ACN-rich mixtures (> 70 vol%). Therefore, the authors recommended using the former correlation to estimate diffusion coefficients of small molecular weight compounds in ACN/water mixtures.

Practically, it is more accurate to measure molecular diffusivities under the intended experimental conditions since $D_m$ varies significantly with the nature of the solute molecules, the temperature and the solvent. There are several ways to perform these measurements, e.g., spectroscopic methods (nuclear magnetic resonance) [23], optical methods (dynamic light scattering) [24], the diaphragm-cell method [25], peak parking [26], the Taylor-Aris method [27-29] and by using microfluidic devices [30-31].

For chromatographic practitioners, the peak parking and Taylor-Aris method are most convenient, since they can be performed on an HPLC apparatus. However, the peak parking method is time-consuming and necessitates calibration [32]. Therefore, from a practical point of view, the Taylor-Aris method is the most convenient way to determine $D_m$-values [29]. This method will be discussed in great detail in Chapter 5 of the thesis.

## 1.4. Hydrodynamics of chromatography

In essence, the hydrodynamics of chromatography deal with the relation between the efficiency of a column and the flow dynamics, the properties of the stationary phase and the sample. Generally, if the plate height is plotted against the linear velocity of the mobile phase flowing through the column, a curve with a minimum and a nearly linear increase of the plate height with linear velocity at higher linear velocity is obtained, as illustrated in Figure 1.5. Three equations are commonly used to describe this relationship: the van Deemter equation, the Giddings equation and the Knox equation.

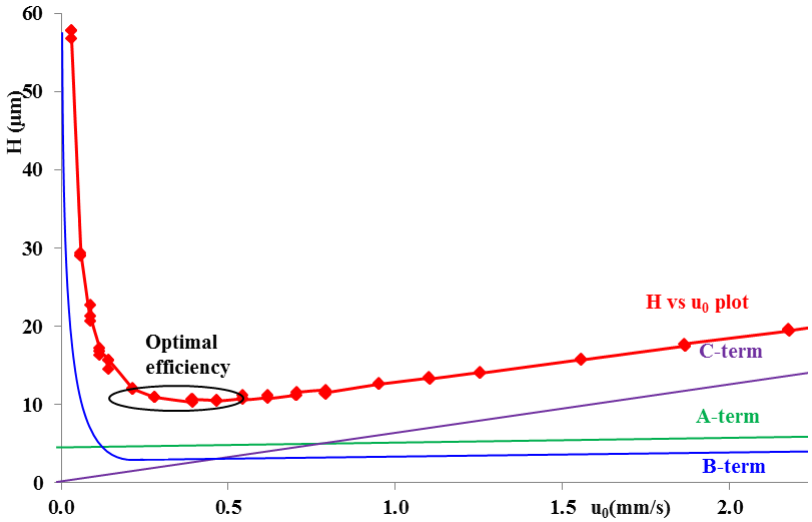


**Figure 1.5:** A curved relationship between plate height (H) and linear velocity ($u_0$). Each independent contribution, eddy dispersion (green, A-term), longitudinal dispersion (blue, B-term), mass transfer resistance (purple, C-term), is plotted independently as a function of the linear velocity.

### 1.4.1. van Deemter equation

The van Deemter equation is the simplest equation describing the relation between plate height (H) and velocity. It is composed of three independent and additive contributions: eddy dispersion (A-term), longitudinal diffusion (B-term) and mass transfer resistance (C-term):

$$H = A + \frac{B}{u} + Cu \qquad (1.27)$$

As shown in Figure 1.5, eddy dispersion forms the largest contribution to band broadening close to the minimum of the plate height curve. For a specific column, a separation is best performed at this minimum, where the velocity is designated as the optimal velocity. In Figure 1.6a, the black lines represent the different flow paths compound molecules can follow when travelling through the column. Since the length of each of these flow paths is different, the velocities encountered in the different interparticle channels can vary quite significantly as well. This will result in band broadening of sample molecules following different flow paths. However, since the ratio of the velocities in the different flow paths is independent of the absolute velocity, band broadening originating from the nonuniformities in a packed bed is independent of the linear velocity.

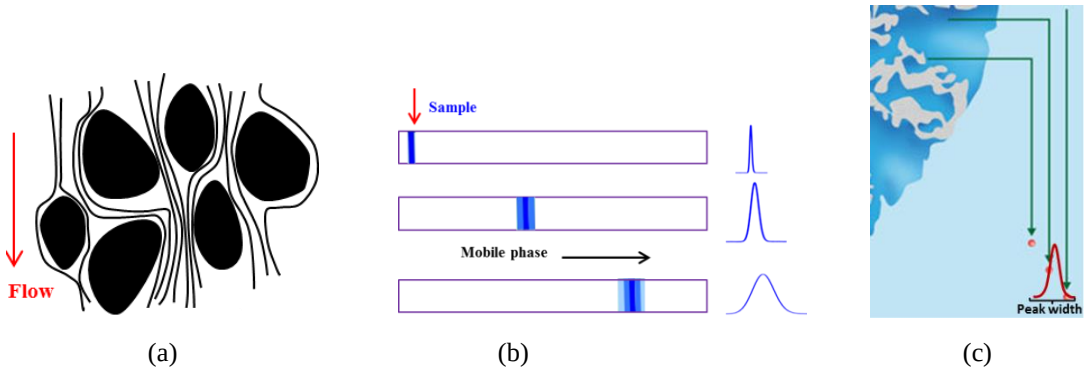


**Figure 1.6:** Schematic representation of the different contributions to the van Deemter equation (a) eddy dispersion, (b) longitudinal diffusion, (c) mass transfer resistance.

The A-term or eddy dispersion is a measure for the heterogeneity of a column, caused by the size and distribution of the interparticle channels and other nonuniformities in the packed bed. It is generally assumed to be proportional to the particle size ($d_p$) of the packed column:

$$A = \lambda_A \cdot d_p \qquad (1.28)$$

The $\lambda_A$-value is between 1 and 1.5 for a well-packed bed. The longitudinal diffusion, or B-term, describes the effect of molecular diffusion in the axial direction due to the concentration difference between the sample plug and the mobile phase, as shown in Figure 1.6b. At lower mobile phase velocities, the sample solute will need more time to pass through the column resulting in more time for longitudinal diffusion. Therefore, the B-term is inversely proportional to the velocity and can be expressed as:

$$B = 2 \cdot \gamma_B \cdot D_m \qquad (1.29)$$

Where $\gamma_B$ is the obstruction factor, describing the extent of "obstruction" in the column slowing down the free movement of molecules.

The C-term, or so-called mass transfer parameter, describes all phenomena that lead to an increase in plate height with increasing velocity, as shown in Figure 1.6c. These phenomena include the mass transfer from the moving mobile zone to the stationary zone, the interaction kinetics between the molecules and the stationary zone, followed by the transfer back to the mobile zone. There are mainly two contributions to this phenomenon: mass transfer in the mobile zone ($C_m$) and mass transfer in the stationary zone ($C_s$).
The C-term can be written as follows:

$$C = C_m\left(\frac{k''}{1+k''}\right)^2 \frac{d_p^2}{D_m} + C_s \frac{k''}{(1+k'')^2} \cdot \frac{d_p^2}{D_{part}} \quad (1.30)$$

Where $d_p$ is the particle size, $D_{part}$ the diffusion coefficient in stationary zone. For most chromatographic separations, the zone retention factor varies between 2 and 10, where the dependence of the mass transfer coefficient on the retention factor is negligible. Therefore, in this practical range of retention factors, the dependence of the plate height on the mass transfer coefficient can roughly be written as:

$$H = C\frac{d_p^2}{D_m}u \quad (1.31)$$

The coefficient $C$ is between 1/10 and 1/5 in most practical cases [33].

### 1.4.2. Giddings equation

Although the Giddings equation (Eq. (1.32)) is quite similar to the van Deemter equation, the former makes up for some of the shortcomings occurring in the latter. For example, in many practical cases, a downward curvature is observed in the plate height curve at high linear velocities that cannot be accounted for by the van Deemter equation. The origin of this problem rests with the assumption that the different contributions to the plate height are independent of each other and their variances are additive.

However, the real situation is far more complex than this and some portions of the eddy dispersion and the mass transfer resistance term should be coupled harmonically. This is due to the fact that the zone spreading originating from the macroscopic and microscopic nonuniformities in the packed bed is caused by the velocity inequalities between different flow paths and that the extent of the zone spreading is largely governed by mobile phase diffusion between fast and slow stream paths.

Both flow and lateral diffusion mechanisms hence work simultaneously to exchange molecules between flow paths of unequal velocities.

$$H = \sum \frac{1}{\frac{1}{A}+\frac{1}{C_m u}} + \frac{B}{u} + C_s \qquad (1.32)$$

### 1.4.3. Knox equation

The Knox equation was proposed by Knox by measuring a large series of plate height data on columns with different particle sizes over a large range of velocities [9,34-36]. The experimentally obtained plate height data were subsequently fitted to the van Deemter equation by adding the third root of the linear velocity to the A-term. Since the Knox equation is an empirical equation, associating a physical meaning to this extra term is not easy [37]. Therefore, the Knox equation is best expressed in its reduced form (see also § 1.5):

$$h = av^{\frac{1}{3}} + \frac{b}{v} + cv \qquad (1.33)$$

The value of *a* generally ranges between 0.8 and 1.0, *b* between 0.8 and 1.5 and *c* between 0.01 and 0.05 [12].

### 1.4.4. Comparison of the different equations

Since there are three frequently used plate height models, selecting the most adequate one to describe the properties of a packed bed can be a big challenge. The van Deemter equation is generally the most practical one, but is conceptually incorrect. The Giddings equation represents the best description of the packed bed, however, the coefficients resulting from curve-fitting can be unreliable [33]. The same holds for the Knox equation. The extent of the discrepancy between the different plate height models depends on the range of reduced velocities evaluated. Generally, there is only little difference between them for reduced velocities up to 20, which is the typical range of interest for practical HPLC columns [38].

There is some discrepancy between the van Deemter equation and the other two equations at reduced velocities above 20, while the Knox and Giddings equations are almost identical up to reduced velocities of 100 [33].

### 1.5. Reduced van Deemter plot

The reduced plate height ($h$) and reduced velocity (ν) are dimensionless parameters, which were first introduced by Giddings. These parameters allow comparing the efficiency of different columns over a broad range of column lengths, particle sizes and mobile phase conditions.

$$h = \frac{H}{d} \tag{1.34}$$

$$v = \frac{u \cdot d}{D_m} \tag{1.35}$$

For packed bed columns, $d$ corresponds to the particle size; for monolithic columns, it refers to the domain size and for open tubular columns, it refers to the capillary inner diameter.

### 1.6. HPLC versus UHPLC

Packed particle columns are generally based on silica as the standard packing material, capable of tolerating temperatures up to 60°C and a pH-range of 2.5 to 7.5. Particles with diameters of 3-5 µm that can withstand pressures up to 400 bar are still the standard in conventional HPLC. However, the demand for more efficient and faster separations has resulted in a large increase in the use of sub-2 µm particle columns. As shown in Eqs. (1.28), (1.30) and (1.31), the minimal plate height ($H_{min}$) decreases with decreasing particle size, resulting in more efficient separations. The optimal mobile phase velocity moreover increases with decreasing particle size, allowing for faster separations. In the C-term regime, smaller particles result in smaller diffusion distances and thus a much flatter plate height curve, allowing to operate at velocities significantly beyond the optimal velocity without sacrificing efficiency. However, column pressure increases with the square of the inverse particle size. As the (optimal) mobile phase velocity increases proportional with the inverse particle size, running smaller particles at their optimal velocity increases pressure drop hence by the third power of particle size. (e.g. going from 5 to 1.7 µm at optimal velocity increases the operating pressure by a factor of 27 for the same column length). The operation of sub-2 µm columns thus requires chromatographic instrumentation allowing higher operating pressures (up to 1200-1500 bar) to take full advantage of their potential. New technologies, such as bridged ethyl hybrid (BEH) and high-density silica particles have also been developed to produce sub-2 µm packings with sufficient mechanical strength to withstand these ultra-high pressures.

## 1.7. Kinetic plot method

The kinetic plot method is a tool to compare LC columns with different packing types, lengths or particle sizes. The approach was first presented by Giddings in 1965 to compare the theoretical limit of the separation speed in GC and LC [39]. Later, Knox used this method to compare the performance of packed bed columns and open-tubular columns [40].
In 1997, Poppe independently used kinetic plots to explore the compromise between speed and efficiency in LC [41]. In 2005, Desmet laid the foundation of the modern kinetic plot method [42-43] and used it to perform a wide comparison of different instruments and chromatographic conditions [44-49].

Meanwhile, kinetic plots were also adapted to gradient conditions by Wang [50]. In 2009, Carr further optimized the kinetic plot method to serve the chromatographic community with a tool that allows rapidly and effectively achieving a specific separation goal or comparing emerging technologies [51]. Recently, Desmet gave an overview of the different, existing kinetic plots and discussed their best use [52].

### 1.7.1. Constructing kinetic plots

Kinetic plots can be established by transforming a series of ($u_0$, H)-data, obtained in a column with permeability ($K_{v0}$) into corresponding $t_0$- and N-values by using Eqs. (1.38) and (1.40). These equations are obtained from the well-established pressure drop (ΔP) equation [53]:

$$u_0 = \frac{\Delta P}{\eta}\frac{K_{v0}}{L} \tag{1.36}$$

(Note that Eq. (1.36) is actually Eq. (1.21) for the case of the linear velocity)
and the basic equation relating column length (L), plate height (H) and plate number (N):

$$L = N \cdot H \tag{1.37}$$

Equations (1.36) and (1.37) are combined into the following expression:

$$\mathrm{N} = \left(\frac{\Delta \mathrm{P}}{\eta}\right)\left[\frac{\mathrm{K_{v0}}}{\mathrm{u_0 H}}\right]_{\mathrm{exp}} \tag{1.38}$$

Inserting Eq. (1.39) into Eq. (1.38),

$$t_0 = \frac{L}{u_0} \tag{1.39}$$

it is found that:

$$t_0 = \left(\frac{\Delta P}{\eta}\right)\left[\frac{K_{v0}}{u_0^2}\right]_{exp} \quad (1.40)$$

These calculations can easily be implemented into a spreadsheet calculator such as MS Excel [54]. In Fig. 1.7b, two representative $t_0$ versus N curves, obtained for two packed bed columns with particle sizes of $d_p$=3.5 µm and 1.8 µm, are shown. Each experimentally obtained ($u_0$, H)-data point in Fig. 1.7a is transformed into the corresponding ($t_0$, N)-data point in Fig. 1.7b using Eqs. (1.38) and (1.40).

The ($t_0$, N)-couple represents the efficiency (N) that can be obtained in a certain time ($t_0$). Since low velocities allow the use of longer columns at the maximum pressure, the data points corresponding to the B-term dominated region of the van Deemter curve are transformed into the long analysis time and high efficiency end of the kinetic plot curve (upper-right side of Fig. 1.7b). Inversely, the data points originating from the C-term dominated region are transformed into the short analysis time and low efficiency end of the plot (lower-left side of Fig. 1.7b).

To consider the ultimate performance limits of a certain column, the pressure (ΔP) in Eqs. (1.38) and (1.40) can be replaced by a freely selectable maximum pressure $\Delta P_{max}$, which can either be the maximum pressure a column can tolerate or the maximum pressure the instrument can deliver. All experimental ($u_0$, H)-couples obtained in a column with arbitrary length and pressure drop can in this way be transformed into (N, $t_0$)-couples representing the maximum number of plates and the corresponding minimal $t_0$-time. Such minimal $t_0$-time would be obtained if the same support would be used in a column that is exactly long enough to yield the maximal allowable pressure at the given $u_0$-velocity. The plot of $t_0$ versus N can directly map the kinetic performance limits of the tested support structure without any further numerical optimization.

Based on the van Deemter curves and permeability data in Fig. 1.7a, it is hard to evaluate which column is better. The 1.8 µm column results in lower plate heights and hence higher efficiencies, whereas the 3.5 µm column has a higher permeability. From the transformed kinetic plot (Fig. 1.7b) it can easily be concluded that the 3.5 µm column should be preferred for separations requiring more than 160.000 plates, while the 1.8 µm column will deliver faster separations when less than 160.000 plates are needed.

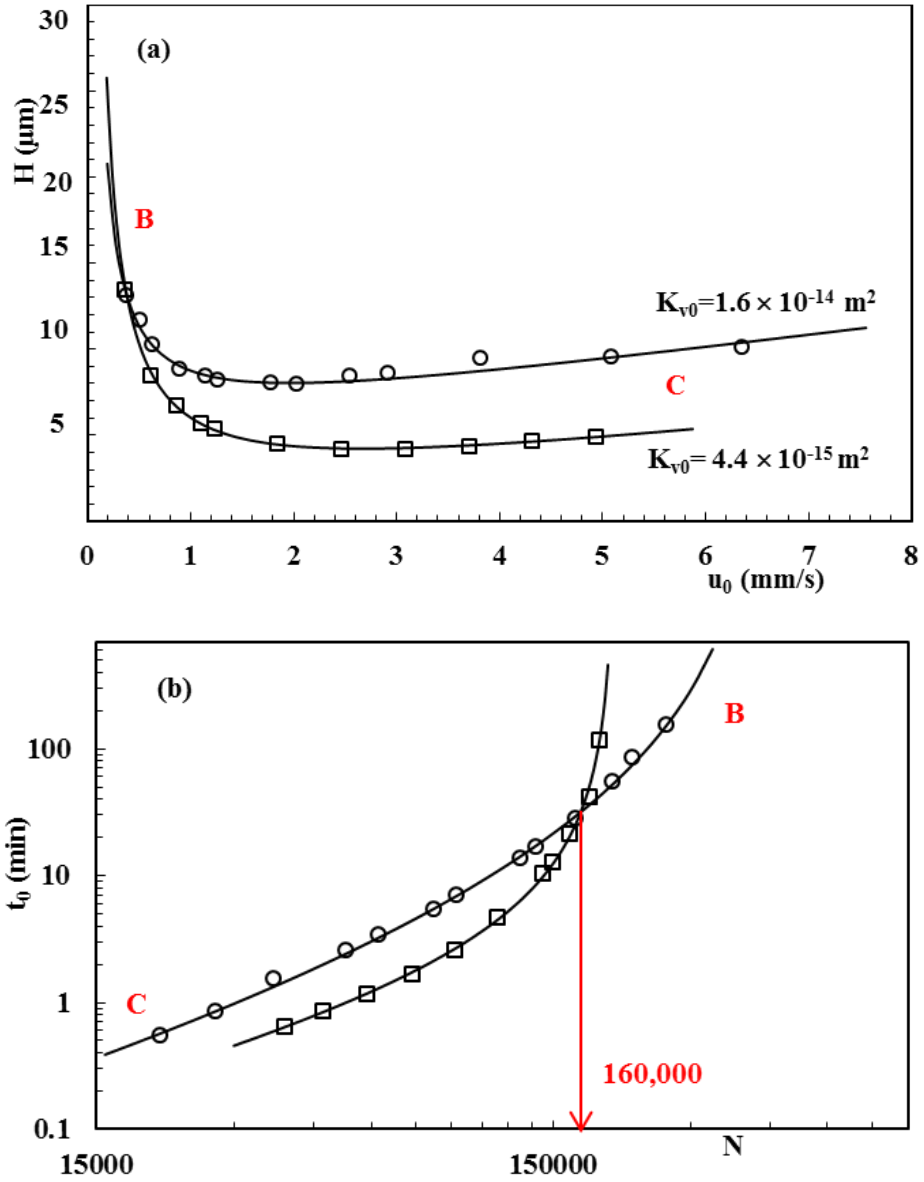


**Figure 1.7: (a)** Van Deemter curves obtained on an Acquity BEH C18 column (2.1×100 mm 1.7 µm) (□) and XBridge C18 column (2.1×150 mm 3.5 µm) (○); **(b)** the corresponding kinetic plot curves were constructed for $\Delta P_{max}$=400 for the 3.5 µm column and for 1000 bar for the 1.8 µm column. The plate count obtained at the crossing point of the two investigated kinetic plot curves is shown. B and C terms are indicated.

### 1.7.2. Comparing chromatographic techniques

Comparing the intrinsic performance potential of columns with new packing structures, one is always confronted with two pieces of information: plate height and column permeability. The former describes the band broadening, the latter the pressure drop characteristics of the column. Both parameters are more or less independent and there are no exact rules to decide whether one should prefer a support yielding small plate heights with a large flow resistance or the opposite.

The van Deemter plot is traditionally used to assess the column performance. However, it does not offer any information on the permeability. Unfortunately, this problem still remains when switching to reduced plate heights ($h_{min}=H_{min}/d_{ref}$), another very popular approach to compare different support types [55-56]. For reduced van Deemter plots, it is also very hard to find a general reference length ($d_{ref}$) that is valid for any type of support [57-58]. Another frequently used quality parameter that offers combined information on the permeability and minimal plate height of a support, is the minimum separation impedance [59]:

$$E_{min} = \frac{H_{min}^2}{K_v} \tag{1.41}$$

This approach is valid for one specific column length only [42]. To meet with the shortcomings existing in most current comparison techniques, the kinetic plot method has been developed to compare the separation performance of different packing structures and operating conditions in a uniform and standardized way**.** Using the kinetic plot method, the performance of a chromatographic system is no longer expressed in terms of absolute or reduced plate heights, but in a more universal and practically relevant unit: the required time versus the obtained efficiency (N), or resolution, or peak capacity. The information obtained from a kinetic plot is maximally generalized. The situation is not only limited to a column with a certain length or to a certain amount of plates, but yields conditions for all possible plate counts and column lengths. An additional advantage is that the kinetic plots can be established without having to define a reference length and hence allow comparing the performance of differently shaped and sized LC supports. Moreover, kinetic plots can be very easily established using Eqs. (1.38) and (1.40). Therefore, it is expected that this performance comparison technique will be used more frequently in the future.In conclusion, the answer to the question which technique is the best one is never unique and almost always depends on the desired efficiency or resolution. Moreover, the answer also depends on the evaluation criterion being used, e.g., a system yielding a fast critical pair analysis [60] can perform badly when one aims for the maximum peak capacity in a certain elution window [40].

## 1.8. Types of liquid chromatography

Based on the retention mechanism, the most popular liquid chromatographic techniques are reversed phase liquid chromatography (RPLC), normal phase liquid chromatography (NPLC), hydrophilic interaction liquid chromatography (HILIC), size-exclusion chromatography (SEC) and ion-exchange chromatography. This thesis mainly focuses on RPLC and HILIC.

### 1.8.1. Reversed phase liquid chromatography

It is estimated that around 90% of all analytical separations of low-molecular weight samples is performed using RPLC [33]. This technique utilizes apolar stationary phases and polar mobile phases. The broad variety in separation and retention characteristics encountered in columns obtained from different manufacturers is attributed to differences in base silica and surface derivatization.

The surface of reversed-phase packings is hydrophobic. Around 600 different stationary phases for RPLC are manufactured worldwide. The most popular types are alkyl ligands bonded to silica gels and among those the octyl (C8-) and octadecyl (C18-) bonded phases are used most frequently. The hydrophobic surface of the stationary phase interacts with the hydrophobic part of the molecules in the sample. The higher the lipophilicity of the analyte is, the higher the retention will be. Generally, silica-based bonded phases are prepared by reacting the silanols on the surface of the silica gel with chlorosilanes, as shown in Figure 1.8.

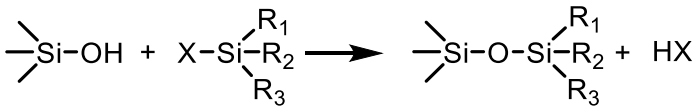


**Figure 1.8:** The bonding reaction for derivatization of silica surface by chlorosilanes.

Where $R_2$ is the alkyl ligand; $R_1$ and $R_3$ can either be short hydrocarbon groups (usually methyl groups) or additional functional groups that can bind to the surface or a neighboring silane. The amount of ligand that can be bonded to the surface is limited by the steric hindrance of the head group that attaches the ligand to the surface. The fully hydroxylated silica has a silanol content of 8 μmol/$m^2$. However, only half of these will usually be bonded to the silica surface [33].

The rest of the original silanol groups can hence still interact with the analyte molecules, leading to increased retention and peak tailing. An end capping procedure is often applied to remove these residual silanols by reacting them with a smaller, less sterically hindered, highly reactive silane, such as trimethylchlorosilane to improve the reversed-phase column packing. A complete removal of all residual surface silanols is, however, not possible.

The retention mechanism in RPLC is generally driven by adsorption at the stationary phase/mobile phase interface and partitioning into the stationary phase. The eluents used in RPLC are polar solvents or mixtures thereof. Among those, water is the weakest eluent, while methanol and acetonitrile are the most popular and strongest eluents. The lower the polarity of a solvent is, the higher its elution strength will be. A minimum of 5 vol% of organic modifier is required to ensure full contact between mobile and stationary phases. Acetonitrile is the preferred organic modifier in RPLC, due to the fact that acetonitrile-based mobile phases result in up to 2-fold lower pressure drops than methanol-based mobile phases when used at the same flow rate. The diffusion properties of solutes in acetonitrile-based mobile phases are also more favorable than in methanol-based mobile phases. For ionic or ionizable analytes, a buffered mobile phase should always be used to ensure reproducible results.

### 1.8.2. Hydrophilic interaction liquid chromatography

Today, mainstream liquid chromatography is dominated by RPLC that results in fast column equilibration and efficient separation of analytes with a broad range in polarity. For some weakly or moderately hydrophilic compounds, ion-exchange chromatography [61] or ion-pairing RPLC [62] can be used. However, for a large group of strongly polar compounds that cannot be ionized in solution, it is impossible to obtain sufficient retention on either stationary phase. This problem can be overcome to a certain extent by using normal-phase liquid chromatography, wherein a purely organic mobile phase is employed. However, strongly polar compounds are often not sufficiently soluble in nonpolar organic solvents, limiting the applicability of NPLC. Nowadays, the above problems are largely solved by the development of hydrophilic interaction liquid chromatography (HILIC) [63].

In HILIC, a polar stationary phase is used to retain polar analytes that are eluted by a mixture of organic solvent (usually ACN, > 70 vol%) and water (or buffer). HILIC has been described as a variant of NPLC, since both modes have a polar stationary phase and nonpolar mobile phase in common, but the separation mechanism in HILIC is different and more complicated than that of NPLC [64].

### 1.8.2.1. Stationary phase

In HILIC, bare silica is the most commonly used stationary phase [65]. To accommodate various applications, however, the family of HILIC stationary phases with various support materials and surface modifications, including many silica-bonded or organic-polymer stationary phases and materials with hybrid support or mixed-mode functionalities, is continuously expanding [66]. UHPLC columns (packed with sub-2 μm fully-porous particles) [67], columns filled with superficially porous particles [68] and monolithic columns [69] have also recently joined the HILIC family. Bonded silica phases such as diol, amino, amide and others are usually prepared by chemically modifying the silica gel surface with polar functional groups.

**Table 1.1.:** Selected stationary phases used in HILIC separations

| Packing materials | References |
|---|---|
| Underivatized silica stationary phases that contain functional groups such as siloxanes, silanols with (or without) a small quantity of metals | [70] |
| Polymeric structures of poly (succinimide) derivatives | [71] |
| Amino bonded phases | [72] |
| Diol bonded phases | [73] |
| Amide bonded phases | [72] |
| Alkylamide | [74] |
| Mix-mode | [74] |
| Cyano bonded phases | [75] |
| Polyethylene glycol/silica (HS PEG) | [76] |
| “click” ß-cyclodextrin | [77] |
| “click” saccharides(“click” maltose) | [78] |
| “click” dipeptide | [79] |
| Zwitterionic sulfobetaine bonded phases (ZIC-HILIC) | [80] |
| Cationic exchangers bonded phases | [81] |
| Mix-mode RP/anionic exchangers bonded phases | [82] |

The structural variations of HILIC stationary phases are wider than those in RPLC columns. Moreover, HILIC stationary phases can also be grouped into neutral polar and ionic surfaces. Different types of separation materials have different retention characteristics and separation selectivities. Table 1.1 shows some selected stationary phases used in HILIC separations [66].

### 1.8.2.2. Mobile phase

HILIC can be distinguished from NPLC by the fact that the mobile phases are mixtures of water-miscible polar organic solvents containing water or buffer (min. 3 vol%), wherein water acts as the strong eluent. The selected organic solvent in the HILIC mobile phase has a large influence on the obtained retention; the higher the percentage of organic solvent, the larger the retention of the polar compounds will be [83]. Usually, ACN is preferred as organic solvent, since it results in sufficient sample retention and good peak shapes [84], but in principle any aprotic solvent that is miscible with water (e.g. THF, dioxane) can be used. In cases where water as the protic solvent is too strong, retention can be increased by partly substituting water with a polar organic solvent, such as methanol, ethanol and isopropanol. In HILIC, the pH and ionic strength of the mobile phase can significantly affect the retention and separation selectivity of ionizable compounds.

Ammonium acetate, ammonium formate, ammonium phosphate and trifluoroacetic acid are commonly used as buffer salts or ionic additives to improve peak shape and to manipulate the retention of the analytes, although the separation also depends on the properties of the stationary phase [64, 66]. In addition, and owing to the large percentage of organic modifier in the mobile phase, HILIC can easily be coupled to mass spectrometry, especially in the electrospray ionization (ESI) mode, resulting in better sensitivities and lower limits of detection [85].

### 1.8.2.3. Retention mechanism

Although the retention mechanism in HILIC is not yet fully understood, it is commonly believed that it is based on the differential distribution of the analytes between the organic-rich mobile phase and the water-enriched multilayer adsorbed onto the hydrophilic surface of the stationary phase, as is shown in Figure 1.10. The retention phenomenon actually depends on various types of interaction between the analyte and the stationary phase, the analyte and the mobile phase, and the stationary and mobile phases, such as chemical interactions, physical interactions, intermolecular interactions and hydrophobic interactions [86].However, the real separation mechanism of HILIC involves various combinations of partitioning and electrostatic interactions or hydrogen bonding with the stationary phase [70]. The extent of each contribution depends on the particular conditions employed [87], such as the stationary phase, buffer conditions, type of organic solvent etc.

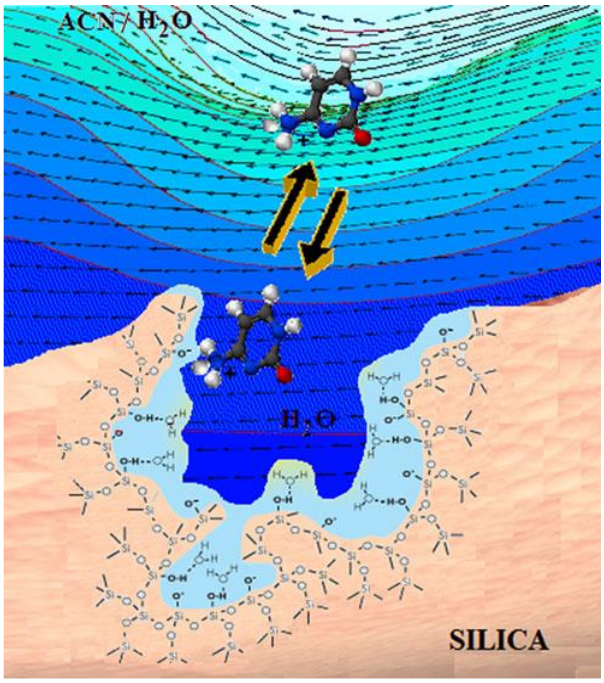


**Figure 1.10:** Overview of the separation mechanism in a HILIC system.(Figure reprinted with permission from [66])

## 1.9. Comparison of RPLC and HILIC

In general, the advantages of HILIC have been summarized as follows: (i) good peak shapes can be obtained for bases, (ii) MS sensitivity is enhanced due to the high organic content of the mobile phase, (iii) direct injection of extracts eluted from $C_{18}$ solid-phase extraction columns with solvents of high organic content is possible, (iv) the elution order of solutes is different and generally opposite to that in RPLC separations, (v) good retention of polar compounds, and (vi) higher flow rates are possible due to the high organic content of the mobile phase.

In addition, polar samples always show good solubility in HILIC mobile phases, overcoming the sample solubility issues encountered in NPLC. Ion pair reagents are not required in HILIC, making coupling to MS detection convenient. In contrast to RPLC, gradient elution in HILIC begins with a low-polarity organic solvent and elutes polar analytes by increasing the polar aqueous content [65, 88]. Other advantages of the HILIC technology have recently also been explored, including the use of long columns to achieve highly efficient separations, a superior loading capacity for charged basic solutes and the potential of fast analysis due to the good mass transfer characteristics of the columns operated in mobile phases with low viscosity [68].

Nevertheless, HILIC also shows some drawbacks including: (i) the separation mechanism is at present less well understood, thus, it may be difficult to predict the effect of a change in conditions on the separation outcome, (ii) the technique does not have the broad applicability of RPLC, e.g., neutral and non-polar analytes generally show very little retention in HILIC. In addition, ionized acidic analytes (negatively charged ions) also show little retention due to the repulsion of the ions from negatively charged silanol groups on some silica-based columns. (iii) HILIC is potentially an environmentally less friendly technique, as it consumes much larger volumes of organic solvents [89].

### 1.10. References

[1] Naing, N. N.; Li, S. F. Y.; Lee, H. K., J. Chromatogr. A 2015, 1426, 69-76.

[2] Chen, F.; Gong, Z.; Kelly, B. C., J. Chromatogr. A 2015, 1383, 104-111.

[3] Planche, C.; Ratel, J.; Mercier, F.; Blinet, P.; Debrauwer, L.; Engel, E., J. Chromatogr. A 2015, 1392, 74-81.

[4] Knolhoff, A. M.; Croley, T. R., J. Chromatogr. A 2016, 1428, 86-96.

[5] Yin, P.; Xu, G., J. Chromatogr. A 2014, 1374, 1-13.

[6] Denadai, M.; Cass, Q. B., J. Catogr. A 2015, 1418, 177-184.

[7] Guo, L.; Tan, S.; Li, X.; Lee, H. K., J. Chromatogr. A 2016, 1438, 1-9.

[8] Caltabiano, A. M.; Foley, J. P.; Barth, H. G., J. Chromatogr. A 2016, 1437, 74-87.

[9] Knox, J. H., J. Chromatogr. Sci. 1977, 15, 352-364.

[10] Cabooter, D.; Billen, J.; Terryn, H.; Lynen, F.; Sandra, P.; Desmet, G., J. Chromatogr. A 2008, 1178, 108-117.

[11] Cabooter, D.; Lynen, F.; Sandra, P.; Desmet, G., J. Chromatogr., A 2007, 1157, 131-141.

[12] Guiochon, G., J. Chromatogr. A 2006, 1126, 6-49.

[13] Halász, I.; Vogtel, P., Angew. Chem., Int. Ed. Engl. 1980, 19, 24-28.

[14] Broeckhoven, K. Understanding the effects of velocity, pressure, temperature and composition gradients in HPLC. Vrije Universiteit Brussel, Brussel, 2010.

[15] Bruce, E.; Poling, E. B.; John, M.; Prausnitz, J. M.; John, P.; O′Connell, J. P., The properties of gases and liquids. McGraw-Hill Education, New York, 1987.

[16] Karaiskakis, G.; Gavril, D., J. Chromatogr. A 2004, 1037, 147-189.

[17] Li, J.; Carr, P. W., Anal. Chem. 1997, 69, 2530-2536.

[18] Northrop, J. H.; Anson, M. L., J. Gen. Physiol. 1929, 12, 543-554.

[19] Song, H.; Desmet, G.; Cabooter, D., Anal. Chem. 2015, 87, 12331-12339.

[20] Wilke, C. R.; Chang, P., AIChE J. 1955, 1, 264-270.

[21] Scheibel, E. G., Ind. Eng. Chem. 1954, 46, 2007-2008.

[22] Hayduk, W.; Laudie, H., AIChE J. 1974, 20, 611-615.

[23] Stejskal, E. O.; Tanner, J. E., J.Chem. Phys. 1965, 42, 288-292.

[24] Krahn, W.; Schweiger, G.; Lucas, K., J. Phys. Chem. 1983, 87, 4515-4519.

[25] Stokes, R. H., J. Am. Chem. Soc. 1950, 72, 763-767.

[26] Miyabe, K.; Ando, N.; Guiochon, G., J. Chromatogr. A 2009, 1216, 4377-4382.

[27] Taylor, G., Proc R Soc A 1953, 219, 186-203.

[28] Ouano, A. C., Ind. Eng. Chem. Fund. 1972, 11, 268-271.

[29] Atwood, J. G.; Goldstein, J., J.Phys. Chem.1984, 88, 1875-1885.

[30] Miložič, N.; Lubej, M.; Novak, U.; Žnidaršič-Plazl, P.; Plazl, I., Chem. Biochem. Eng. Q. 2014, 28, 215-223.

[31] Häusler, E.; Domagalski, P.; Ottens, M.; Bardow, A., Chem. Eng. Sci. 2012, 72, 45-50.

[32] Miyabe, K.; Nagai, J.-i.; Guiochon, G., Chem. Eng. Sci. 2010, 65, 3859-3864.

[33] Neue, U. D., HPLC Columns, Theory, Technology and Practice. Wilet-VCH, New York, 1997.

[34] Grushka, E.; Snyder, L. R.; Knox, J. H., J. Chromatogr. Sci. 1975, 13, 25-37.

[35] Knox, J. H.; Parcher, J. F., Anal. Chem. 1969, 41, 1599-1606.

[36] Knox, J. H.; McLaren, L., Anal. Chem. 1963, 35, 449-454.

[37] Done, J. N.; Knox, J. H., J. Chromatogr. Sci. 1972, 10, 606-612.

[38] Usher, K. M.; Simmons, C. R.; Dorsey, J. G., J. Chromatogr. A 2008, 1200, 122-128.

[39] Giddings, J. C., Anal. Chem. 1965, 37, 60-63.

[40] Knox, J. H.; Saleem, M., J. Chromatogr. Sci. 1969, 7, 614-622.

[41] Poppe, H., J. Chromatogr. A 1997, 778, 3-21.

[42] Desmet, G.; Clicq, D.; Gzil, P., Anal. Chem. 2005, 77, 4058-4070.

[43] Desmet, G.; Clicq, D.; Nguyen, D. T. T.; Guillarme, D.; Rudaz, S.; Veuthey, J.-L.; Vervoort, N.; Torok, G.; Cabooter, D.; Gzil, P., Anal. Chem. 2006, 78, 2150-2162.

[44] Eeltink, S.; Gzil, P.; Kok, W. T.; Schoenmakers, P. J.; Desmet, G., J. Chromatogr. A 2006, 1130, 108-114.

[45] Cabooter, D.; Heinisch, S.; Rocca, J. L.; Clicq, D.; Desmet, G., J. Chromatogr. A 2007, 1143 , 121-133.

[46] Clicq, D.; Heinisch, S.; Rocca, J. L.; Cabooter, D.; Gzil, P.; Desmet, G., J. Chromatogr. A 2007, 1146, 193-201.

[47] Billen, J.; Guillarme, D.; Rudaz, S.; Veuthey, J. L.; Ritchie, H.; Grady, B.; Desmet, G., J. Chromatogr. A 2007, 1161, 224-233.

[48] Cabooter, D.; Billen, J.; Terryn, H.; Lynen, F.; Sandra, P.; Desmet, G., J. Chromatogr. A 2008, 1204, 1-10.

[49] Heinisch, S.; Desmet, G.; Clicq, D.; Rocca, J.-L., J. Chromatogr. A 2008, 1203, 124-136.

[50] Wang, X.; Stoll, D. R.; Carr, P. W.; Schoenmakers, P. J., J. Chromatogr. A 2006, 1125, 177-181.

[51] Carr, P. W.; Wang, X.; Stoll, D. R., Anal. Chem. 2009, 81, 5342-5353.

[52] Desmet, G.; Cabooter, D.; Broeckhoven, K., Anal. Chem. 2015, 87, 8593-8602.

[53] Katz, E. D.; Ogan, K.; Scott, R. P. W., J. Chromatogr. Library, 1985, 32, 403-434.

[54] Desmet, G.; Cabooter, D.; Gzil, P., LC-GC Europe 2005, 18, 8.

[55] Tanaka, N.; Kobayashi, H.; Nakanishi, K.; Minakuchi, H.; Ishizuka, N., Anal. Chem. 2001, 73, 420 A-429 A.

[56] Knox, J. H., J. Chromatogr. A 2002, 960, 7-18.

[57] Knox, J. H., J. Chromatogr. A 1999, 831, 3-15.

[58] Leinweber, F. C.; Tallarek, U., J. Chromatogr. A 2003, 1006, 207-228.

[59] Knox, J. H., J. Chromatogr. Sci. 1980, 18, 453-461.

[60] Scott, R. P. W., J. Chromatogr. A 1990, 517, 297-304.

[61] Nordborg, A.; Hilder, E. F., Anal. Bioanal. Chem. 2009, 394, 71-84.

[62] Dai, J.; Carr, P. W., J. Chromatogr. A 2009, 1216, 6695-6705.

[63] Alpert, A. J., J. Chromatogr. A 1990, 499, 177-196.

[64] Jandera, P., Anal. Chim. Acta 2011, 692, 1-25.

[65] McCalley, D. V., J. Chromatogr. A 2007, 1171, 46-55.

[66] Buszewski, B.; Noga, S., Anal. Bioanal. Chem. 2012, 402, 231-247.

[67] Li, Y.; Cheng, S.; Dai, P.; Liang, X.; Ke, Y., Chem. Commun. 2009, 9, 1085-1087.

[68] McCalley, D. V., J. Chromatogr. A 2008, 1193, 85-91.

[69] Jiang, Z.; Smith, N. W.; Liu, Z., J. Chromatogr. A 2011, 1218, 2350-2361.

[70] Hemström, P.; Irgum, K., J. Sep. Sci. 2006, 29, 1784-1821.

[71] Alpert, A. J.; Shukla, M.; Shukla, A. K.; Zieske, L. R.; Yuen, S. W.; Ferguson, M. A. J.; Mehlert, A.; Pauly, M.; Orlando, R., J. Chromatogr. A 1994, 676, 191-202.

[72] Strege, M. A., Anal. Chem. 1998, 70, 2439-2445.

[73] Tanaka, H.; Zhou, X.; Masayoshi, O., J. Chromatogr. A 2003, 987, 119-125.

[74] Buszewski, B.; Jezierska, M.; Wełniak, M.; Kaliszan, R., J. Chromatogr. A 1999, 845, 433-445.

[75] Kaczmarski, K.; Prus, W.; Kowalska, T., J. Chromatogr. A 2000, 869 , 57-64.

[76] Rong, L.; Takeuchi, T., J. Chromatogr. A 2004, 1042, 131-135.

[77] Guo, Z.; Jin, Y.; Liang, T.; Liu, Y.; Xu, Q.; Liang, X.; Lei, A., J. Chromatogr. A 2009, 1216, 257-263.

[78] Fu, Q.; Liang, T.; Zhang, X.; Du, Y.; Guo, Z.; Liang, X., Carbohydr. Res. 2010, 345, 2690-2697.

[79] Xue, M.; Huang, H.; Ke, Y.; Chu, C.; jin, Y.; Liang, X., J. Chromatogr. A 2009, 1216, 8623-8629.

[80] Strege, M. A.; Stevenson, S.; Lawrence, S. M., Anal. Chem. 2000, 72, 4629-4633.

[81] Lindner, H.; Sarg, B.; Meraner, C.; Helliger, W., J. Chromatogr. A 1996, 743, 137-144.

[82] Lämmerhofer, M.; Richter, M.; Wu, J.; Nogueira, R.; Bicker, W.; Lindner, W., J. Sep. Sci. 2008, 31, 2572-2588.

[83] Hao, Z.; Xiao, B.; Weng, N., J. Sep. Sci. 2008, 31, 1449-1464.

[84] Jandera, P., Anal. Chim. Acta 2011, 692, 1-25.

[85] Periat, A.; Boccard, J.; Veuthey, J.-L.; Rudaz, S.; Guillarme, D., J. Chromatogr. A 2013, 1312, 49-57.

[86] Kaliszan, R., Chem. Rev. 2007, 107, 3212-3246.

[87] Naidong, W., J. Chromatogr. B 2003, 796, 209-224.

[88] Cubbon, S.; Bradbury, T.; Wilson, J.; Thomas-Oates, J., Anal. Chem. 2007, 79, 8911-8918.

[89] McCalley, D. V., J. Chromatogr. A 2010, 1217, 858-880

# Chapter 2

# Scope of the Thesis

The aim of this thesis is to perform a thorough fundamental comparison of HILIC and RPLC to assess the true merits of HILIC for pharmaceutical applications. In **Chapter 3**, commercially available RPLC and HILIC columns will be used to investigate the column packing characteristics and band broadening phenomena. Subsequently, the intrinsic gain in separation speed that can be obtained by switching from HPLC to UHPLC conditions will be studied and compared under HILIC and RPLC conditions, first by using the kinetic plot method, then by applying it to a pharmaceutically relevant sample consisting of tetracycline (TC) and its main impurities 4-epitetracycline (ETC), anhydrotetracycline (ATC) and 4-epianhydrotetracycline (EATC).

In **Chapter 4,** an evaluation of column performance under HILIC and RPLC conditions for columns with identical packing structures will be performed by using an innovative protocol, developed for the adequate removal of the stationary phase of RPLC columns. This procedure allows studying the same column first under RPLC and subsequently under HILIC conditions.

Since an accurate knowledge of molecular diffusion coefficients ($D_m$) in different mobile phases is crucial in fundamental column performance studies, in **Chapter 5** the Taylor-Aris methodology is employed to measure molecular diffusion coefficients of 45 polar and apolar compounds in a wide range of mobile phase compositions typically used in RPLC and HILIC studies. The influence of the buffer concentration is also investigated.

In **Chapter 6**, the future perspectives are elucidated. The developed stripping protocol will be applied to a set of selected test compounds displaying a broader range of zone retention factors (k"= 0 to 10) to evaluate band broadening under RPLC and HILIC conditions, and to investigate the differences in intra-particle diffusion under both conditions. Once the intra-particle diffusivity is accurately known, the different contributions to eddy dispersion will be investigated to obtain a thorough understanding of the extent to which column end fitting design, sample distribution and collection in the column, wall and border effects influence the overall band spreading in RPLC and HILIC columns. This could potentially lead to the proposition of new column designs and formats, separately optimized for HILIC and RPLC separations.

# Chapter 3

# Evaluation and Comparison of the Kinetic Performance of Ultra-High Performance Liquid Chromatography and High-Performance Liquid Chromatography Columns in Hydrophilic Interaction Liquid Chromatography and Reversed-Phase Conditions

Parts of this chapter have been published in:

- **Huiying Song**, Erwin Adams, Gert Desmet, Deirdre Cabooter, Evaluation and comparison of the kinetic performance of ultra-high performance liquid chromatography and high-performance liquid chromatography columns in hydrophilic interaction and reversed-phase liquid chromatography conditions. *Journal of Chromatography A*, 1369 (2014) 83-91.

**Abstract**

An intrinsic performance comparison is made of the reduction in analysis time that can be obtained when switching from HPLC to UHPLC column formats in HILIC and reversed-phase conditions. A detailed overview of the packing characteristics of both stationary phase types is given first. It is demonstrated that HILIC columns demonstrate higher external porosity values than their reversed-phase counterparts resulting in lower flow resistance values. Column total porosity values determined from the elution time of a small marker molecule are shown to depend strongly on the composition of the mobile phase. To omit errors that might arise from an over- or underestimation of the column void time, all plate height and kinetic plot data are therefore expressed as a function of the interstitial velocity. Although only a limited number of columns are evaluated in this study, it is shown that the column efficiency of the HILIC columns is lower than that of their reversed-phase counterparts, at least for the samples evaluated here. Despite this lower efficiency, the kinetic performance of both stationary phase types is similar, due to the much lower viscosity of the mobile phases typically used in HILIC conditions. Finally, it is demonstrated that a similar, yet slightly larger reduction in analysis time can be obtained when switching from HPLC column formats to UHPLC formats in HILIC compared to reversed-phase conditions. This is also demonstrated for the practical separation of tetracycline and its main impurities.

**Keywords:** HILIC; RPLC; Kinetic plot; Porosity; Flow resistance; Tetracycline

## 3.1. Introduction

The recent revival of HILIC has led to the introduction of a large number of stationary phases for HILIC that are available both in HPLC and UHPLC column formats. Columns with particle sizes of 3.0-3.5 µm are commonly used for HPLC applications. To enhance the analysis speed and efficiency of LC analyses, sub-2 µm particle size columns operated under ultra-high pressure conditions have been introduced for both RP and HILIC [1-3]. The gain in separation performance that can be obtained by switching from conventional HPLC to UHPLC conditions is well-quantified and has been extensively demonstrated for RPLC separations [4]. A number of publications also exist that focus on the comparison in separation performance between RPLC and HILIC columns, e.g., for the separation and quantification of ephedrines [5-6], the quantification of peptides [7] and, more fundamentally, the comparison of the intra-particle diffusivity between these two technologies [8]. Recently, McCalley et al. published a paper on the comparison of sub-2 µm column formats on the one hand and 3.5 µm particle column formats on the other hand, of bare silica HILIC and $C_{18}$ RP columns from a fundamental point-of-view [9]. A comparison of reduced plate height curves of both column selectivities using basic and neutral solutes revealed smaller b-term coefficients for the HILIC columns, despite the larger solute diffusivity in the acetonitrile-rich mobile phases encountered in HILIC mode. This finding was attributed to the enhanced surface diffusion in the layer of acetonitrile on the surface of the RPLC stationary phases, which increases the b-term coefficient. Reduced c-term coefficients were found to be higher in HILIC than in RPLC, which was attributed to slower adsorption-desorption kinetics in HILIC. Kinetic plots moreover revealed that HILIC can present a significant improvement in performance when high efficiencies are required, resulting from the low viscosity of typical HILIC mobile phases and the low b-term coefficients.

No quantitative comparison of the gain in separation performance that can be obtained by switching from HPLC to UHPLC column formats in RPLC conditions on the one hand versus HILIC conditions on the other hand has, however, been made up to now. For this purpose, van Deemter and kinetic plot curves will be used in this study. A generic test mixture that can be applied to both HILIC and RPLC conditions under similar retention conditions will be defined. Subsequently, the findings obtained for test compounds will be extrapolated to a practical comparison using pharmaceutical sample consisting of tetracycline (TC) and its main impurities. Tetracyclines are widely used as veterinary medicines and growth additives

in animal feeds and water [10].

It has been shown that only a small amount of the used tetracyclines (veterinary or food additives) is metabolized or absorbed in animals, while most of the unmetabolized form is released in excreta [11], entering into the environment and disrupting the indigenous microbial population. Therefore, many researchers focus on method development for the determination of TCs in environmental samples. It has been demonstrated that TCs can be separated by RPLC [12], NPLC and HILIC [13-15], making this sample ideally suited for a practical comparison of the separation modes evaluated in this study.

## 3.2. Experimental

### 3.2.1. Chemicals and columns

Dimethyl sulfoxide (DMSO), perchloric acid, ammonium acetate and thymidine were obtained from Sigma-Aldrich (Steinheim, Germany). Cytosine, guanine, thymine, guanosine, adenosine, adenine and uracil from Janssen chimica (Geel, Belgium). Milli-Q water was prepared using a Milli-Q gradient water purification system from Millipore (Bedford, MA, USA). HPLC grade acetonitrile (ACN) and dichloromethane (analytical grade) were purchased from Fisher Chemicals (Erembodegem, Belgium) and tri-ammonium citrate was also obtained from Fisher Chemicals (Leicestershire, UK). HPLC grade tetrahydrofuran (THF) was from VWR (Leuven, Belgium). Glacial acetic acid was obtained from Merck (Darmstadt, Germany) and acenaphthene from Merck (Hohenbrunn, Germany). Tetracycline (TC), 4-epitetracycline (ETC), anhydrotetracycline (ATC), 4-epianhydrotetracycline (EATC), thiourea and citric acid were all from Acros (Geel, Belgium).

The chemical structures of TC and its main impurities are shown in Fig. 3.1. Details of the six evaluated columns are shown in Table 3.1. Polystyrene standards with 12 different molecular weights ranging between 500 Da and 2,000,000 Da were used for inverse size exclusion chromatography (ISEC) experiments and were also purchased from Sigma-Aldrich (Bornem, Belgium).

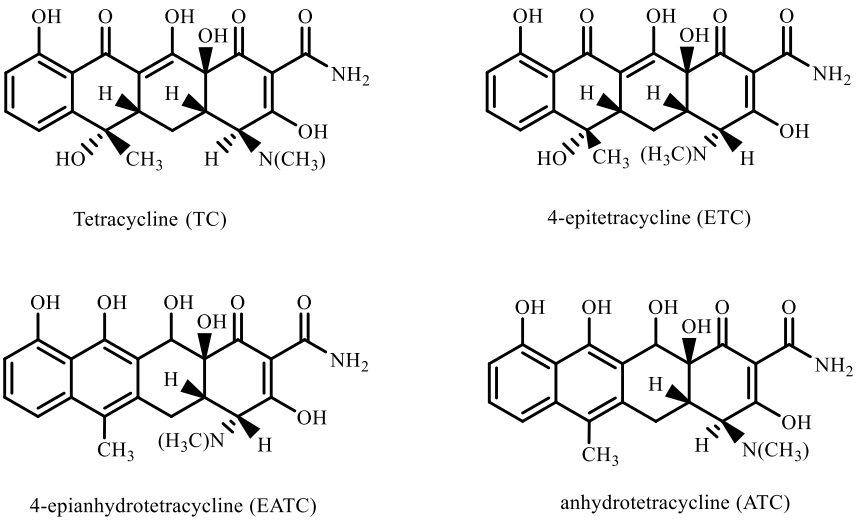


**Figure 3.1:** Chemical structure of TC and its related impurities

### 3.2.2. Apparatus

All HPLC experiments were performed on a UHPLC series 275 (Perkin Elmer, Massachusetts, USA) equipped with an autosampler, a binary pump, a forced-air oven and a variable wavelength detector with a detector cell of 2.6 µL. The maximum operating pressure of the system was 690 bar (10,000 psi). A stainless steel viper (125 µm I.D.) with heat exchanger (2 µL) (Dionex, Amsterdam, the Netherlands) was used between the injector and the inlet of the column. Between the outlet of the column and the detector, PEEK tubing with an internal diameter of 125 µm was used. The tubing was not altered during the experiments to avoid changing the extra-column volume. The overall system volume was determined to be 13 µL. Chromera software (Perkin Elmer) was used to control the UHPLC system and for data acquisition and analysis. The absorbance was measured at a wavelength of 254 nm for the test sample (theoretical evaluation and comparison of column performance) and at 300 nm for the tetracycline analysis. The column temperature was kept constant at 30℃.

UHPLC experiments were performed on an Infinity 1290 system (Agilent Technologies, Waldbronn, Germany) equipped with an autosampler, a quaternary pump and a diode-array detector with a detector cell of 1.0 µL. The maximum operating pressure of the system was 1200 bar. Peeksil vipers (75 µm I.D.) were used to connect the column to the system. The tubing was not altered during the experiments to avoid changing the extra-column volume. The overall system volume was determined to be 8.4 µL.

Chemstation software (Agilent Technologies) was used to control the UHPLC system and for data acquisition and analysis. The absorbance was measured at a wavelength of 300 nm for the tetracycline analysis.

### 3.2.3. Sample preparation

Stock solutions of thymine, adenosine, uracil, adenosine, cytosine and thymidine were prepared in a concentration of 1000 ppm in $H_2O$. Guanosine and adenine were dissolved separately in a concentration of 1000 ppm in DMSO. Guanine (1000 ppm) was dissolved in 0.1 M NaOH solution. Thiourea and acenaphthene were individually dissolved in a concentration of 1000 ppm in water and acetonitrile, respectively. Fresh test samples were prepared daily by mixing and diluting stock solutions in the mobile phase for the evaluation of the column performance according to Table 3.1. Injection volumes were 0.5 µL.

TC, ETC, ATC and EATC were dissolved in methanol, individually, to prepare stock solutions with a concentration of 1000 ppm each. Stock solutions were wrapped with aluminum foil to avoid compound degradation and afterwards were mixed and diluted in the corresponding mobile phase for column evaluation (Tables 3.2 and 3.3). The sample solutions were kept refrigerated until analysis. A refrigerated autosampler set at 4℃ was used to preserve the stability of the solutions during analysis.

### 3.2.4. Methodology for the determination of column porosities

External porosity values ($\varepsilon_e$) were measured experimentally by inverse size exclusion chromatography (ISEC) using a set of twelve polystyrene standards (MW= 500; 2000; 3000; 10,000; 20,000; 30,000; 70,000; 150,000; 300,000; 700,000; 1,000,000; 2,000,000). Each standard was dissolved in a concentration of 0.1 mg/mL in pure tetrahydrofuran. The flow rate was set at 0.4 mL/min for the 2.1 mm I.D. HPLC columns, at 0.2 mL/min for the 2.1 mm I.D. UHPLC columns and at 0.8 mL/min for the 4.6 mm I.D. HPLC column to operate all columns at similar column pressures. Injection volumes were 1 µL and the detection wavelength was 254 nm. Each injection was performed in triplicate and the obtained retention volumes averaged. Retention volumes were corrected for the extra-column volume of the system. The elution volumes of the polystyrene standards were subsequently plotted against the cubic root of their molecular weight ($MW^{1/3}$). External porosities were derived by extrapolating the exclusion branches of the ISEC plots to $MW^{1/3}= 0$ [16].

Column dead volumes and total porosities were assessed from the elution time of an unretained marker (thiourea for RP columns and acenaphtene for HILIC columns) using different mixtures of acetonitrile and water. Additionally, pycnometric measurements were performed using THF and dichloromethane as pure liquids, with densities of $\rho_{THF}$= 0.886 g/cm³ and $\rho_{CH2Cl2}$= 1.322 g/cm³, respectively [16].

### 3.2.5. Methodology for column evaluation and theoretical comparison

For the theoretical evaluation of the column performance of RPLC and HILIC columns, a mobile phase consisting of ACN and ammonium acetate ($NH_4Ac$) buffer in varying ratios was used to keep the retention factor of the last eluting compound constant on all columns ($k''_{last}$ ~10). The use of the zone retention factor k" was preferred over the phase retention factor k′ (based on the column void time $t_0$) for reasons that will be elaborated in Section 3.3.2. The zone retention factor k" can be calculated as:

$$k'' = \frac{t_R \cdot L}{u_i} \tag{3.1}$$

with $t_R$ the analyte retention time, L the column length and $u_i$ the interstitial velocity:

$$u_i = \frac{F}{\varepsilon_e \pi r^2} \tag{3.2}$$

where F is the mobile phase flow rate. Stock ammonium acetate solutions were prepared by dissolving the appropriate amount of ammonium acetate in water and adjusting to pH 6.0 by diluted acetic acid. The concentration of ammonium acetate in the total mobile phase was kept constant at ~19.5 mM for all columns in all intrinsic performance measurement experiments (see Table 3.1). These experiments were performed in isocratic mode. Plate heights were measured for at least 10 different velocities on every considered column to construct van Deemter curves. The viscosities of the mobile phases (η) were calculated according to Li and Carr [17]. Diffusion coefficients ($D_m$) were measured using the open tubular Taylor-Aris method at a flow rate of 0.1 mL/min at 30°C (Table 3.1). The internal diameter and length of the PEEK tubing used was 0.05277 cm and 1524 cm, respectively, the coil diameter was 12 cm [17]. Column efficiency ($N_{col}$) and asymmetry factors ($A_s$) were determined from peak widths at 10% of the peak height ($w_{0.1}$). All reported plate height and column permeability data were obtained after correction for the system band broadening ($\sigma^2_{sys}$), dead time ($t_{sys}$) and pressure ($\Delta P_{sys}$), determined by removing the column from the system and replacing it with a zero dead-volume connector under the same experimental conditons as for the plate height measurements [18].

**Table 3.1:** Composition of mobile phase and sample used for the theoretical evaluation of the six columns. Details on column dimensions and stationary phases are given.

| Columns | Manufacturer | Dimensions (mm) | Mode | $d_p$ (µm) | ACN/$NH_4Ac$ vol/vol %/% | $NH_4Ac$ (mM) | $k''_{last}$ | $D_{mol,last}$ ($m^2/s$) | Sample concentration (ppm) |
|---|---|---|---|---|---|---|---|---|---|
| Ace C18 | Achrom | 4.6 × 150 | RP | 3.0 | 2.6/97.4 | 19.5 | 10.8 | $0.77 \times 10^{-9}$ | Thiourea 20, thymine 40, |
| XBridge C18 | Waters | 2.1 × 150 | RP | 3.5 | 1.8/98.2 | 19.4 | 10.0 | $0.78 \times 10^{-9}$ | guanosine 40, |
| Acquity BEH C18 | Waters | 2.1 × 100 | RP | 1.7 | 2.0/98.0 | 19.6 | 11.1 | $0.77 \times 10^{-9}$ | thymidine 80, adenosine 80 |
| XBridgeAmide HILIC | Waters | 2.1 × 150 | HILIC | 3.5 | 89.0/11.0 | 19.5 | 9.5 | $1.53 \times 10^{-9}$ | Acenaphthene 80, uracil 25, |
| XBridge HILIC | Waters | 2.1 × 150 | HILIC | 3.5 | 93.0/7.0 | 19.5 | 11.1 | $1.69 \times 10^{-9}$ | adenosine 25, |
| Acquity HILIC BEH | Waters | 2.1 × 100 | HILIC | 1.7 | 93.2/6.8 | 19.0 | 10.2 | $1.69 \times 10^{-9}$ | cytosine 60, guanine 50 |



**Table 3.2:** Mobile phase composition, obtained retention factors (k') and critical pair resolution ($R_{s,\,cri}$) for the three HILIC columns evaluated for the analysis of tetracyclines at maximum column pressure.

| Columns | Dimension (mm) | $d_p$ (µm) | Tri-ammonium citrate(mM) | ACN/buffer | $R_{s,crit}$ | Inj. Vol (µL) | $t_0$ (min) | $k'_1$ | $k'_2$ | $k'_3$ | $k'_4$ | $P_{max}$ (bar) | Sample concentration (ppm) |
|---|---|---|---|---|---|---|---|---|---|---|---|---|---|
| XBridge Amide HILIC | 2.1×150 | 3.5 | 6.23 | 93/7 | 1.7 | 1 | 0.199 | 0.72 | 2.40 | 3.77 | 4.36 | 310 | TC 40, ETC 30, |
| XBridge HILIC | 2.1×150 | 3.5 | 1.20 | 97/3 | 2.5 | 1 | 0.215 | 0.30 | 1.26 | 2.25 | 3.77 | 313 | EATC 12, ATC 5 |
| ACQUITY HILIC BEH | 2.1×100 | 1.7 | 1.25 | 97/3 | 2.5 | 1 | 0.119 | 0.32 | 1.20 | 2.00 | 3.20 | 967 | TC 40, ETC 30, EATC 12, ATC 5 |

The subscript "total" refers to the experimentally measured efficiency, analysis time and pressure; the subscript "col" refers to the pure column efficiency obtained after correction:

$$N_{col} = \frac{\left(t_{R,total} - t_{R,sys}\right)^2}{\sigma^2_{total} - \sigma^2_{sys}} \quad (3.3)$$

$$H_{col} = \frac{L}{N_{col}} \quad (3.4)$$

$$K_{vi} = \frac{u_i \eta L}{\Delta P_{total} - \Delta P_{sys}} \quad (3.5)$$

Note that column permeabilities ($K_{vi}$) were originally calculated based on the interstitial velocity $u_i$. To avoid any misinterpretation that might arise from correction errors, column performance was assessed from plate height data obtained for adenosine (k"∼10.6) on RPLC columns and guanine (k"∼10.3) on HILIC columns.

The maximum difference between corrected and uncorrected plate heights for all columns at all evaluated flow rates, was always lower than 7%. Plate height data were subsequently fitted to the van Deemter equation:

$$H_{col} = A + \frac{B}{u_i} + C u_i \quad (3.6)$$

Where A, B and C are the eddy diffusion, longitudinal dispersion and resistance to mass transfer coefficients respectively.

### 3.2.6. Methodology for the construction of kinetic plots

Based on experimental van Deemter data ($u_i$, $H_{col}$) and column permeability values ($K_{vi}$), kinetic plots were constructed to visualize the potential of the two investigated analytical systems. Two equations were used to transform the experimental data into extrapolated plots of interstitial elution time versus efficiency, based on Desmet et al. [19-20]:

$$N = \frac{\Delta P_{max}}{\eta}\left(\frac{K_{vi}}{u_i H}\right) \quad (3.7)$$

$$t_i = \frac{\Delta P_{max}}{\eta}\left(\frac{K_{vi}}{u_i^2}\right) \quad (3.8)$$

Where η and $\Delta P_{max}$ represent the mobile-phase viscosity (Pa.s) and the maximum allowed column or instrument pressure, respectively. Data-processing and curve fitting were done using the Kinetic Plot Creator 3.1 (CHIS, Vrije Universiteit Brussel, Belgium).

### 3.2.7. Application to a pharmaceutically relevant sample

The analyses of tetracyclines were carried out in isocratic mode for the HILIC columns and in gradient mode for the RPLC columns. The goal was to obtain comparable separation qualities (critical pair resolution $R_{s,crit} > 1.5$) and elution windows ($k'_{last}$=4-5) on both column types.

Ammonium citrate, adjusted to pH= 3.5 with citric acid (Table 3.2) was chosen as the buffer component and acetonitrile as the organic modifier for the HILIC separations. The mobile phase composition was adjusted for each column to get sufficient resolution for the critical pair ($R_{s,crit} > 1.7$) and comparable elution windows ($k'_{last}$= 3.8 ± 0.6) on all HILIC columns (see Table 3.2).

For RPLC columns, all gradient experiments were performed using the same mobile phase A (DMSO-1M $HClO_4$-$H_2O$, 500:50:450 v/v/v) and B (DMSO-1M $HClO_4$, 950:50 v/v). The gradient start concentration ($\phi_0$), end concentration ($\phi_e$) and steepness (related to the gradient time $t_G$) were adapted for each column to keep the ratio of $t_G/t_0$ constant at 4.4 and the apparent retention factors ($k'$) for the first eluting compound (ETC) and last eluting compound (ATC) at $k'_1$ = 1.32 and $k'_{last}$ = 5.0, respectively. The ratio of $t_{delay}/t_0$ ($t_{delay}=t_{dwell}+t_{isocratic\ hold}$, with $t_{delay}$ the total delay time, $t_{dwell}$ the system dwell time and $t_{isocratic\ hold}$ the time of the applied isocratic hold at the start of the gradient) was kept constant as well to maintain the selectivity of the separation.

The column void time ($t_0$) of each column was determined from the elution time of thiourea, corrected for the system void time ($t_{ext}$, obtained by replacing the column by a zero-dead volume connector). Table 3.4 shows the gradient profiles that were used on the RPLC columns at maximum system pressure.

**Table 3.3:** Obtained retention factors (k') and critical pair resolution ($R_{s,crit}$) for the two reversed-phase columns evaluated for the analysis of tetracyclines at maximum pressure. The sample concentration was 40 ppm TC, 30 ppm ETC, 12 ppm EATC and 5 ppm ATC.

| Columns | Dimension (mm) | $d_p$ (µm) | $t_0$ (min) | $k'_1$ | $k'_2$ | $k'_3$ | $k'_4$ | $R_{s,crit}$ | Inj. vol(µL) | $P_{max}$ (bar) |
|---|---|---|---|---|---|---|---|---|---|---|
| XBridge C18 | 2.1×150 | 3.5 | 2.44 | 1.32 | 1.54 | 4.84 | 5.08 | 1.8 | 1 | 342 |
| Acquity C18 BEH | 2.1×100 | 1.7 | 1.34 | 1.32 | 1.53 | 4.73 | 4.98 | 1.7 | 1 | 951 |

**Table 3.4:** Gradient programs applied for the separation of TC and its main impurities on two RP columns at maximum column pressure. Applied flow rates are indicated.

| XBridge C18 2.1×150 mm, 3µm (F=0.12mL/min) | | ACQUITY BEH C18 2.1×100 mm, 1.7 µm (F=0.15mL/min) | |
|---|---|---|---|
| Time (min) | Mobile phase B(% v/v) | Time (min) | Mobile phase B(% v/v) |
| 0 | 25 | 0 | 27 |
| 1.78 | 25 | 0 | 27 |
| 10.85 | 58 | 5.95 | 58 |
| 1.09 | 58 | 0.59 | 58 |
| 1.09 | 25 | 0.59 | 27 |
| 26.9 | 25 | 14.76 | 27 |

## 3.3. Results and discussion

### 3.3.1. Determination of a suitable test mixture

A test mixture was defined that could be applied to both RPLC and HILIC-type stationary phases under similar retention conditions, to allow for an intrinsic evaluation and comparison of the column performance of both phases, regardless of their selectivity. Different nucleosides and nucleobases were selected as test molecules (Table 3.1), due to their relatively polar nature and comparable characteristics (small molecular weight compounds with MW= 111-280 and log P values between -0.12 and -1.72). Representative chromatograms, obtained at the optimal flow rate on RPLC and HILIC columns with similar dimensions are shown in Fig. 3.2. As can be deduced from these figures, good peak shapes are obtained on both column types (asymmetry factor $A_s$= 1.0 - 1.3 for all compounds) within similar elution windows (k"~ 2-3 for the first eluting peak and k"~ 10 for the last eluting peak) using similar compounds.

Although very low concentrations of ACN (~ 2% volume) were required to obtain sufficient retention for all compounds on the reversed-phase columns, phase dewetting did not occur to the best of our knowledge. This can be deduced from the fact that clear retention was obtained for the different compounds in the test mixture, that peak shapes were excellent under these conditions and that retention times were reproducible at all flow rates considered during the van Deemter measurements (RSD < 1.0 %) [21].

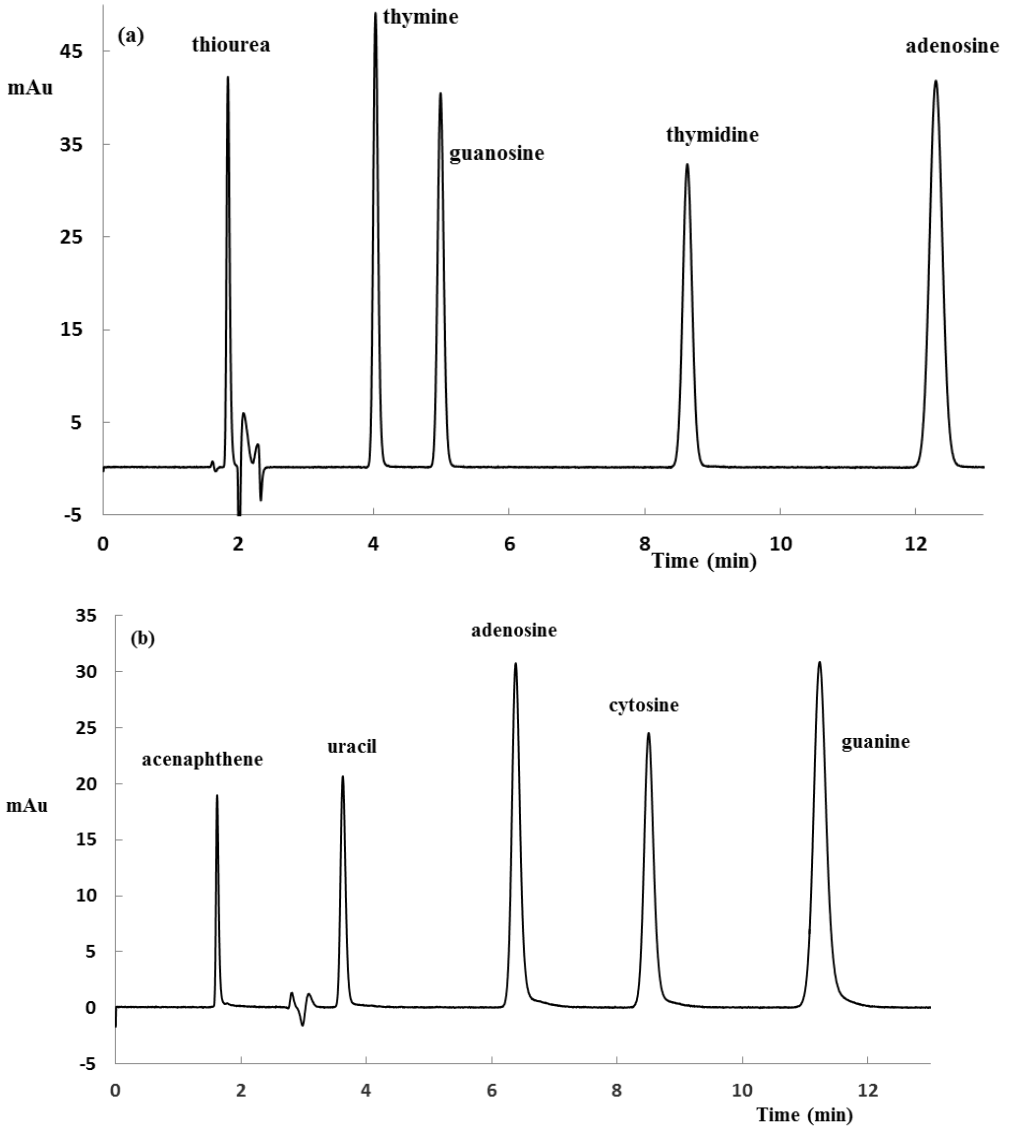


**Figure 3.2:** Chromatograms of test mixture on (a) XBridge C18 2.1 × 100 mm, 3.5 µm (1.8/98.2 vol%/vol% ACN/$NH_4Ac$ buffer) and (b) XBridge Amide HILIC 2.1 × 100 mm, 3.5 µm (89/11 vol%/vol% ACN/$NH_4Ac$ buffer) in isocratic conditions at the optimal flow rate (0.2 mL/min). Mobile phase compositions are also shown in Table 1.

### 3.3.2. Column permeability

Column permeability ($K_{v0}$) and flow resistance values ($\phi_0 = d_p^2/K_{v0}$) were originally calculated from the same set of data used for the construction of the plate height curves (§ 3.2.5, data see Table 3.5, $K_{v0}$ and $\phi_0$ VD). Despite the similarity in dimensions between e.g., the XBridge $C_{18}$ and XBridge HILIC column, and the Acquity $C_{18}$ and Acquity HILIC column, significantly larger permeability values (on average a factor 1.8) were observed for the HILIC columns in comparison with their RPLC counterparts. As all permeability values were originally calculated using the linear velocity of the mobile phase ($u_0$, determined from the elution time of an unretained marker) and viscosity values calculated according to [17], it was investigated

whether errors or discrepancies in one of these parameters could explain the large observed differences in permeability, or whether they were rather related to intrinsic differences in column structure. For this purpose, pressure and $t_0$- measurements were repeated for each individual column, but now using a fixed mobile phase composition of ACN/$H_2O$ 50/50 vol%/vol% at a fixed flow rate of 0.25 mL/min. Under these conditions, possible inaccuracies in viscosity values can be omitted. To avoid possible errors in $u_0$-values, permeabilities were first recalculated based on the superficial velocity $u_s$:

$$u_s = F/S \tag{3.9}$$

With F the volumetric flow rate ($m^3/s$) and S the cross-section of the column ($m^2$). Looking at the superficially based permeability values $K_{vs}$ and corresponding flow resistances $\phi_s$ obtained for all columns under these conditions (Table 3.6), it is observed that the HILIC columns still yield a higher permeability than their RPLC counterparts (on average a factor of ~1.5), but this difference has already decreased significantly. To explain the observed differences in $K_{vs}$, values of $\varepsilon_e$ were subsequently calculated by fitting the experimentally measured values of $K_{vs}$ to Kozeny-Carman's law for different values of $\varepsilon_e$ until a perfect match was found:

$$K_{vs} = \frac{d_p^2}{180} \frac{\varepsilon_e^3}{(1-\varepsilon_e)^2} \tag{3.10}$$

The obtained values of $\varepsilon_e$ are also shown in Table 3.6 and indicate systematically higher external porosity values for the HILIC columns ($\varepsilon_e$ ~ 43%) in comparison to the RPLC columns ($\varepsilon_e$ ~ 40%).

To verify the accuracy of the obtained $\varepsilon_e$–values, inverse size exclusion (ISEC) experiments were additionally performed and the resulting values of $\varepsilon_e$ are presented in Table 3.6. Considering the accuracy of the ISEC experimental protocol lies within 1% [16], a relatively satisfactory agreement between the data derived from the Kozeny-Carman equation and the ISEC experiments is obtained. More importantly, the previous observation of higher $\varepsilon_e$–values for the HILIC columns ($\varepsilon_e$ (ISEC) ~ 42%) compared to the RP columns ($\varepsilon_e$ (ISEC) ~ 38%) is maintained. These differences in external porosity could be related to differences in packing procedure or particle size distribution (PSD) despite the fact that most of the columns originated from the same vendor. In any case, the higher external porosity $\varepsilon_e$ of the HILIC columns, presents a first explanation for the higher observed values of $K_{v0}$ and $K_{vs}$.

**Table 3.5:** Obtained reduced van Deemter coefficients from curve fitting for the six evaluated columns. Column permeability ($K_{v0}$ VD) and flow resistance ($\phi_0$ VD) values based on the linear velocity of the mobile phase ($u_0$) during the plate height measurements are also given.

| Columns | Dimensions (mm) | Mode | $d_p$ (µm) | A | B | C | $u_{i,opt}$ (mm/s) | $H_{min}$ (µm) | $K_{v0}$ VD ($m^2$) | $\phi_0$ VD |
|---|---|---|---|---|---|---|---|---|---|---|
| Ace C18 | 4.6 × 150 | RP | 3.0 | 0.55 | 5.77 | 0.12 | 1.79 | 6.59 | $1.1 \times 10^{-14}$ | 796 |
| XBridge C18 | 2.1 × 150 | RP | 3.5 | 1.43 | 3.82 | 0.05 | 1.98 | 7.93 | $1.6 \times 10^{-14}$ | 785 |
| Acquity BEH C18 | 2.1 × 100 | RP | 1.7 | 0.45 | 5.97 | 0.17 | 2.66 | 4.24 | $4.4 \times 10^{-15}$ | 664 |
| XBridgeAmide HILIC | 2.1 × 150 | HILIC | 3.5 | 1.74 | 1.99 | 0.20 | 1.39 | 10.4 | $3.0 \times 10^{-14}$ | 404 |
| XBridge HILIC | 2.1 × 150 | HILIC | 3.5 | 2.19 | 2.27 | 0.13 | 2.10 | 11.6 | $2.5 \times 10^{-14}$ | 484 |
| Acquity HILIC BEH | 2.1 × 100 | HILIC | 1.7 | 1.19 | 3.25 | 0.25 | 3.54 | 4.92 | $6.5 \times 10^{-15}$ | 447 |

**Table 3.6:** Flow characteristics of the evaluated columns: permeability, porosity and flow resistance measures, obtained using different methodologies and under different mobile phase compositions. KC= Based on Kozeny-Carman's law, ISEC= obtained from inverse-size exclusion measurements, VD= determined from the elution time of an unretained marker under the mobile phase conditions used for the plate height measurements, 50:50= determined from the elution time of an unretained marker in a mobile phase consisting of 50/50 ACN/$H_20$ vol%/vol%, pycno= determined via pycnometry measurements.

| Columns | Dimensions (mm) | Mode | $d_p$(µm) | $u_s$(mm/s) | $K_{vs}$ ($m^2$) | $\phi_s$ | $\varepsilon_e$ (KC) | $\varepsilon_e$ (ISEC) | $\varepsilon_T$ (VD) | $\varepsilon_T$(50/50) | $\varepsilon_T$ (pycno) | $K_{vi}$ ($m^2$) |
|---|---|---|---|---|---|---|---|---|---|---|---|---|
| Ace C18 | 4.6 × 150 | RP | 3.0 | 0.25 | $8.11 \times 10^{-14}$ | 1110 | 0.3915 | 0.3624 | 0.7180 | 0.5762 | 0.6645 | $2.24 \times 10^{-14}$ |
| XBridge C18 | 2.1 × 150 | RP | 3.5 | 1.20 | $1.07 \times 10^{-14}$ | 1148 | 0.3884 | 0.3784 | 0.7088 | 0.5810 | 0.6487 | $2.82 \times 10^{-14}$ |
| Acquity BEH C18 | 2.1 × 100 | RP | 1.7 | 1.20 | $3.12 \times 10^{-15}$ | 925 | 0.4084 | 0.3894 | 0.7279 | 0.6033 | 0.6558 | $8.02 \times 10^{-15}$ |
| XBridge Amide HILIC | 2.1 × 150 | HILIC | 3.5 | 1.20 | $1.69 \times 10^{-14}$ | 725 | 0.4314 | 0.4147 | 0.5818 | 0.5970 | 0.7258 | $4.08 \times 10^{-14}$ |
| XBridge HILIC | 2.1 × 150 | HILIC | 3.5 | 1.20 | $1.64 \times 10^{-14}$ | 748 | 0.4284 | 0.4229 | 0.6906 | 0.7454 | 0.7581 | $3.87 \times 10^{-14}$ |
| Acquity HILIC BEH | 2.1 × 100 | HILIC | 1.7 | 1.20 | $4.10 \times 10^{-15}$ | 705 | 0.4340 | 0.4336 | 0.6787 | 0.7433 | 0.7691 | $9.45 \times 10^{-15}$ |

Total porosity values ($\varepsilon_T$) were subsequently calculated for HILIC and RPLC columns from the elution time of their respective $t_0$-markers (thiourea for RPLC columns and acenapthene for HILIC columns) using a mobile phase composition of ACN/$H_2O$ 50/50 vol%/vol%:

$$\varepsilon_T = \frac{V_0}{V_G} = \frac{t_0 \cdot F}{V_G} \quad (3.11)$$

Where $V_0$ is the void volume of the column (mL) and $V_G$ is the geometrical volume of the column (mL), calculated as $V_G = \pi r^2 L$. These values were compared with $\varepsilon_T$–values deduced from the elution time of the $t_0$-marker during the van Deemter experiments at the same fixed flow rate of 0.25 mL/min (~ 2 vol% ACN for the RP columns and ~ 92 vol% ACN for the HILIC columns). Finally, $\varepsilon_T$–values were also determined via pycnometry. All obtained values are displayed in Table 3.6. It has been suggested that the "true" or "maximum" column dead volume and hence column total porosity can be assessed from pycnometry measurements [22-24]. Focussing on the reversed-phase columns first, the $\varepsilon_T$-values obtained from the elution volume of thiourea are significantly higher when a small percentage of ACN (~ 2 vol% ACN) is used in the mobile phase, indicating some retention of the "unretained" marker occurs. The $\varepsilon_T$-values deduced from the elution volumes of thiourea in a mobile phase containing 50 vol% ACN on the other hand, are much smaller than those obtained by pycnometry. This suggests that thiourea is excluded from a substantial fraction of the internal pore volume under these conditions and could indicate the formation of a multilayer of ACN at the $C_{18}$-bonded surface area of the pores by the preferential adsorption of ACN. Since the solubility of thiourea is low in this ACN-rich layer inside the mesopores, it is likely excluded from this region, explaining the small observed $\varepsilon_T$-values in comparison with the pycnometry values.

The results for the pure silica HILIC columns (XBridge and Acquity HILIC) on the other hand, suggest that the values of $\varepsilon_T$ deduced from the elution volumes of acenapthene during the plate height measurements (hence in a high vol% ACN) are underestimated in comparison with the values obtained via pycnometry. This can be attributed to the formation of a water-rich mobile phase layer on the surface of the pores, since water will be adsorbed more strongly on the surface of silica than ACN. Due to the limited solubility of acenaphthene in water, it will largely be absent in this water-rich layer and rather partition in the ACN-rich mobile phase, explaining why the $\varepsilon_T$-values obtained in an ACN-rich mobile phase are lower than the pycnometry values [25].

As the water content increases to 50 vol%, the thickness of the water layer increases but also the difference in polarity between the mobile phase and this water layer decreases, allowing acenaphthene to partition into the water layer [25]. This results in values of $\varepsilon_T$ that are larger in 50 vol%ACN than in ~92 vol% of ACN (as used for the plate height measurements) for bare silica columns. The $\varepsilon_T$-values obtained from the elution time of acenapthene for the Amide HILIC column are smaller than those of the bare silica columns and more similar for both mobile phase compositions. This is probably due to the formation of a thicker water layer at the surface of the mesopores due to the presence of the polar amide groups. Considering the originally calculated values of $K_{v0}$ ($K_{v0}$VD in Table 3.5) are directly related to the elution volume or elution time ($t_0$) of the "unretained" marker:

$$K_{v0} = \frac{L^2 \eta}{t_0 \Delta P} \tag{3.12}$$

The overestimation of $t_0$ during the plate height measurements on the RP columns and its underestimation during the plate height measurements on the HILIC columns, provides a second explanation for the large difference in observed $K_{v0}$-values between HILIC and RP columns. The above discussion illustrates how difficult it is to accurately assess the column dead volume and $t_0$-time when different column stationary phase types (such as HILIC and RP columns) are to be compared under different mobile phase conditions. For the remainder of the study, it was therefore decided to express all plate height and kinetic plot data as a function of the interstitial velocity $u_i$ and the interstitial column permeability $K_{vi}$, which is anyhow fundamentally more sound [26-28]:

$$K_{vi} = \frac{K_{vs}}{\varepsilon_e} \tag{3.13}$$

With $\varepsilon_e$ the external porosity value determined via ISEC measurements. Although we also could have used the $\varepsilon_e$-values derived from Kozeny–Carman's law, we decided to work with the ISEC $\varepsilon_e$-values because these are based on fewer assumptions.

### 3.3.3. Column evaluation using plate height models

Fig. 3.3 shows the plate height curves obtained on all investigated columns. To compare column efficiency, van Deemter plots for the last eluting compound in the chromatogram were selected (adenosine (k"= 10.6 ± 0.6) for the RPLC columns and guanine (k" = 10.3 ± 0.8) for the HILIC columns).

Comparing the van Deemter plots of RPLC and HILIC columns with same particle size (Fig. 3.3 and Table 3.5), the minimum plate heights ($H_{min}$) obtained for the HILIC columns are consistently higher than those on RPLC columns with the same particle size. This is also reflected in the higher A-term values obtained for the HILIC columns. Despite the higher solute diffusivity obtained in HILIC conditions due to the large ACN content (Table 3.1), the B-term values obtained for the HILIC columns are systematically lower than those obtained for their RPLC counterparts, while the C-term values are higher. Although these findings seem counter-intuitive, they are in agreement with those made by McCalley et al. [9] and suggest that diffusion is slowed down considerably by the water-rich layer in the mesopores of the HILIC columns. Finally, the lower viscosity of the ACN-rich mobile phase, allows the HILIC columns to be operated at much higher interstitial velocities, before the upper pressure of the column is reached.

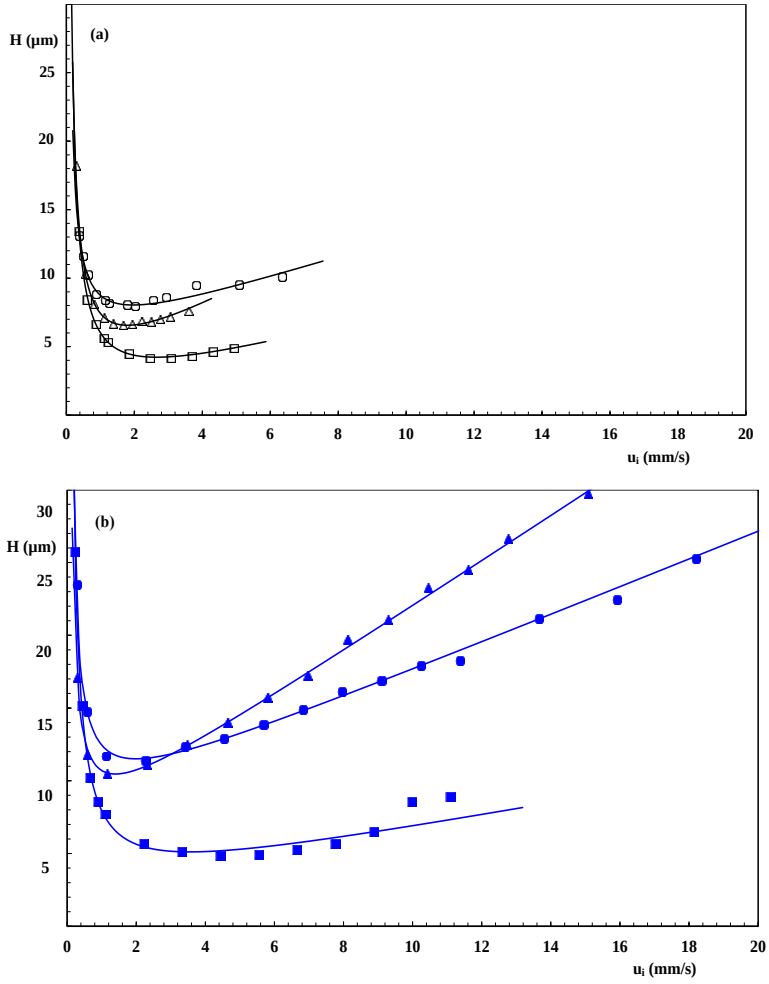


**Figure 3.3:** van Deemter curves of plate height (H) versus interstitial velocity ($u_i$) for (a) adenosine (k" = 10.6 ± 0.6) on reversed phase columns and (b) guanine (k" = 10.3 ± 0.8) on HILIC columns. ACE $C_{18}$ column 4.6 × 150 mm, 3.0 µm (Δ); XBridge $C_{18}$ 2.1 × 150 mm, 3.5 µm (○); Acquity UHPLC BEH $C_{18}$ 2.1 × 100 mm, 1.7 µm (□); XBridge Amide 2.1 × 100 mm, 3.5 µm (▲); XBridge HILIC 2.1 × 150 mm, 3.5 µm (●); Acquity HILIC BEH 2.1 × 100 mm, 1.7 µm (■). Open, black symbols refer to reversed phase columns, closed, blue symbols to HILIC columns. Mobile phase conditions are given in Table 3.1

To compare the intrinsic efficiency of columns packed with different particle sizes and different porosities, the reduced form of the van Deemter plot is more suited as it allows normalizing these differences. Fig. 3.4 shows that the difference in reduced plate heights (*h*) between the different particle sizes is relatively small, both for the RPLC and HILIC stationary phases, be it that in both cases the C-term slope is slightly steeper for the sub-2 µm particles in comparison with the 3.0-3.5 µm particles. This could be an indication of viscous heating leading to a decrease in column efficiency at high operating pressures [4], especially considering all experiments were conducted in a forced-air oven. From the reduced van Deemter plots, the larger B-term and smaller C-term of the RPLC columns compared to the HILIC columns is also clearly evident. As shown in Fig. 3.4, all columns yield minimum reduced plate heights between 2.0 and 3.2 and can therefore be considered as relatively "well-packed" [27].

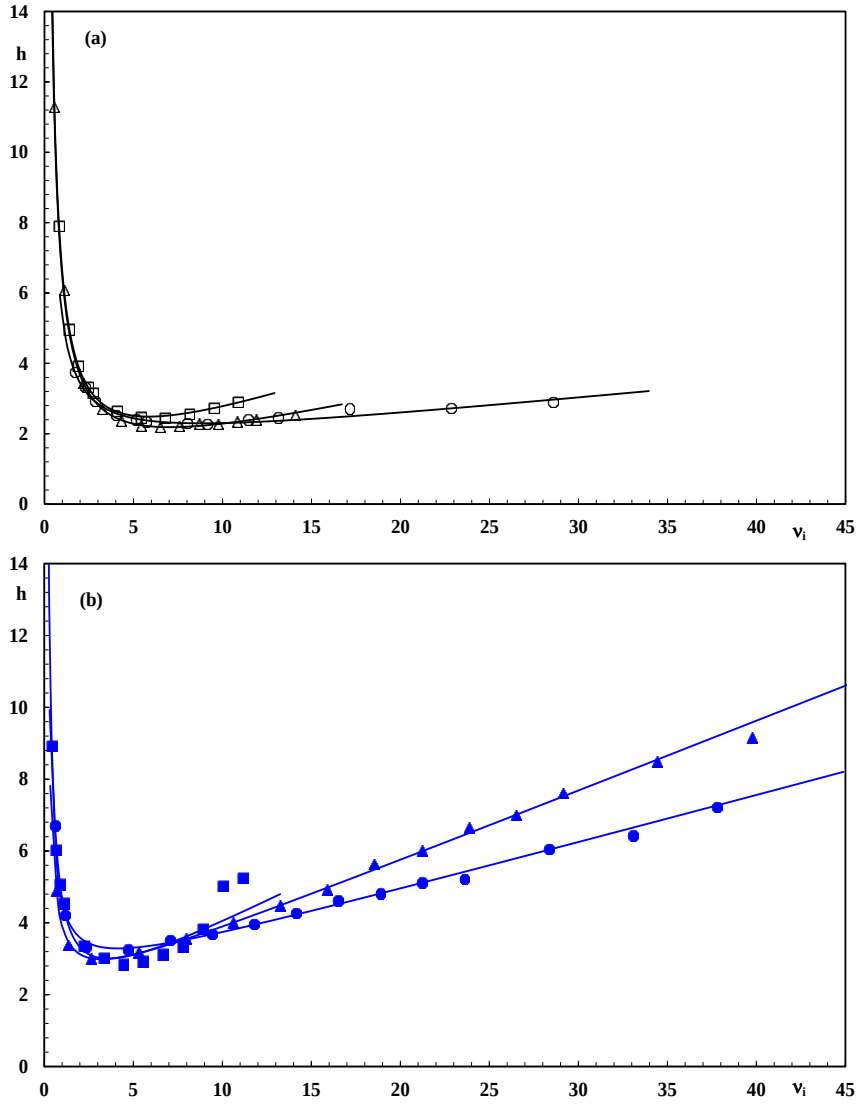


**Figure 3.4:** Reduced van Deemter plots of h versus $\nu_i$ for (a) adenosine (k" = 10.6 ± 0.6) on reversed phase columns and (b) guanine on HILIC columns (k" = 10.3 ± 0.8), same columns and symbols as in Fig. 3.3.

Comparing the reduced plate heights for the HILIC and RP columns overall, the RPLC columns, however, clearly perform better than the HILIC columns (average $h_{min}$= 2.2 for the RP columns versus average $h_{min}$= 3.0 for the HILIC columns) indicating a better overall packing quality. To obtain a complete picture of the column performance, information on column permeability was subsequently also taken into account.

### 3.3.4. Kinetic plot evaluation of the HILIC and RP columns

#### 3.3.4.1. Reduced kinetic plots

To assess the packing quality of the different column supports evaluated in this study in a more comprehensive way, reduced kinetic plots of $u_i$-based impedance number $E_i$ versus $N_{opt}/N$ were constructed for all stationary phases [19-20]. Both measures can be calculated without having to define a characteristic length or diameter, as can be seen in the following equations:

$$E_i = \frac{H^2}{K_{vi}} = h^2 \phi \tag{3.14}$$

$$\frac{N_{opt}}{N} = \frac{u_i H}{u_{i,opt} H_{min}} = \frac{\nu_i h}{v_{i,opt} h_{min}} \tag{3.15}$$

$E_i$ and $N_{opt}/N$ are only dependent on the dimensionless variables $h$ (the reduced plate height), $\nu_i$ (the reduced interstitial mobile phase velocity) and $\phi$ (the flow resistance) and can be calculated without having to specify the actual size of the particles. The reduced form of a kinetic plot yields the same type of information as the reduced form of a van Deemter plot: columns with different particle sizes, packed with the same packing quality, with the same intra-particle diffusion characteristics and the same retention factors, will yield coinciding curves. The lower this curve, the better packed the column is. The reduced kinetic plot, however, has a second important advantage over the reduced van Deemter plot in that it also incorporates information on the flow resistance [29-30]. To compare the packing quality of the supports discussed in Figs. 3.3 and 3.4, plots of $E_i$ versus $N_{opt}/N$ were constructed using Eqs.(3.14) and (3.15), and are shown in Fig. 3.5. Considering the obtained plots of $E_i$ versus $N_{opt}/N$ in Fig. 3.5, it can be deduced that especially the Waters Xbridge 3.5 µm and Waters Acquity sub-2 µm RPLC columns have a very similar reduced kinetic performance ($E_{i,min}$~ 2200) and hence very similar packing structures, while the ACE $C_{18}$ 3.0 µm column has a considerably lower $E_{i,min}$- value of 1900, which could be attributed to its lower minimum plate height ($h_{min}$= 2.0).

As was already evident from the (reduced) van Deemter curves in Figs. 3.3-3.4 and the external porosity values in Table 3.6, the reduced kinetic plots of the HILIC columns suggest a less good packing quality, approaching rather a value of $E_{i,min}$~ 2500-2700.

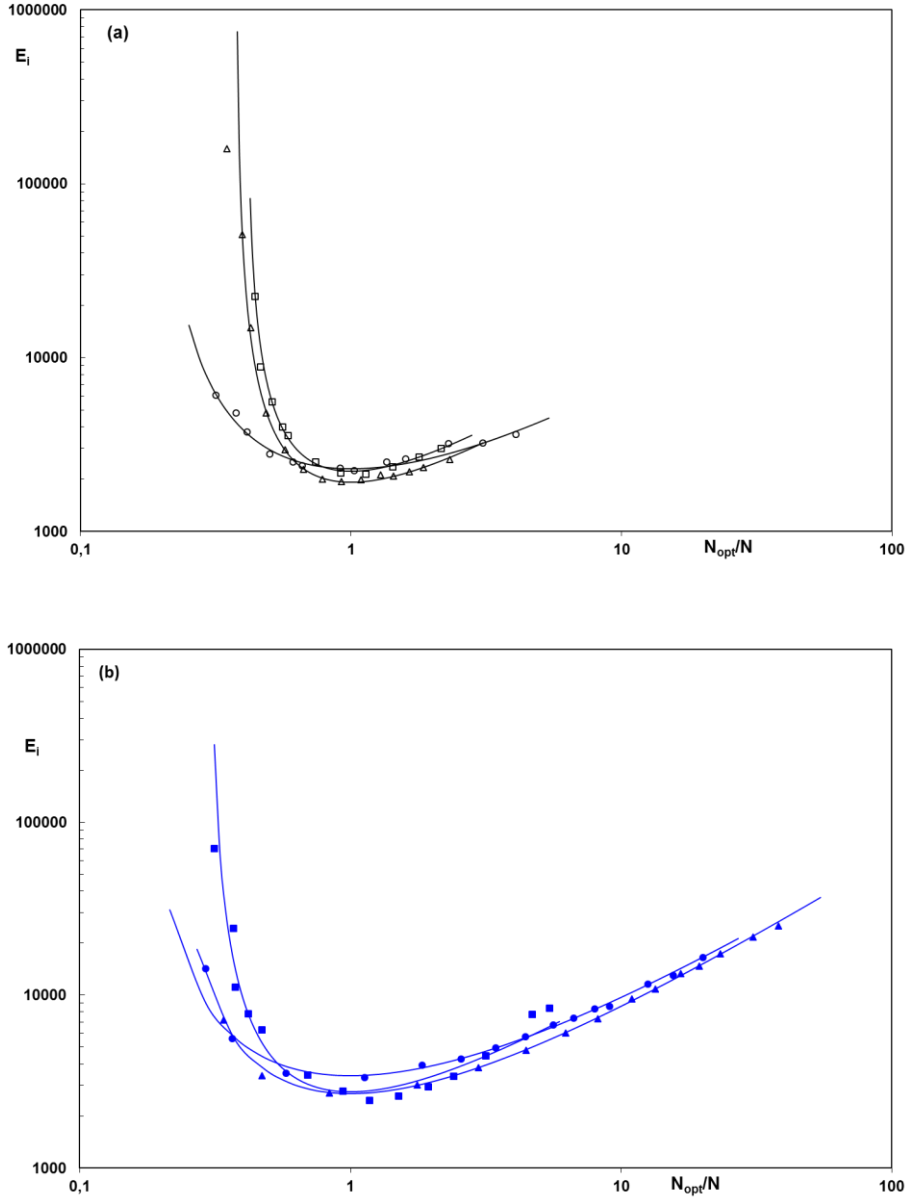


**Figure 3.5:** Reduced kinetic curves of $E_i$ versus $N_{opt}/N$ for (a) adenosine (k" = 10.6 ± 0.6) on reversed phase columns and (b) guanine on HILIC columns (k" = 10.3 ± 0.8), same columns and same symbols as in Fig. 3.3.

### 3.3.4.2. Kinetic plots of interstitial time ($t_i$) versus plate count

To assess the intrinsic gain obtained by switching from a conventional HPLC column operated at 400 bar to a sub-2 µm packed column operated at 1000 bar, kinetic plots of interstitial time ($t_i$= L/$u_i$) versus column plate count (N) were subsequently constructed for all columns at their respective maximum operating pressures (Fig. 3.6).

For the construction of these plots, values of $K_{vi}$ and $t_i$ were again deduced from the interstitial velocity $u_i$ to avoid any misinterpretation that might arise from an erroneous assessment of the column dead volume. For the interpretation of the plots, columns with the same packing quality should mainly be considered (as determined from the reduced kinetic plots in Fig. 3.5) as they show the pure performance increase that will result from the use of smaller particles at higher pressures.

As can be deduced from Fig. 3.6, the sub-2 µm columns clearly perform better than the conventional columns for both RPLC and HILIC columns in the entire practically relevant range of plate counts ($N \leq 150{,}000$), achieving separations faster than 3.0-3.5 µm columns at any given efficiency in this range. Whereas the superior efficiency of the sub-2 µm columns was already assessed from Fig. 3.3, Fig. 3.6 now directly shows the gain in analysis time that can be obtained when switching from a 3.0-3.5 µm column to a sub-2 µm column to obtain the same plate count (N). For reversed phase columns, a gain in analysis time of some 2.4 times can be obtained in the practically relevant range of 20,000 to 100,000 plates (see arrows added to Fig. 3.6a as examples for the gain in analysis time that can be obtained at N= 40,000 and N= 80,000), while this range is larger for the HILIC columns (similar arrows added to Fig. 3.6b, where a gain of a factor 3.2 is obtained).

On the other hand, the range of plate counts wherein the HILIC sub-2 µm perform better than their conventional counterparts is clearly larger than for the RP columns: a significant gain in analysis time is obtained for plate counts up to 250,000 plates, whereas this range is limited to maximum 160,000 plates for RPLC columns. This can be attributed to the lower viscosity of the mobile phase typically used for HILIC analyses, which allows to operate longer columns at higher mobile phase velocities at the maximum pressure and therefore allows exploiting the B-term region of the kinetic plots (upper right part of the plots in Fig. 3.6) where high efficiencies can be attained to a larger extent. It must also be remarked that the HILIC columns in general seem to perform equally well as their RPLC counterparts, despite their lower packing quality (as shown in Fig. 3.5) and their higher intrinsic $\varepsilon_e$-values. The main difference between the reduced kinetic plots in Fig. 3.5 and their “absolute” form in Fig. 3.6 is that the latter takes the applied pressures and viscosity of the mobile phases into account. As is evident from Fig. 3.6, the lower viscosity of the HILIC mobile phases is able to compensate the less advantageous packing quality of these columns quite well, resulting in performances that are comparable to those of their RP counterparts.

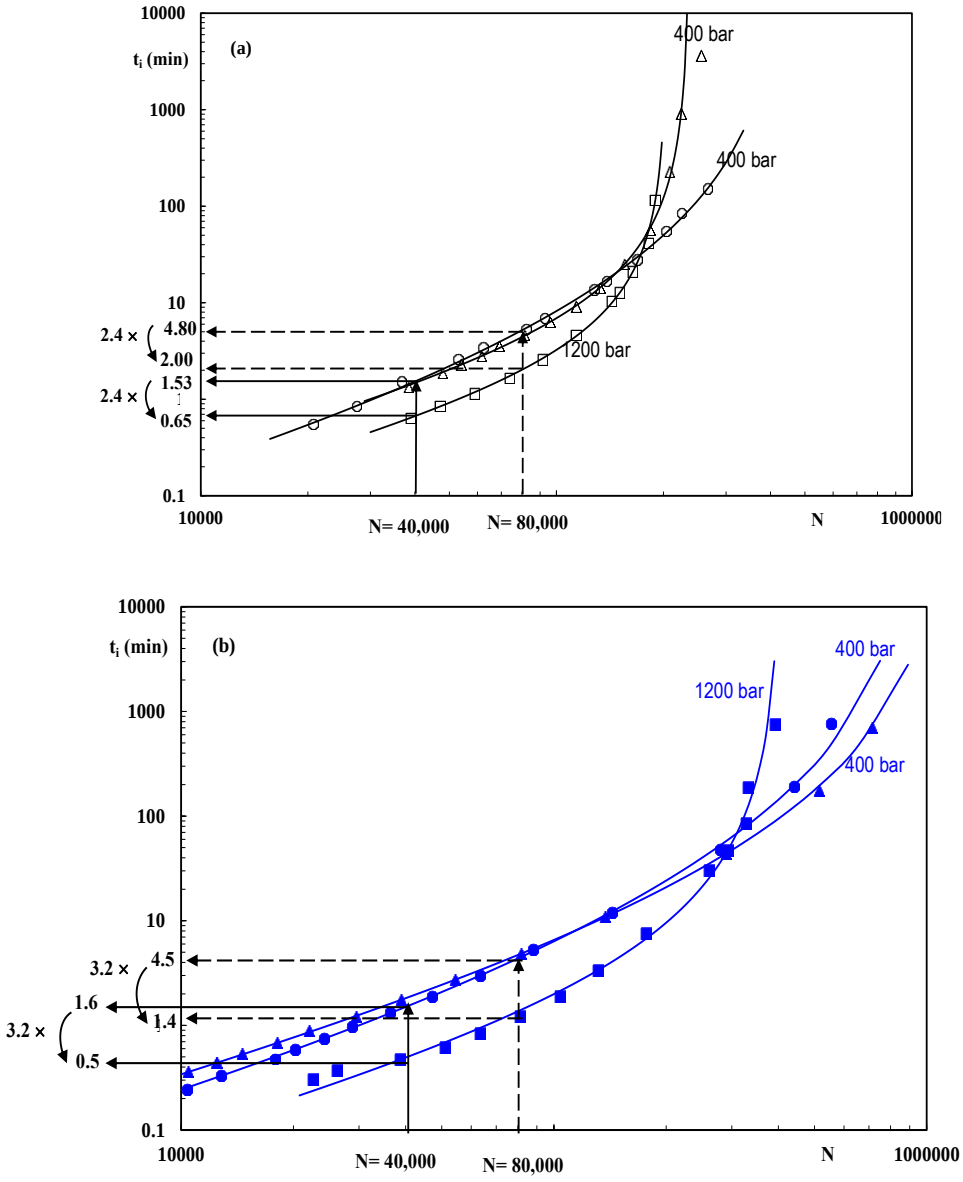


**Figure 3.6:** Kinetic curves of $t_i$ versus N for (a) adenosine (k" = 10.6 ± 0.6) on reversed phase columns and (b) guanine on HILIC columns (k" = 10.3 ± 0.8), same columns and same symbols as in Fig. 3.3. The maximum operating pressures of the columns are shown. The arrows indicate the $t_i$-times corresponding with a plate count of 40,000 and 80,000.

### 3.3.5. Comparison of HILIC and RPLC columns for tetracycline analysis

To allow for a more practical evaluation of the difference column types and stationary phases, and to verify the observations made from the kinetic plots in Section 3.3.4.2, a more complex and pharmaceutically relevant sample consisting of TC and its main impurities ETC, ATC and EATC was applied to both RPLC and HILIC stationary phases in conventional and sub-2 µm columns. Only columns from the same vendor were considered to assure that columns with similar packing qualities would be compared.

All columns were operated at the maximum instrument pressure (~400 bar for the 3.0-3.5 µm columns and ~1000 bar for the sub-2 µm columns). Although the selectivities obtained on both stationary phase types are completely different (compare Fig. 3.7 and 3.8), the set criteria of baseline separation for all compounds ($R_s \geq 1.5$) and sufficiently large elution windows ($k'_{last}$~4.5) were met under all conditions.

Comparing the analysis times on the HILIC columns, a decrease in analysis time of some 2.1 times is obtained when switching from conventional HPLC to UHPLC conditions (Fig. 3.7). A similar, though slightly smaller decrease in analysis time is observed for the tetracycline analysis using RPLC columns when switching from HPLC to UHPLC: the gain in analysis time in this case amounts up to some 1.8 times (Fig. 3.8). These practical chromatograms, although crude in their comparison method, seem to confirm the observations that were made from the kinetic plots in section 3.3.4.2: slightly larger gains in analysis time can be expected when switching from HPLC to UHPLC conditions for HILIC compared to RPLC stationary phases, when column formats with similar packing qualities are being compared.

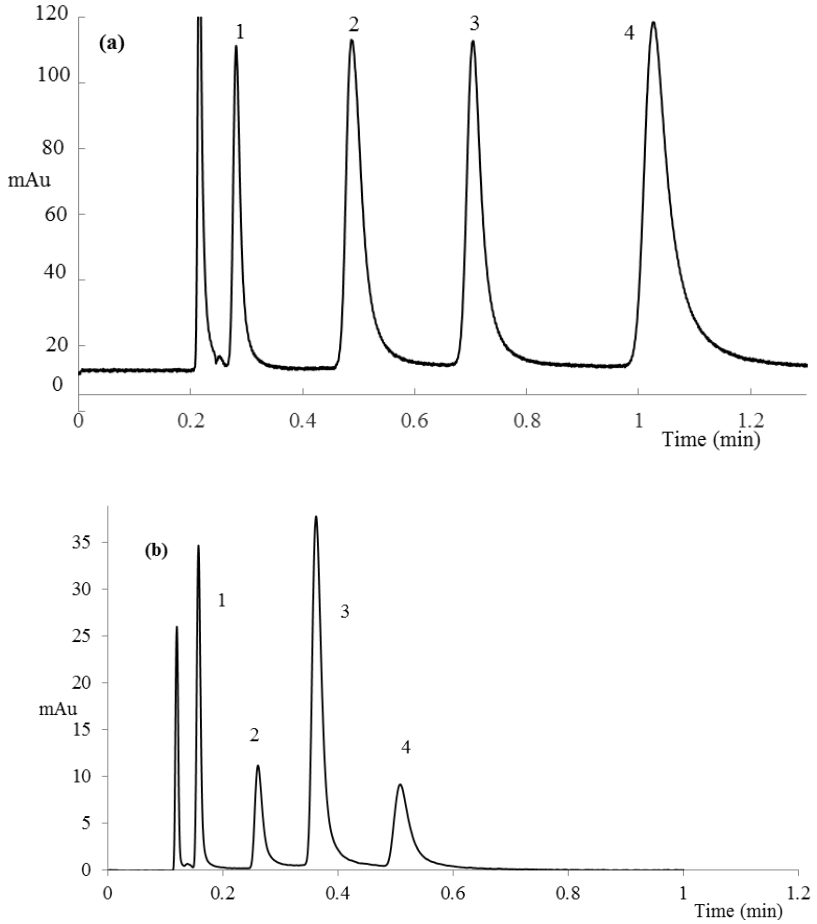


**Figure 3.7:** Chromatograms obtained for tetracycline and its main impurities at the maximum column pressure on (a) XBridge HILIC 3.5 µm 2.1 × 150 mm (400 bar) and (b) Acquity HILIC BEH 1.7 µm 2.1 × 100 mm (1000 bar). Peak identification: 1: ATC, 2: TC, 3: EATC, 4: ETC

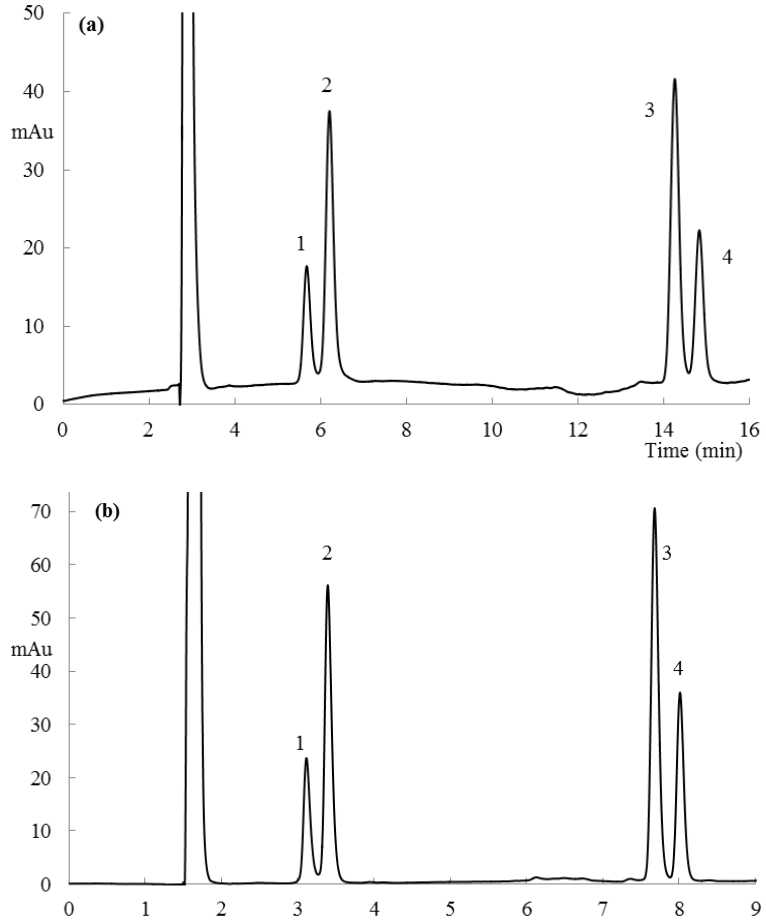


**Figure 3.8:** Chromatograms obtained for tetracycline and its main impurities at the maximum column pressure on (a) XBridge C18 3.5 µm 2.1 × 150 mm (400 bar) and (b) Acquity C18 BEH 1.7 µm 2.1 × 100 mm (1000 bar). Gradient conditions see Table 3.4. Peak identification: 1: ETC, 2: TC, 3: EATC, 4: ATC

## 3.4. Conclusions

A column performance comparison, wherein the gain in performance that can be obtained by switching from HPLC column formats to UHPLC columns is assessed, is made for HILIC columns on the one hand, and RPLC columns on the other hand.

It is demonstrated that $u_0$-based column permeabilities ($K_{v0}$) can be severely underestimated for reversed-phase columns when highly retentive mobile phases are used, as this can lead to a clear overestimation of the $t_0$-based void volume of the column. For HILIC columns, $K_{v0}$-values seem to be rather overestimated in highly retentive mobile phases due to the exclusion of the apolar $t_0$-marker from part of the mesopore volume, resulting in an underestimation of the $t_0$-based void volume. To avoid any errors that might arise from an inaccurate assessment of the column dead volume, all plate height and kinetic plot data are therefore expressed as a function of the interstitial velocity $u_i$ in this study.

Column permeabilities are first calculated based on the superficial velocity $u_s$ and are shown to be slightly larger for HILIC columns than for their RPLC counterparts, mainly due to their larger external porosity.

Van Deemter measurements reveal a slightly worse efficiency for the HILIC columns, at least for the columns and sample evaluated in this study. The systematically larger permeability values observed for the HILIC columns cannot compensate for these low efficiencies in reduced kinetic plots of $E_i$ versus $N_{opt}/N$, suggesting a lower packing quality for the HILIC columns. Despite this lower packing quality, the absolute kinetic performance of the 3.5 µm and sub-2µm HILIC and RPLC columns evaluated here is quite comparable, which can largely be attributed to the lower viscosity of the mobile phases typically employed for HILIC columns. The reduction in analysis time that can be obtained by switching from HPLC to UHPLC conditions is also quite similar for both stationary phase types. These theoretical findings are finally also demonstrated for the practical separation of tetracycline and its main impurities.

### 3.5. References

[1] MacNair, J. E.; Lewis, K. C.; Jorgenson, J. W., Anal. Chem. 1997, 69, 983-989.

[2] Lippert, J. A.; Xin, B.; Wu, N.; Lee, M. L., J. Microcol. Sep.1999, 11, 631-643.

[3] Wu, N.; Lippert, J. A.; Lee, M. L., J. Chromatogr. A 2001, 911, 1-12.

[4] Cabooter, D.; Billen, J.; Terryn, H.; Lynen, F.; Sandra, P.; Desmet, G., J. Chromatogr. A 2008, 1204, 1-10.

[5] Heaton, J.; Gray, N.; Cowan, D. A.; Plumb, R. S.; Legido-Quigley, C.; Smith, N. W., J. Chromatogr. A 2012, 1228, 329-337.

[6] Gray, N.; Heaton, J.; Musenga, A.; Cowan, D. A.; Plumb, R. S.; Smith, N. W., J. Chromatogr. A 2013, 1289, 37-46.

[7] Simon, R.; Enjalbert, Q.; Biarc, J.; Lemoine, J.; Salvador, A., J. Chromatogr. A 2012, 1264, 31-39.

[8] Gritti, F.; Guiochon, G., J. Chromatogr. A 2013, 1297, 85-95.

[9] Heaton, J. C.; Wang, X.; Barber, W. E.; Buckenmaier, S. M.; McCalley, D. V., J. Chromatogr. A 2014, 1328, 7-15.

[10] Oka, H.; Ito, Y.; Matsumoto, H., J. Chromatogr. A 2000, 882, 109-133.

[11] Sarmah, A. K.; Meyer, M. T.; Boxall, A. B. A., Chemosphere 2006, 65, 725-759.

[12] Diana, J.; Vandenbosch, L.; De Spiegeleer, B.; Hoogmartens, J.; Adams, E., J. Pharm. Biomed. Anal. 2005, 39, 523-530.

[13] Li, R.; Zhang, Y.; Lee, C. C.; Liu, L.; Huang, Y., J. Sep. Sci. 2011, 34, 1508-1516.

[14] Li, R.; Yuan, Q.; Zhang, Y.; Ling, J.; Han, T., J. Liq. Chromatogr. Relat. Technol. 2011, 34, 511-520.

[15] Valette, J. C.; Demesmay, C.; Rocca, L. J.; Verdon, E., Chromatographia 2004, 59, 55-60.

[16] Gritti, F.; Guiochon, G., J. Chromatogr. A 2013, 1280, 35-50.

[17] Li, J.; Carr, P. W., Anal. Chem. 1997, 69, 2530-2536.

[18] McCalley, D. V., J. Chromatogr. A 2010, 1217, 4561-4567.

[19] Desmet, G.; Clicq, D.; Gzil, P., Anal. Chem. 2005, 77, 4058-4070.

[20] Billen, J.; Guillarme, D.; Rudaz, S.; Veuthey, J. L.; Ritchie, H.; Grady, B.; Desmet, G., J. Chromatogr. A 2007, 1161, 224-233.

[21] Matthew Przybyciel, R. E. M., LC-GC Europe 15(2002)1-5.

[22] McCormick, R. M.; Karger, B. L., Anal. Chem. 1980, 52, 2249-2257.

[23] Knox, J. H.; Kaliszan, R., J. Chromatogr. A 1985, 349, 211-234.

[24] Rimmer, C. A.; Simmons, C. R.; Dorsey, J. G., J. Chromatogr. A 2002, 965, 219-232.

[25] McCalley, D. V.; Neue, U. D., J. Chromatogr. A 2008, 1192, 225-229.

[26] Knox, J. H.; Scott, H. P., J. Chromatogr. A 1983, 282, 297-313.

[27] Desmet, G.; Broeckhoven, K., Anal. Chem. 2008, 80, 8076-8088.

[28] Horvath, C.; Lin, H.-J., J. Chromatogr. A 1976, 126, 401-420.

[29] Neue, U. D., HPLC Columns, Theory, Technology and Practice. Wilet-VCH: New York 1997.

[30] Bristow, P. A.; Knox, J. H., Chromatographia 1977, 10, 279-289.

# Chapter 4

# Evaluation of the Kinetic Performance Differences between Hydrophilic-Interaction Liquid Chromatography and Reversed-Phase Liquid Chromatography under Conditions of Identical Packing Structure

This chapter has been published in:

- **Huiying Song,** Gert Desmet, Deirdre Cabooter, Evaluation of the kinetic performance differences between hydrophilic-interaction liquid chromatography and reversed-phase liquid chromatography under conditions of identical packing structure, *Analytical Chemistry*, 87 (2015) 12331-12339.

**Abstract**

A protocol using trifluoroacetic acid at a temperature of 60°C is developed for the adequate removal of the stationary phase of reversed-phase liquid chromatography (RPLC) columns. This procedure allows for studying the same column first under RPLC and subsequently under hydrophilic interaction chromatography (HILIC) conditions to isolate intrinsic differences between mass transfer properties in HILIC and RPLC from differences in packing quality. The established procedure allows for a complete removal of the stationary phase (confirmed by retention studies and thermogravimetry analyses) while leaving the structure of the packing unaffected (witnessed by an unchanged external porosity and pressure drop). Accurate plate height analysis comparing compounds at the same zone retention factor indicates a significant difference in reduced c-term (typically 40-80% larger under HILIC conditions), despite the columns otherwise being identical. Correcting for the known contributions of longitudinal diffusion (*b*-term) and particle mass transfer ($c_m$- and $c_s$-term) to focus on band broadening originating from eddy dispersion, similar strong differences are observed (differences of some h=0.3 up to 1.2). These findings show that the interior structure and the retention mechanism of the particles have a very strong effect on the observed eddy diffusion, a factor typically ascribed to phenomena occurring outside the particles. This also implies that comparing the quality of packings of different particle types is virtually impossible without the availability of a sound model to correct for the intra-particle effect on the observed eddy dispersion.

**Keywords:** HILIC; RPLC; Stationary phase removal; Kinetic performance; Identical packing conditions

## 4.1. Introduction

Despite the increasing interest in HILIC, only a few studies comparing the kinetic performance of HILIC and RPLC have been performed. Band broadening in packed particle columns is usually described by the general plate height model [1-6]:

$$h = h_{inhom} + \frac{2}{\nu_i}\frac{D_{eff}}{D_m}(1 + k") + \frac{2}{\alpha}\frac{k"^2}{(1+k")^2}\frac{\varepsilon_e}{1-\varepsilon_e}\frac{\nu_i}{Sh_m} + \frac{2}{\alpha}\frac{k"}{(1+k")^2}\frac{\nu_i}{Sh_{part}\frac{D_{part}}{D_m}} \qquad (4.1)$$

Wherein h is the reduced plate height, $\nu_i$ the reduced velocity, $D_{eff}$, $D_{part}$ and $D_m$ are the effective, intra-particle and bulk molecular diffusion coefficients, respectively, k" is the zone retention factor, $\varepsilon_e$ is the external porosity, $\alpha$ is a geometrical constant and $Sh_m$ and $Sh_{part}$ are the Sherwood numbers relating to the mobile and the intra-particle zones, respectively. The expressions for the b–, $c_m$– and $c_s$–terms (the second, third and fourth term in Eq. (4.1), respectively), representing the effective longitudinal diffusion contribution and the resistance to mass transfer in the mobile and stationary zones, are generally accepted [7-10]. The first term ($h_{inhom}$) relates to band broadening originating from flow heterogeneities in the bed, traditionally referred to as eddy diffusion. This term includes contributions from trans-channel, short-range inter-channel and trans-column eddy dispersion [11].

Although some studies indicate the optimum column efficiencies in HILIC and RPLC to be comparable, it has been demonstrated that the individual mass transfer phenomena leading to these column efficiencies are inherently different in HILIC and RPLC [12-14]. In HILIC, lower b-terms and higher $c_s$-terms are typically observed in comparison with RPLC. These have been attributed to differences in intra-particle diffusion, and more specifically surface diffusion. Because the radial mass transfer between neighboring regions (short-range as well as long-range) in the column occurs partly through the particles, these differences in intra-particle diffusion can also alter eddy dispersion and mass transfer resistance across the particles. The extent to which this can occur, however, is not well known, due to the lack of our theoretical knowledge. In addition, some interesting experimental observations have recently been published including the observation that the trans-column eddy-dispersion term in HILIC does not tend to zero for low reduced velocities [12].

Moreover, it was reported that mass transfer resistance across HILIC particles increases with increasing retention factor [13]. Because the dominant factor in the $c_s$-term is proportional to $k''/(1+ k'')^2$, this suggests a decrease of the intra-particle mass transfer resistance ($D_{part}/D_m$ indeed decreases with increasing k", but typically this effect is not as strong as the decrease of the $k''/(1+ k'')^2$ factor).

A drawback of the earlier-cited studies comparing mass transfer phenomena in HILIC and RPLC is that they have been performed on different columns, which is nearly inevitable. Even when obtaining these columns from the same manufacturer using the same native silica, differences in packing quality can never be excluded (considering that many manufacturers pack their HILIC and RPLC columns in different ways). In fact, in Chapter 3 it was observed that HILIC columns made of the same silica material as their RPLC counterparts had significantly higher external porosities, pointing at important differences in packing structure [15]. Such differences can of course bias any observed difference in fundamental mass transfer properties between HILIC and RPLC.

The goal of this study, therefore, was to make an evaluation of column performance under HILIC and RPLC conditions for columns with identical packing structures. This was done by first measuring the full kinetic performance of C18-coated silica particle columns under RPLC conditions. Subsequently, the stationary phase coating of the RPLC columns was removed to obtain a bare silica column with identical packing characteristics. Finally, the kinetic performance of these columns was reassessed, but now under HILIC conditions. An accurate assessment of the effective and intra-particle diffusion under RPLC and HILIC conditions was made via peak parking experiments. Subsequently, the b-, $c_m$, and $c_s$-term contributions to band broadening were subtracted from the experimental plate heights to directly compare the remaining band-broadening sources (related to eddy dispersion). These are commonly attributed to the packing structure, which, using the approach adopted in the present study, is identical under both HILIC and RPLC conditions.

## 4.2. Experimental section

### 4.2.1. Chemicals and Columns

Ammonium acetate, thymidine, trifluoroacetic acid (TFA) and thiourea were obtained from Sigma-Aldrich (Steinheim, Germany); cytosine, guanosine, adenosine and from Janssen chimica (Geel, Belgium), the structures and log P values of these compounds are shown in Fig. 4.1. Milli-Q water was prepared in the lab using a Milli-Q gradient water purification system from Millipore (Bedford, MA, USA). HPLC-grade acetonitrile (ACN) and dichloromethane (analytical grade) were from Fisher Chemicals (Erembodegem, Belgium). HPLC grade tetrahydrofuran (THF) was from VWR (Leuven, Belgium). Glacial acetic acid was obtained from Merck (Darmstadt, Germany) and acenaphthene from Merck (Hohenbrunn, Germany). Polystyrene standards with MW ranging between 500 and 2.000.000 Da for ISEC experiments were from Sigma–Aldrich (Bornem, Belgium).

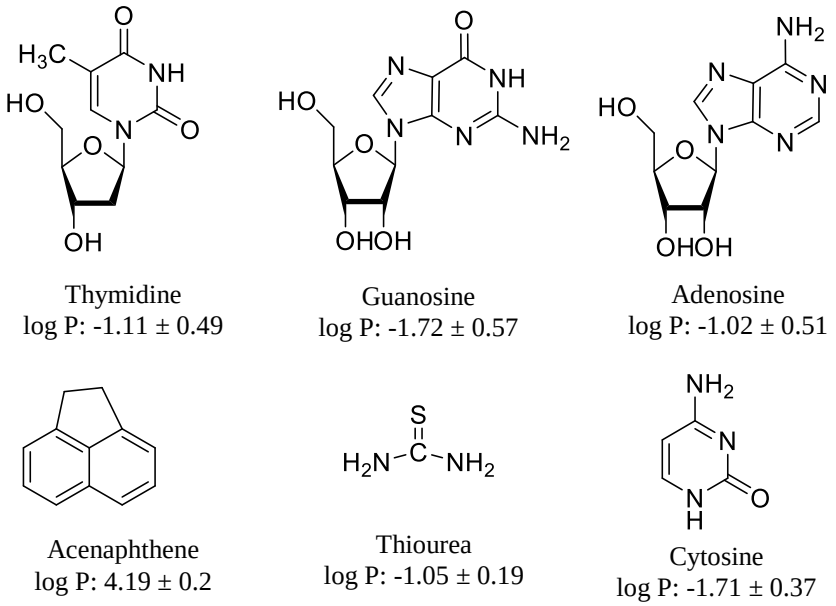


Figure 4.1: Chemical structures and log P values for the six compounds used for the evaluation of the kinetic performance under HILIC and RPLC conditions. (log P values were predicted by ACD/ChemSketch 2015.2.5)

ZORBAX Eclipse Plus C18 (4.6 × 50 mm) columns with particle sizes of 5 µm (column 1 and column 2) and 1.8 µm (column 3 and column 4) were purchased from Agilent Technologies (Diegem, Belgium). The 1.8 µm particle columns were used for the initial development of the stripping protocol (including thermogravimetric analyses). The 5 µm particle columns were used to assess band broadening phenomena, because these columns are less prone to extra-column band broadening and viscous heating effects.

### 4.2.2. Apparatus

All band broadening and column pressure measurements were performed on an ultra-high performance liquid chromatograph (UHPLC) Agilent 1290 system (Agilent Technologies, Waldbronn, Geremany) with a pressure limit of 1200 bar. The instrument was equipped with a quaternary pump, an autosampler and a diode array detector (DAD) with a flow cell of 1 µL. Absorbances were measured at 254 nm. Viper tubing (75 µm × 550 mm, Thermo Scientific, Germering, Germany) was used between the injector and the inlet of the column. Between the outlet of the column and the detector, viper tubing with the following dimensions with the following dimensions was used: 75 µm × 125 mm. The overall system volume was 9 µL. Data acquisition and instrument control were performed by Chemstation software (Agilent Technologies). Column stripping and peak parking experiments were performed on an Ultimate 3000 HPLC system (Thermo Scientific) equipped with a high pressure pump (LPG-3400A), autosampler (WPS-3000SL) and UV/VIS variable wavelength detector (VWD-3400) with a flow cell of 11 µL. Absorbances were measured at 254 nm. Viper tubing used to connect the column to the system were the same as the Agilent 1290 system. The overall system volume was 20 µL. Data acquisition and instrument control were performed by Chromeleon software (Thermo Scientific).

Molecular diffusion coefficient ($D_m$) measurements and inverse size exclusion chromatography (ISEC) experiments were carried out on a Perkin Elmer 275 UHPLC system (Perkin Elmer, Massachusetts, USA) equipped with a binary high pressure pump (maximum operating pressure: 690 bar), an autosampler, and a variable wavelength detector with a flow cell of 2.6 µL. The detection wavelength was set at 254 nm. A stainless steel viper (125 µm I.D.) was used between the injector and the inlet of the column. Between the outlet of the column and the detector, PEEK tubing with an internal diameter of 125 µm was used. The overall system volume was 15 µL. Chromera software (Perkin Elmer) was used for system operation and data analysis.

### 4.2.3. Methodology

#### 4.2.3.1. Sample preparation

Stock solutions of thymine, adenosine, uracil, cytosine and thymidine were prepared in a concentration of 1000 ppm in $H_2O$. Guanosine was dissolved in a concentration of 10000 ppm in DMSO. Thiourea and acenaphthene were dissolved in a concentration of 1000 ppm in $H_2O$

and ACN, respectively. Fresh test samples were prepared daily by mixing and diluting stock solutions in the mobile phase. Final concentrations of the compounds in the test samples are shown in Table 4.1.

#### 4.2.3.2. Stationary phase stripping

The procedure to strip the stationary phase of the reversed-phase columns, was based on a protocol developed to study column stability under low-pH conditions [16]. First the column was equilibrated with 50:50 ACN/$H_2O$ (v/v) for 1 hour at a flow rate of 0.5 mL/min and a temperature of 30°C. This was followed by three injections of acenaphthene (20 ppm), to assess the initial elution volume of acenaphthene. Subsequently, the column was flushed with 3% TFA in ACN for 60 min at a flow rate of 0.5 mL/min and a temperature of 60°C to fully wet the column bed. Then the column was exposed to 3% TFA in $H_2O$ (pH=0.9) for 120 min at a flow rate of 0.5 mL/min and a temperature of 60°C to hydrolyze the siloxane bond connecting the octadecyl functional groups to the silica surface [17]. Finally, the column was flushed again with 3% TFA in ACN for 60 min at a flow rate of 0.5 mL/min and a temperature of 60°C, to desorb any residual hydrolyzed phase that was not removed in the previous step and to ensure the phase was fully solvated for the next exposure cycle. After each stripping cycle, the retention volume of acenaphthene was monitored in 50:50 ACN/$H_2O$ (v/v) at a flow rate of 0.5 mL/min and a temperature of 30°C. The stripping sequence was repeated until the retention volume of acenaphthene reached a constant value.

#### 4.2.3.3. Thermogravimetry experiments

The stationary phase material of stripped and unstripped Zorbax Eclipse C18 columns with a particle size of 1.8 µm (columns 3 and 4) was removed by opening the columns and flushing them with a mixture of water/isopropanol (50:50 v/v). The stationary phase material was subsequently dried under vacuum to remove excess solvent. Thermogravimetry experiments were performed on a TGA Q500 system (TA Instruments, New Castle, DE, USA) and data were acquired and interpreted using Q series Advantage software (TA Instruments). Approximately 5 mg of stationary phase was placed on a pretarred platinum sample pan and the weight recorded. The sample was heated from room temperature to 600°C using a linear gradient at a rate of 5°C/min. The temperature was then maintained at 600°C until a stable weight was observed (typically after 150 min). Throughout the experiments air was used as the purge gas, and the weight of the sample was continuously recorded.

**Table 4.1:** Column dimensions and chromatographic conditions used to evaluate the performance of the columns before and after stripping.

| Col. | Stationary Phase | Dimensions | Before Stripping/RPLC | | | | | After Stripping/HILIC | | | | |
|---|---|---|---|---|---|---|---|---|---|---|---|---|
| | | | ACN/$NH_4A$ c(v/v, %/%) | buffer conc. (mM) | compounds (conc. ppm) | k″ | $D_m$ ($\times 10^{-9}$ m²/s) | ACN/$NH_4A$ c(v/v, %/%) | buffer conc. (mM) | compounds (conc. ppm) | k″ | $D_m$ ($\times 10^{-9}$ m²/s) |
| 1 | ZORBAX Eclipse Plus C18 | 4.6×50mm 5 µm | 2.5/97.5 | 9.95 | guanosine 40 | 5.5 | 0.59 | 92.5/7.5 | 10.27 | adenosine 50 | 5.6 | 1.29 |
| | | | | | thymidine 170 | 9.5 | 0.61 | 92.2/7.8 | 10.45 | cytosine 120 | 9.8 | 1.62 |
| | | | | | adenosine 85 | 16.5 | 0.60 | 92.5/7.5 | 10.27 | guanosine 120 | 16.5 | 1.19 |
| 2 | ZORBAX Eclipse Plus C18 | 4.6×50mm 5µm | 2.5/97.5 | 9.95 | guanosine 40 | 5.3 | 0.59 | 92.5/7.5 | 10.27 | adenosine 50 | 5.4 | 1.29 |
| | | | | | thymidine 170 | 9.3 | 0.61 | 92.2/7.8 | 10.45 | cytosine 120 | 9.5 | 1.62 |
| | | | | | adenosine 85 | 15.9 | 0.60 | 92.5/7.5 | 10.27 | guanosine 120 | 15.4 | 1.19 |

#### 4.2.3.4. Plate height measurements

For the theoretical evaluation of the column performance before and after stripping, all experiments were performed in isocratic mode using a mobile phase consisting of ACN and 10 mM ammonium acetate buffer (pH 6.0). The composition of the mobile phase (Table 4.1) was adapted in such a way that similar zone retention factors k" were obtained at the optimum velocities for the test compounds under HILIC and RPLC conditions [15]. The zone retention factor k" is defined as:

$$k'' = \frac{t_R \cdot u_i}{L} - 1 \tag{4.2}$$

$$u_i = \frac{F}{\varepsilon_e \pi r^2} \tag{4.3}$$

Where $u_i$ is the interstitial velocity, r is the column radius, L is the column length, $t_R$ is the analyte retention time and $F$ is the flow rate. Chromatograms were recorded for at least 20 different velocities on every considered column to construct plate height curves. All elution times ($t_R$) and peak variances ($\sigma^2$) were determined from the first and the second central moments, respectively, and corrected for the system contribution [18].

#### 4.2.3.5. Column porosity measurements

External porosity values ($\varepsilon_e$) of the unstripped and stripped columns were measured experimentally by ISEC using a set of twelve polystyrene standards as described in [15]. The flow rate was set at 0.4 mL/min. Injection volumes were 1 µL and the detection wavelength was 254 nm. External porosity values of the unstripped columns were additionally verified via total pore blocking experiments as described in [19-20,36-37]. Total porosity values ($\varepsilon_T$) were assessed by pycnometry measurements using THF and dichloromethane to sequentially fill the columns before weighing [21-22].

#### 4.2.3.6. Column pressure measurements

Column pressures were measured on each column before and after stripping for three different mobile phases (50:50 ACN/$H_2O$ (v/v), 5:95 ACN/$H_2O$ (v/v) and 95:5 ACN/$H_2O$ (v/v)) at flow rates of 0.5 mL/min and 0.75 mL/min. The viscosities of the different mobile phases ($\eta$) were calculated according to Guillarme et al. [18].

#### 4.2.3.7. Peak parking experiments

Reduced b-term coefficients were measured using the arrested elution method [23-24]. The analyte of interest was injected onto the column at a flow rate of 0.5 mL/min and arrested for a specific parking time ($t_{park}$= 1 min, 15 min, 30 min, 45 min, 60 min or 90 min). Afterwards, the flow was resumed and the analyte peak was eluted towards the detector. By plotting the obtained peak variances $\sigma^2_x$ against the applied parking time $t_{park}$, a plot with a straight line was obtained. The effective diffusion coefficient ($D_{eff}$) was subsequently calculated from the slope of this line [23, 25-26]:

$$\sigma_x^2 = 2 \cdot D_{eff} \cdot t_{park} \tag{4.4}$$

Bulk diffusion coefficients ($D_m$) were measured at 22.5°C using the open tubular Taylor-Aris method [27], which will extensively be discussed in Chapter 5. From the experimentally determined values of $D_{eff}$ and $D_m$, the reduced b-term coefficient was calculated as follows [23]:

$$b = 2\frac{D_{eff}}{D_m}(1 + k'') \tag{4.5}$$

### 4.3. Results and Discussion

#### 4.3.1. Stationary phase stripping

Fig. 4.2 shows the retention times of acenaphthene in 50:50 ACN/$H_2O$ (v/v) after each stripping cycle. A clear decrease in retention time is observed from an initial value of 16.12 min, to a constant value of 1.02 min (± 0.5%) after a total stripping time of some 270 hours, entailing 135 stripping cycles. The dashed line and open symbols show the retention times obtained for uracil under the same experimental conditions. The constant and similar values of the elution times for uracil and acenaphthene at the end of the stripping procedure indicate a complete lack of retention for both molecules and hence point at the complete removal of the stationary phase. Note that the retention time of uracil at time-point zero, before any stripping of the stationary phase has occurred, is slightly lower (t= 0.80 min) than the values obtained for acenaphthene and uracil at the end of the stripping procedure. This points at the exclusion of uracil from the multilayer of ACN at the C18-bonded surface area of the pores [15]. With the removal of the stationary phase, a larger portion of the mesopore volume becomes accessible for uracil resulting in a constant elution time of 1.14 min.

Note that the retention time of uracil at time-point zero, before any stripping of the stationary phase has occurred, is slightly lower (t= 0.80 min) than the values obtained for acenaphthene and uracil at the end of the stripping procedure. This value is slightly larger than the value obtained for acenaphthene at the end of the stripping procedure and indicates that acenaphthene is slightly excluded from the water-rich layer formed at the silica surface under HILIC conditions.

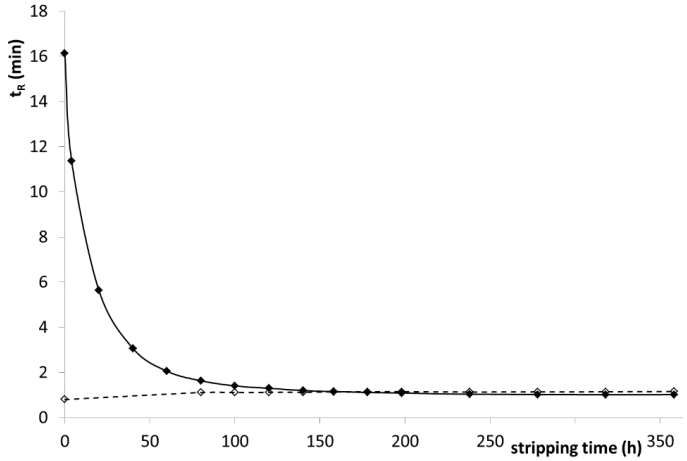


**Figure 4.2:** Retention loss for a Zorbax Eclipse Plus C18 column (4.6 × 50 mm, $d_p$= 5.0 µm) as a function of the stripping time (expressed as the time during which the column was flushed with 3% TFA in $H_2O$). Retention loss was measured via the elution time of acenaphthene (full line and symbols) at a flow rate of 0.5 mL/min in a mobile phase consisting of 50:50 ACN/$H_2O$ (v/v). The dashed line and open symbols represent the elution time of uracil, measured under the same conditions.

As an additional verification, thermogravimetric analyses were executed on intact Zorbax Eclipse C18 material with a particle size of 1.8 µm (column 3) and on the same material (obtained from a different column, column 4) after stripping the stationary phase. For this purpose, and following a protocol described by Lumley et al. [28], the stationary phase material collected from columns 3 and 4 was heated from room temperature to 600°C and the weight loss recorded. The obtained results are shown in Fig. 4.3.

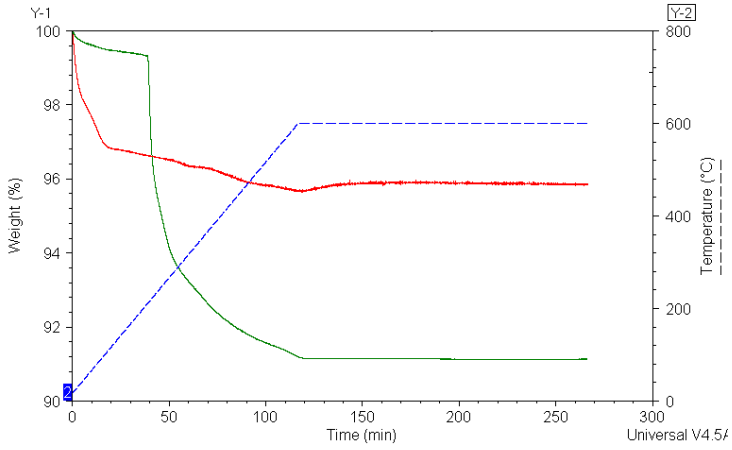


**Figure 4.3:** TGA traces obtained for the Zorbax Eclipse Plus C18 stationary phase ($d_p$= 1.8 µm), before stripping (green trace) and after stripping (red trace). The temperature program is shown in blue.

The C18-coated sample (before stripping, green trace) displays a small weight loss during the first 40 min of the experiment (T < 200°C) which is related to the removal of residual solvent in the stationary phase. Between 200°C and 600°C, the weight loss is much more pronounced and decreases from 99.3% to 91%. Bonded phase content was calculated as the weight difference between 200°C and 600°C, relative to the sample weight at 200°C [29]. This resulted in a value of 8.4%, in excellent agreement with the carbon load of 9%, specified by the manufacturer. The stripped sample (red trace) showed a much larger initial decrease in weight during the first 20 min of the experiment (T < 120°C) indicating a larger percentage of residual solvent was still present in this sample. Subsequently, the weight decreased from 96.8% to 96.0%. This weight loss most probably resulted from the loss of strongly hydrogen-bonded water on the silanol groups, of which removal only starts at 200°C and is not complete until about 650°C [30], instead of the combustion of carbon. This was confirmed by taking the first derivative of the TGA traces (Fig. 4.4).

For the C18-coated particles, a clear peak corresponding with the combustion of carbon was observed after 40 min (corresponding with a temperature of 200°C), while at this point no peaks were observed in the trace of the stripped sample. The smaller peaks that can be observed at the beginning of the trace correspond with the evaporation of the residual solvents. These results confirm that C18-layer was adequately stripped from the coated particles during the stripping procedure and hence bare silica was obtained.

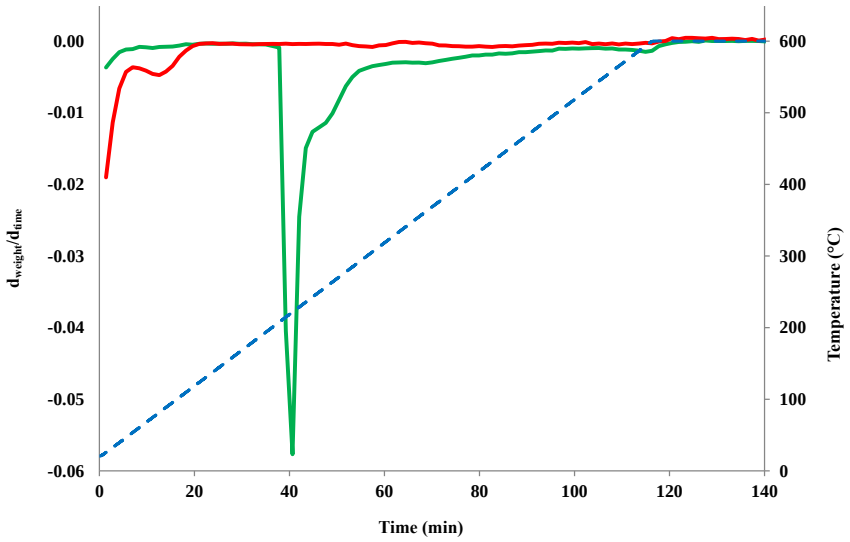


**Figure 4.4:** Derivative curves of $d_{weight}/d_{time}$ versus time of the TGA traces shown in Figure 4.3 of the main manuscript. These curves were obtained for the Zorbax Eclipse Plus C18 stationary phase ($d_p$= 1.8 µm), before stripping (green trace) and after stripping (red trace). The temperature program is shown in blue.

### 4.3.2. Assessment of mechanical packing characteristics

To verify whether the packing structure of the columns remained intact after stripping the stationary phase, the external porosity $\varepsilon_e$ of the 5 µm particle columns (columns 1 and 2) was assessed before and after the stripping procedure. This was done via inverse size exclusion chromatography (ISEC). The external porosity of the RPLC columns was additionally verified via total pore blocking (TPB) experiments. The obtained external porosity values are shown in Table 4.2. Considering the accuracy of the ISEC experimental protocol lies within 1% [22], an excellent agreement is found between $\varepsilon_e$-values before and after stripping. These results suggest that the external porosity of the columns is maintained during stripping and the packing structure hence remains intact.

**Table 4.2:** Column porosities measured on the columns before and after stripping. External porosities ($\varepsilon_e$) were measured via total pore blocking (TPB) and inverse-size exclusion (ISEC) experiments. Total porosities ($\varepsilon_T$) were measured via pycnometry.

| Column | Before Stripping/RPLC | | | | After Stripping/HILIC | | |
|---|---|---|---|---|---|---|---|
| | $\varepsilon_e$ (ISEC) | $\varepsilon_e$ (TPB) | $\varepsilon_T$ (pycnometry) | $\varepsilon_i$ | $\varepsilon_e$ (ISEC) | $\varepsilon_T$ (pycnometry) | $\varepsilon_i$ |
| 1 | 0.3836 | 0.3827 | 0.5571 | 0.2815 | 0.3894 | 0.6728 | 0.4641 |
| 2 | 0.3947 | 0.3945 | 0.5695 | 0.2888 | 0.3958 | 0.6897 | 0.4864 |

A second important check for an unchanged packing structure is that column pressure before and after stripping remains the same (provided the flow rate and mobile phase are kept identical). Combining Darcy's law and Kozeny-Carman's law, the following expression for column pressure (ΔP) can be obtained:

$$\Delta P = \frac{F}{\pi r^2} \cdot \frac{\eta \cdot L}{d_p^2} \cdot \frac{180(1-\varepsilon_e)^2}{\varepsilon_e^3} \tag{4.6}$$

Wherein $\eta$ is the mobile phase viscosity and $d_p$ the particle size. Assuming the column structure remains intact during the stripping procedure, geometrical parameters such as particle size, external porosity and obviously column radius and length should remain unaffected. Consequently, the column pressure should only change upon changing the mobile phase composition and flow rate. Table 4.3 shows the pressure values that were obtained on columns 1 and 2 before and after stripping for different mobile phase compositions and flow rates. The pressure values are perfectly maintained for all considered flow rates and mobile phase compositions. Again, these results suggest the packing structure of the column remains intact during the stripping procedure.

**Table 4.3**: Total pressures (bar) obtained before and after stripping of the stationary phase. Flow rates, mobile phase compositions and viscosities are given.

| Col. | Mobile phase | | Before Stripping/RPLC | | After Stripping/HILIC | |
|---|---|---|---|---|---|---|
| | (ACN/$H_2O$) | viscosity (cP) | 0.50 mL/min | 0.75 mL/min | 0.50 mL/min | 0.75 mL/min |
| 1 | 5/95 | 0.973 | 81 | 120 | 80 | 118 |
| | 50/50 | 0.890 | 72 | 107 | 70 | 104 |
| | 95/5 | 0.436 | 33 | 49 | 32 | 48 |
| 2 | 5/95 | 0.973 | 80 | 118 | 80 | 119 |
| | 50/50 | 0.890 | 70 | 104 | 70 | 104 |
| | 95/5 | 0.436 | 32 | 48 | 32 | 48 |

Total column porosities $\varepsilon_T$ were determined before and after stripping via pycnometry experiments and are also displayed in Table 4.2. As expected, a significantly larger total porosity is observed after stripping the stationary phase. Since it was already demonstrated that the external porosity of the columns remained intact during stripping, these differences must be found in the internal pore structure of the column. Internal porosity values ($\varepsilon_i$) were therefore calculated as:

$$\varepsilon_i = \frac{\varepsilon_T - \varepsilon_e}{1 - \varepsilon_e} \tag{4.7}$$

The obtained $\varepsilon_i$-values are also displayed in Table 4.2 and indicate a significant increase in internal porosity upon removal of the stationary phase. Under the assumption that the mesopores are cylindrical with a fixed pore size and the total length of the pores (L) is maintained during the stripping, the ratio of the internal porosities of the stripped and unstripped column can be written as:

$$\frac{\varepsilon_{i,unstripped}}{\varepsilon_{i,stripped}} = \frac{\pi r^2_{unstripped} L}{\pi r^2_{stripped} L} = \frac{r^2_{unstripped}}{r^2_{stripped}} \sim 0.60 \tag{4.8}$$

According to the manufacturer, the pore size (diameter) of the base silica Zorbax Eclipse material (=$r_{stripped}$) is 95 Å. Following Eq. (4.8), this leads to a pore size of 73-74 Å for the unstripped C18 material (=$r_{unstripped}$). The pore size hence increases with some 20 Å after removal of the stationary phase, which is in the order of magnitude of two times the length of an extended C18 chain [31].

### 4.3.3. Evaluation of column performance

To fairly compare the column's efficiency under HILIC and RPLC conditions, test molecules that can be used under RPLC and HILIC conditions were selected, and the mobile phase composition was adapted in such a way that a similar retention window was obtained under RPLC conditions (before stripping) and under HILIC conditions (after stripping). As can be seen in Table 4.1, this implied using a large percentage of ACN for the HILIC measurements, while a largely aqueous mobile phase was used in RPLC. The concentration of the buffer in the mobile phase was maintained at ~10 mM in all instances. Fig. 4.5 shows chromatograms that were obtained on the same column (column 1) before and after stripping the stationary phase at a flow rate of 1 mL/min. Because it was impossible to use exactly the same test mixture under both conditions, compounds with similar characteristics were selected (nucleobases and nucleotides) to obtain a similar retention window. The chromatograms in Fig. 4.5 show that narrow peaks with excellent peak shapes are obtained (asymmetry factors always below 1.1) under both conditions, indicating that column efficiency is not negatively affected by the stripping protocol.

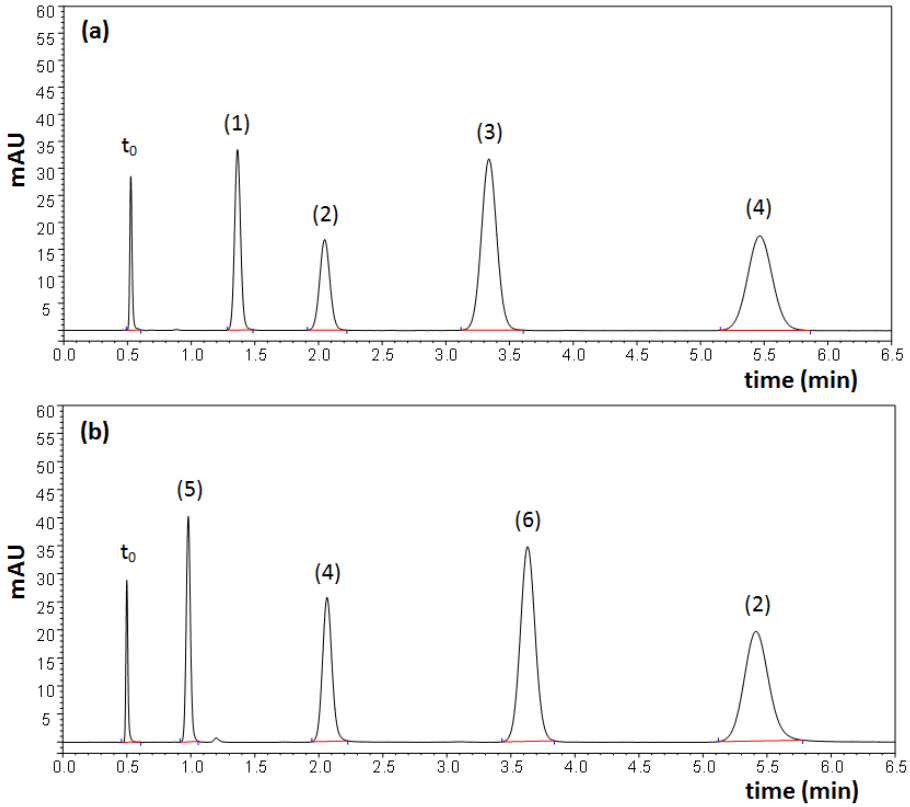


**Figure 4.5:** Chromatograms obtained on a Zorbax Eclipse Plus C18 column (4.6 × 50 mm, $d_p$= 5.0 µm) under **(a)** RPLC conditions (before stripping) and **(b)** HILIC conditions (after stripping). Mobile phase compositions are shown in Table 1. Peak annotation: (1) thymine, (2) guanosine, (3) thymidine, (4) adenosine, (5) uracil, (6) cytosine. The $t_0$-marker under RPLC conditions was thiourea and under HILIC conditions acenaphthene.

Subsequently, plate height curves were constructed by measuring plate heights as a function of the interstitial velocity $u_i$ (defined in Eq. (4.3)). This velocity was preferred over the more customary used $t_0$-based velocity ($u_0$), because $u_i$ can be considered as the fundamental velocity of chromatography since it appears directly (the reduced interstitial velocity $\nu_i$) in the general plate height equation (eq. 4.1). Another reason to prefer $u_i$ over $u_0$ is that, as shown in [32], $t_0$-values based on the elution time of a small, polar marker such as thiourea or uracil, typically tend to be overestimated for RPLC columns when determined in mobile phases with a small percentage of ACN. For HILIC columns operated in mobile phases with a small percentage of water or buffered aqueous phase, $t_0$-values based on the elution time of a small apolar marker, such as acenaphthene, tend to be underestimated, due to the exclusion of the marker from part of the mesoporous volume. To avoid any errors that might arise from an inaccurate assessment of the column dead volume, especially when comparing columns operated under different retention mechanisms, it is therefore safer to plot plate height data as a function of the interstitial velocity.

Fig. 4.6 shows the plate height curves obtained for column 1 (closed symbols) and column 2 (open symbols) operated under RPLC and HILIC conditions for compounds with zone retention factors of k"~5.5, k"~9.5 and k"~16.0. The curves obtained under HILIC conditions clearly show a larger b-term and smaller c-term compared to the curves obtained under RPLC conditions. Bulk diffusion coefficients ($D_m$) for each of the considered compounds were determined experimentally via the Taylor-Aris method, since empirical correlations for the determination of $D_m$, such as the popular Wilke-Chang equation, break down in ACN-rich mobile phases [27]. These values are shown in Table 4.1 and indicate that the $D_m$-values obtained under HILIC conditions are some 2-3 times larger than those obtained under RPLC conditions, explaining the higher observed b-term and lower c-term in HILIC.

To account for the higher bulk diffusion coefficients under HILIC conditions, the plate height curves displayed in Fig. 4.6 were reduced into dimensionless coordinates of h (= $H/d_p$) versus $\nu_i$ (=$u_i \times d_p/D_m$). Curves for compounds (zone retention factors k"= 5.5, 9.5 and 16.5) are shown in Fig. 4.7 and now display higher reduced b-terms under RPLC conditions, while the reduced c-terms appear lower in comparison with the HILIC measurements.To confirm these observations, all dimensionless plate height curves were fitted to a simple van Deemter model. The obtained reduced a-, b- and c-term values are displayed in Table 4.4, together with values of $h_{min}$.

Although the reduced minimum plate heights are systematically slightly higher under HILIC conditions, the values of $h_{min}$ are very similar under HILIC and RPLC conditions, suggesting that the stripping protocol does not affect the performance of the columns. This was already evident from the peak asymmetry values that were perfectly maintained under HILIC and RPLC conditions (Figure 4.5). Despite the crude approximation of the values in Table 4.4, these minimum plate heights are clearly obtained in different ways.

**Table 4.4**: The fitted reduced van Deemter coefficients (FIT) of the columns before and after stripping, the $h_{min}$ values and the b-term coefficients obtained via peak parking (PP) are also shown.

| Column | Before Stripping/RPLC | | | | | | After Stripping/HILIC | | | | |
|---|---|---|---|---|---|---|---|---|---|---|---|
| | k″ | $h_{min}$ | $a_{FIT}$ | $b_{FIT}$ | $b_{PP}$ | $c_{FIT}$ | k″ | $h_{min}$ | $a_{FIT}$ | $b_{FIT}$ | $b_{PP}$ | $c_{FIT}$ |
| 1 | 5.50 | 2.09 | 1.05 | 3.29 | 3.29 | 0.09 | 5.56 | 2.34 | 1.25 | 2.96 | 3.42 | 0.13 |
| | 9.50 | 2.18 | 1.01 | 4.93 | 5.06 | 0.07 | 9.82 | 2.18 | 0.89 | 3.60 | 3.89 | 0.12 |
| | 16.50 | 2.23 | 0.87 | 6.29 | 7.01 | 0.07 | 16.50 | 2.26 | 1.20 | 3.74 | 4.76 | 0.11 |
| 2 | 5.30 | 2.05 | 1.06 | 3.39 | 3.60 | 0.09 | 5.3 | 2.38 | 1.27 | 2.91 | 3.38 | 0.14 |
| | 9.20 | 2.05 | 1.10 | 3.95 | 5.16 | 0.07 | 9.55 | 2.11 | 0.73 | 3.50 | 3.69 | 0.13 |
| | 15.90 | 2.07 | 1.05 | 4.87 | 6.42 | 0.07 | 15.4 | 2.30 | 1.19 | 3.52 | 4.44 | 0.11 |

The b-term values obtained under HILIC conditions are smaller and increase to a much lesser extent with increasing retention factor in comparison with the values obtained under RPLC conditions, whereas the c-term values under HILIC conditions are clearly larger. Similar observations were previously made by other authors that attributed these phenomena to differences in surface diffusion [12-14]. The present study now confirms this for HILIC and RPLC columns with identical packing structures.

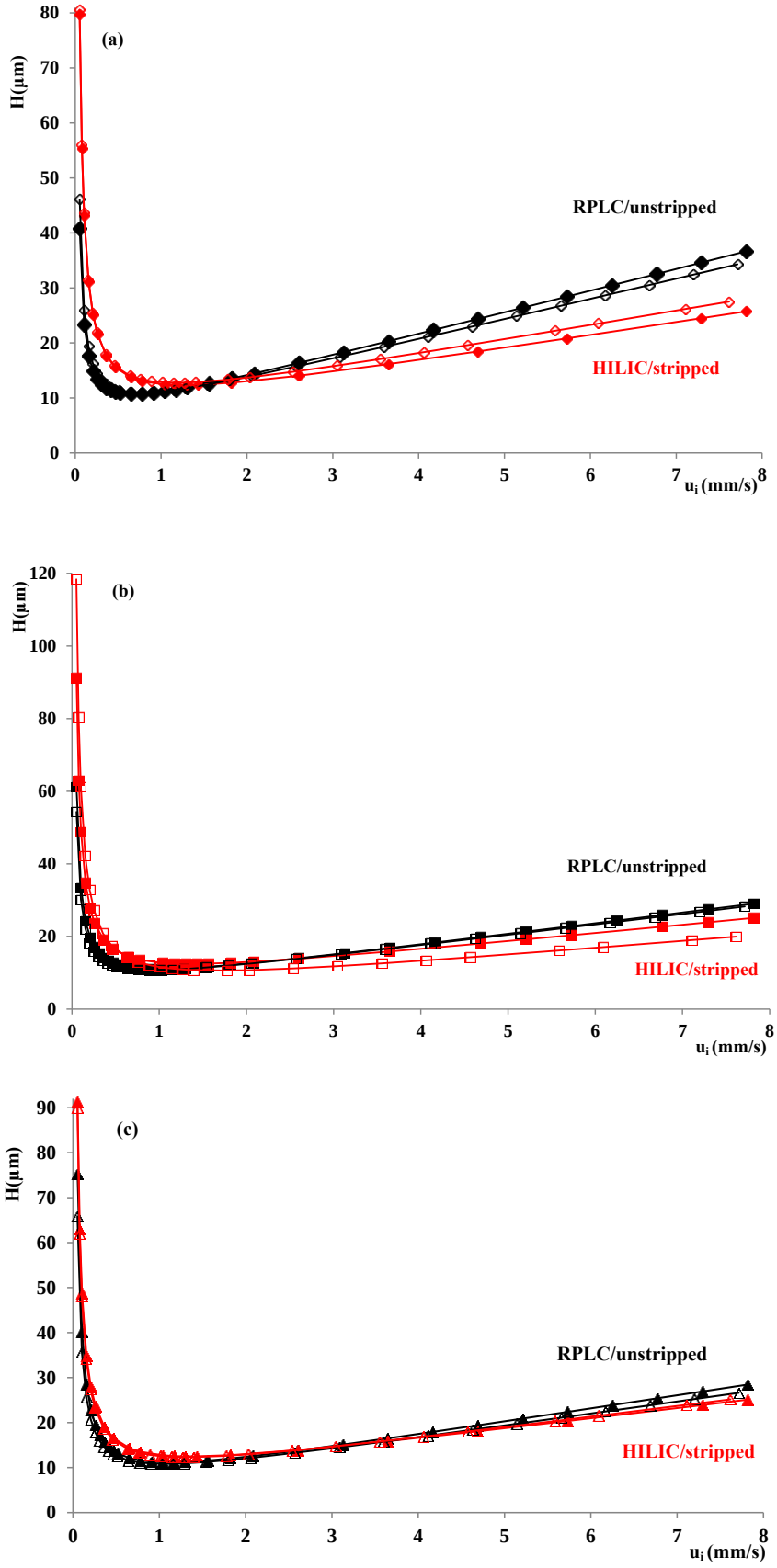


**Figure 4.6:** Plate height curves of H versus $u_i$ obtained under RPLC conditions before stripping (black symbols) and HILIC conditions after stripping (red symbols) for compounds with the following zone retention factors (a) k"= 5.50 (♦), (b) k"= 9.50 (■) and (c) k"= 16.50 (▲). Column 1: closed symbols, column 2: open symbols. Mobile phase conditions are shown in Table 4.1.

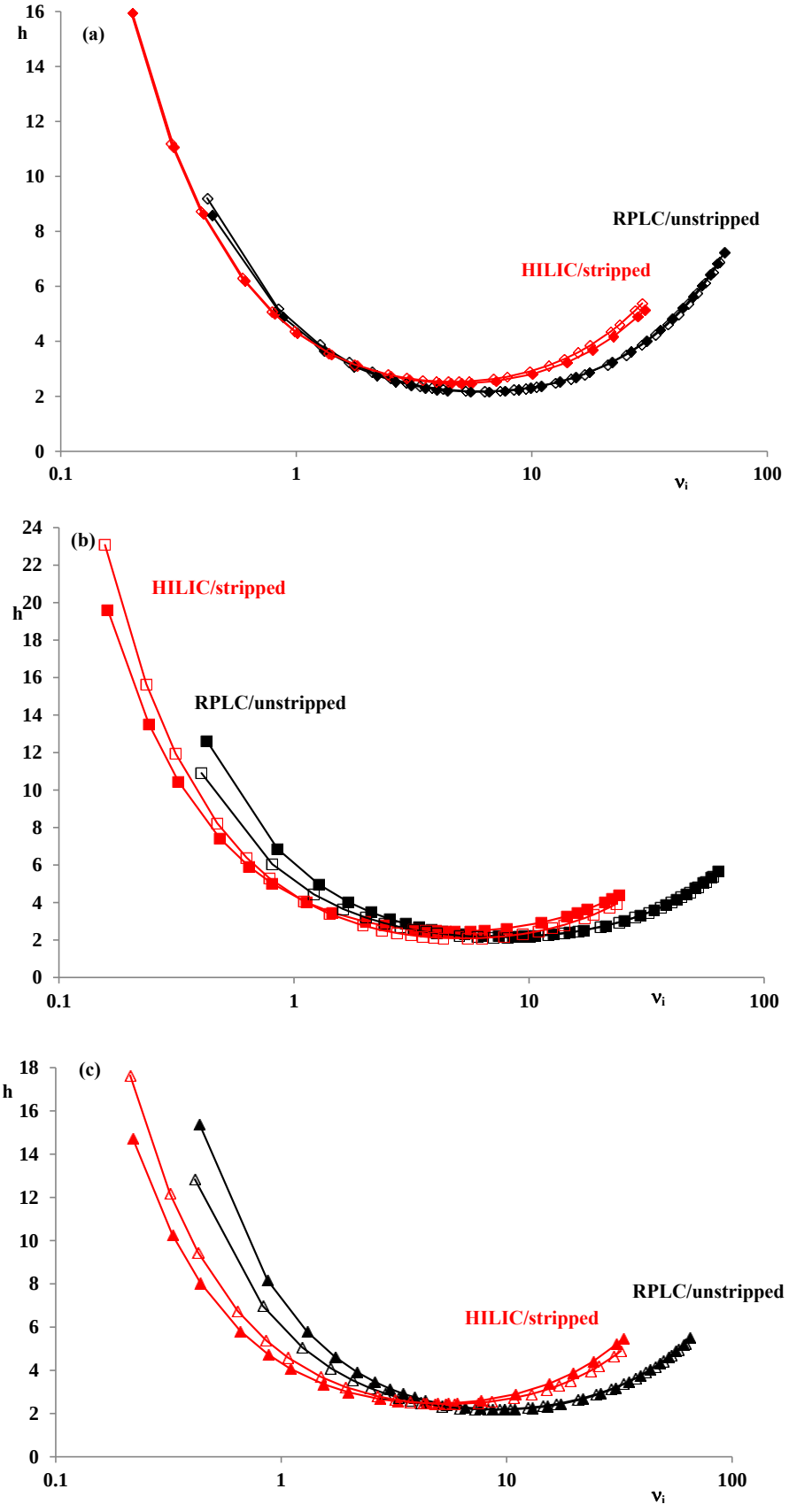


**Figure 4.7:** Reduced plate height curves of h versus $\nu_i$ under RPLC conditions before stripping (black symbols) and HILIC conditions after stripping (red symbols) for compounds with the following zone retention factors (a) k"= 5.50 (♦), k"= 9.50 (■) and (c) k"= 16.50 (▲). Column 1: full symbols, column 2: open symbols. Mobile phase compositions are shown in Table 4.1.

To investigate these observations in more detail, the contribution to band broadening originating from longitudinal diffusion (b-term) was additionally assessed by peak parking experiments. Fig. 4.8 depicts plots of $\sigma_x^2/D_m$ as a function of the parking time $t_{park}$ for each investigated compound, which are, according to Eqs. (4.4) and (4.5), directly proportional to their observed b-term coefficients.

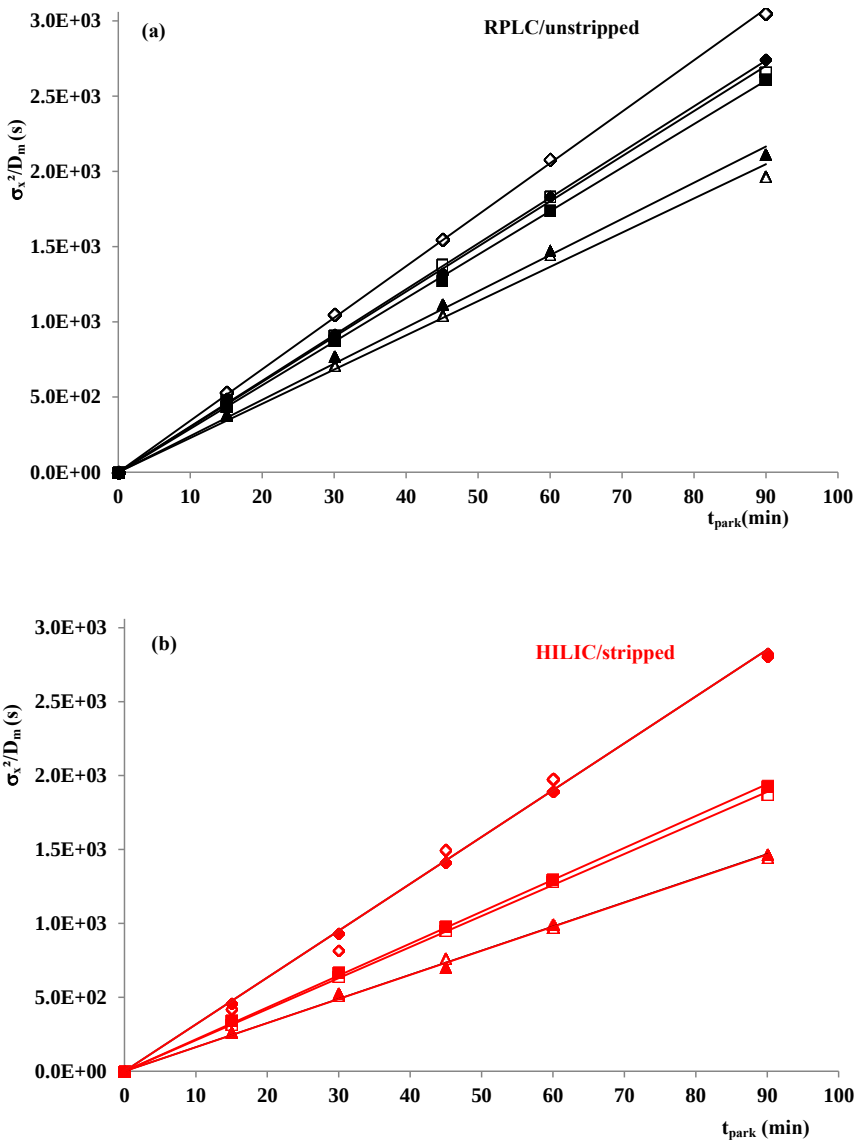


**Figure 4.8:** Curves of $\sigma^2_x/D_m$ versus $t_{park}$ obtained under **(a)** RPLC conditions before stripping (black symbols) and **(b)** HILIC conditions after stripping (red symbols). Retention factors of the compounds are $k_3$"= 5.50 (♦), $k_4$"= 9.50 (■) and $k_5$"= 16.50 (▲). Column 1: full symbols, column 2: open symbols. Mobile phase conditions are given in Table 4.1.

Since the zone retention factors of these compounds were maintained under RPLC and HILIC conditions, these plots confirm that the b-term coefficients in RPLC are larger than in HILIC, as was also evident from the reduced plate height curves in Fig. 4.7.

The exact values of the b-term coefficients obtained via peak parking are presented in Table 4.4 and are in good correspondence with the values obtained via curve fitting, confirming the earlier observed trends. To obtain a deeper understanding of the relation between the inner particle morphology and the observed $D_{eff}$-values, the contribution of the diffusion experienced by the analytes when residing outside the particles should be eliminated.

In [26] it was shown that the effective diffusion coefficient $D_{eff}$, occurring in the expression for the longitudinal diffusion in Eq. (4.1), can accurately be modeled via an effective medium theory-based expression of the form:

$$\frac{D_{eff}}{D_m} = \frac{1}{\varepsilon_e(1+k'')} \frac{1+2\beta_1(1-\varepsilon_e)-\varepsilon_e\zeta_2\beta_1^2}{1-\beta_1(1-\varepsilon_e)-\varepsilon_e\zeta_2\beta_1^2} \quad (4.9)$$

In this equation, $\zeta_2$ is a geometrical three-point parameter that depends on the microscopic geometry of the packed bed and amounts to 0.20-0.30 for random packings with an external porosity of some $\varepsilon_e$= 0.387 [32]. Since the interstitial geometry of the columns considered in this study remained unaffected before and after stripping, the same value of $\zeta_2$ could be used for the stripped and the unstripped columns. An arbitrary value of $\zeta_2$= 0.20 was thus assigned to the three-point parameter and used to extract the values of the polarizability constant $\beta_1$ from the experimentally determined value of $D_{eff}/D_m$ according to Eq. (4.9). This allowed for calculating the relative particle permeability $\alpha_{part}$:

$$\alpha_{part} = \frac{1+2\beta_1}{1-\beta_1} \quad (4.10)$$

from which the intra-particle diffusion coefficient $D_{part}/D_m$ could be deduced:

$$\frac{D_{part}}{D_m} = \alpha_{part} \frac{1-\varepsilon_e}{\varepsilon_e k''} \quad (4.11)$$

The values of $D_{part}/D_m$ as a function of zone retention factor are depicted in Fig. 4.9 and show that whereas intra-particle diffusivity under HILIC and RPLC are relatively similar for compounds with a zone retention factor of k"~5 ($D_{part}/D_m$=0.14-0.15), these values clearly decrease under HILIC conditions towards a value of 0.08 with increasing retention factor. Under RPLC conditions, they remain constant around a value of 0.15 for all considered retention factors. The higher values of $D_{part}/D_m$ under RPLC conditions can be explained as a direct consequence of the higher surface diffusion in the stationary phase under RPLC conditions.

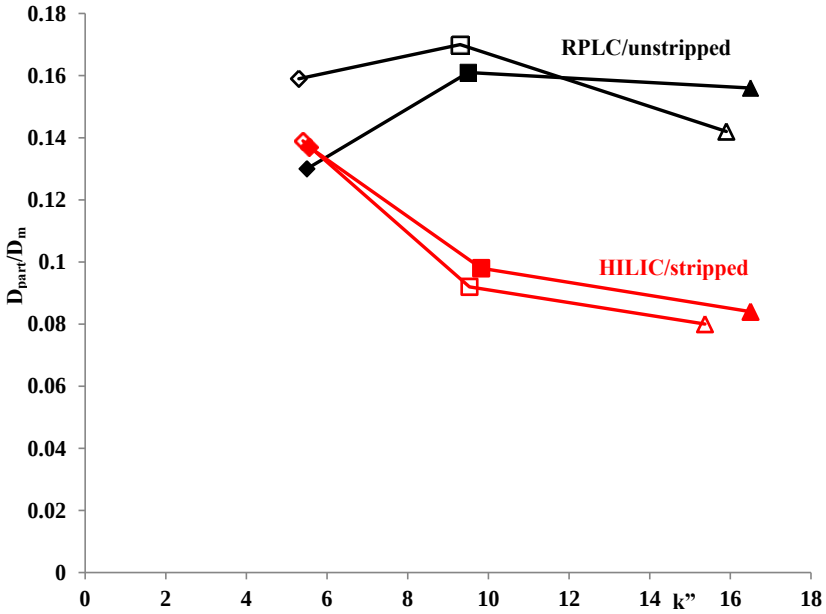


**Figure 4.9:** Curves of $D_{part}/D_m$ versus k” obtained under **(a)** RPLC conditions before stripping (black symbols) and **(b)** HILIC conditions after stripping (red symbols). Retention factors of the compounds are $k_3$”= 5.50 (♦), $k_4$”= 9.50 (■) and $k_5$”= 16.50 (▲). Column 1: full symbols, column 2: open symbols. Mobile phase compositions shown in Table 4.1.

The accurate knowledge of the $D_{part}/D_m$-values allows for a precise assessment of the $c_s$-term (fourth term in Eq. (4.1)). In [6] it has been demonstrated that the value of the geometrical constant $\alpha$ appearing in Eq. (4.1) equals 6 for spherical particles, while $Sh_{part}$= 10, independent of the particle size or retention mechanism. With these values, the $c_s$-terms were calculated for HILIC and RPLC conditions and are shown in Fig. 4.10a as a function of the reduced interstitial velocity. Whereas the $c_s$-values under RPLC conditions clearly decrease with increasing retention factor, this also seems to be the case for the HILIC experiments, despite earlier reports in literature [13]. Resorting to Eq. (4.1), this is a logical consequence of the increasing zone retention factor on the one hand ($c_s$-term is proportional to $k''/(1+k'')^2$) and the only slightly decreasing intra-particle diffusivity with increasing zone retention factor under HILIC conditions on the other hand. Since intra-particle diffusivity under RPLC conditions is overall higher due to enhanced surface diffusion, the $c_s$-terms are generally lower under RPLC conditions, at least for more strongly retained compounds.

The $c_m$-term appearing in eq 4.1 can be calculated using the Wilson and Geankoplis expression for the Sherwood number relating to the mobile zone ($Sh_m$) [33]. Because geometrical parameters ($\alpha$ and $\varepsilon_e$) are identical under HILIC and RPLC conditions, this leads to identical $c_m$-terms in HILIC and RPLC when compounds with the same zone retention factor are compared.

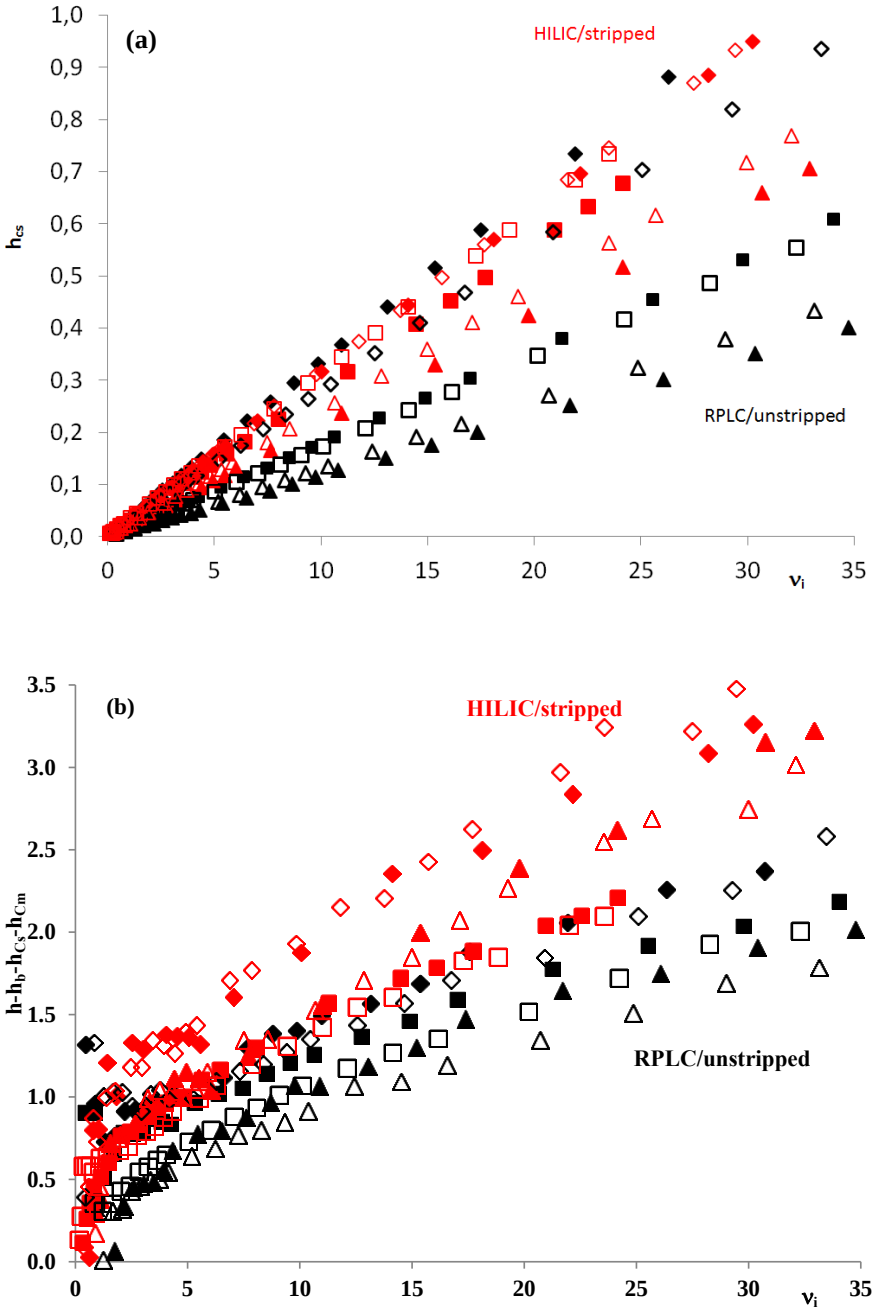


**Figure 4.10: (a)** Curves of $h_{cs}$ versus $\nu_i$ and **(b)** $h-h_b-h_{cs}$ versus $\nu_i$ under RPLC conditions before stripping (black symbols) and HILIC conditions after stripping (red symbols). Retention factors of the compounds are $k_3$"= 5.50 (♦), $k_4$"= 9.50 (■) and $k_5$"= 16.50 (▲).Column 1: full symbols, column 2: open symbols. Mobile phase compositions shown in Table 4.1.

Subtracting the contributions of longitudinal diffusion (b-term) and mass transfer ($c_m$- and $c_s$-term) from the overall observed plate heights, it is now possible to purely focus on band broadening originating from eddy diffusion. These data are shown in Fig. 4.10b and indicate that the contribution to band broadening from eddy dispersion is generally significantly larger for HILIC compared to RPLC conditions (differences in h of 0.3 to 1.2). These results show that both the retention mechanism and the internal structure of the particles have a very strong influence on the observed eddy diffusion.

This is somewhat surprising because this contribution is normally ascribed to phenomena occurring in the interstitial zone (i.e., outside the particles). These observations also imply that one of the traditional paradigms in chromatography, i.e., that there is a one-to-one relation between the eddy dispersion and the packing quality of a column, can no longer be maintained. Hence, differences in eddy dispersion observed among columns from different manufacturers should not only be ascribed to differences in packing quality but also depend strongly on the intra-particle properties.

### 4.4. Conclusions

A new procedure is proposed to study mass transfer phenomena under HILIC and RPLC under identical packing conditions. This procedure entails a detailed characterization of column performance and packing characteristics under RPLC conditions, followed by an adequate removal of the stationary phase to obtain a bare silica column that can be studied under HILIC conditions. Adequate removal of the stationary phase is obtained by submitting the RPLC column to different cycles of sequential flushing with 3% TFA in ACN and $H_2O$ and is confirmed by the lack of retention for small apolar and polar molecules in 50:50 ACN/$H_2O$ (v/v) and by thermogravimetric analyses.

Several experiments demonstrate that the external structure of the packing is not affected by the stripping protocol: the external porosity and pressure characteristics of the column are maintained before and after stripping, while also column efficiency remains unaffected, as demonstrated by excellent peak shapes and peak widths obtained under RPLC and HILIC conditions.

Reduced plate height curves are constructed as a function of the reduced interstitial velocity instead of the more commonly used linear velocity to avoid errors in the assessment of the total column volume. From these curves, it is clear that longitudinal diffusion is decreased in HILIC compared to RPLC. This was already reported in other studies, where this was explained by smaller surface diffusion due to a more localized adsorption mechanism in HILIC. The same principle applies to the stationary zone mass transfer that seems to be decreased under HILIC conditions, leading to higher $c_s$-term values compared to the RPLC analyses. These findings are now demonstrated for the first time in identical columns under HILIC and RPLC conditions.

An accurate assessment of b-, $c_m$- and $c_s$-term contributions to band broadening, facilitated by the fact that all geometrical parameters are kept the same under RPLC and HILIC conditions, reveals that band broadening originating from eddy dispersion is considerably higher under HILIC conditions, compared to RPLC. These findings suggest that the observed eddy dispersion is significantly affected by the interior structure and the retention mechanism of the particles, which is somewhat surprising because eddy dispersion is normally ascribed to phenomena occurring outside the particles. This observation also suggests that the one-to-one relation between eddy dispersion and packing quality of a column no longer holds.

### 4.5. References

[1] Lapidus, L.; Amundson, N. R., J. Phys. Chem. 1952, 56, 984-988.

[2] J. Calvin, G., Dynamics of chromatography, principles and theory. Marcel dekker, INC, New York, 1965.

[3] Huber, J. F. K., J. Chromatogr. Sci. 1969, 7, 85-90.

[4] Kučera, E., J. Chromatogr. A 1965, 19, 237-248.

[5] Horvath, C.; Lin, H.-J., J. Chromatogr. A 1976, 126, 401-420.

[6] Desmet, G.; Broeckhoven, K., Anal. Chem. 2008, 80, 8076-8088.

[7] Gritti, F.; Guiochon, G., J. Chromatogr. A 2012, 1221, 2-40.

[8] Gritti, F.; Guiochon, G., Anal. Chem. 2013, 85, 3017-3035.

[9] Desmet, G.; Broeckhoven, K.; De Smet, J.; Deridder, S.; Baron, G. V.; Gzil, P., J. Chromatogr. A 2008, 1188, 171-188.

[10] Desmet, G.; Deridder, S., J. Chromatogr. A 2011, 1218, 32-45.

[11] Desmet, G., J. Chromatogr. A 2013, 1314, 124-137.

[12] Gritti, F.; Guiochon, G., J. Chromatogr. A 2013, 1302, 55-64.

[13] Gritti, F.; Guiochon, G., J. Chromatogr. A 2013, 1297, 85-95.

[14] Heaton, J. C.; Wang, X.; Barber, W. E.; Buckenmaier, S. M.; McCalley, D. V., J. Chromatogr. A 2014, 1328, 7-15.

[15] Song, H.; Adams, E.; Desmet, G.; Cabooter, D., J. Chromatogr. A 2014, 1369, 83-91.

[16] Trammell, B. C.; Boissel, C. A.; Carignan, C.; O'Shea, D. J.; Hudalla, C. J.; Neue, U. D.; Iraneta, P. C., J. Chromatogr. A 2004, 1060, 153-163.

[17] Cypryk, M.; Apeloig, Y., Organometallics 2002, 21, 2165-2175.

[18] Guillarme, D.; Heinisch, S.; Rocca, J. L., J. Chromatogr. A 2004, 1052, 39-51.

[19] Cabooter, D.; Lynen, F.; Sandra, P.; Desmet, G., J. Chromatogr. A 2007, 1157 , 131-141.

[20] Liekens, A.; Cabooter, D.; Denayer, J.; Desmet, G., J. Chromatogr. A 2010, 1217, 6754-6761.

[21] Cabooter, D.; Billen, J.; Terryn, H.; Lynen, F.; Sandra, P.; Desmet, G., J. Chromatogr. A 2008, 1178, 108-117.

[22] Gritti, F.; Guiochon, G., J. Chromatogr. A 2013, 1280, 35-50.

[23] Knox, J. H.; Scott, H. P., J. Chromatogr. A 1983, 282, 297-313.

[24] Liekens, A.; Denayer, J.; Desmet, G., J. Chromatogr. A 2011, 1218, 4406-4416.

[25] Miyabe, K.; Matsumoto, Y.; Guiochon, G., Anal. Chem. 2007, 79, 1970-1982.

[26] Miyabe, K.; Ando, N.; Guiochon, G., J. Chromatogr. A 2009, 1216, 4377-4382.

[27] Li, J.; Carr, P. W., Anal. Chem. 1997, 69, 2530-2536.

[28] Lumley, B.; Khong, T. M.; Perrett, D., Chromatographia 2004, 60, 59-62.

[29] Schilling, M. R.; Preusser, F.; Gutnikov, G., J. Therm. Anal. 1992, 38, 2483-2490.

[30] Scott, R. P. W.; Traiman, S., J. Chromatogr. A 1980, 196, 193-205.

[31] Rafferty, J. L.; Siepmann, J. I.; Schure, M. R., J. Chromatogr. A 2011, 1218, 2203-2213.

[32] Deridder, S.; Desmet, G., J. Chromatogr. A 2012, 1223, 35-40.

[33] Wilson, E. J.; Geankoplis, C. J., Ind. Eng. Chem. Fund. 1966, 5, 9-14.

# Chapter 5

# Extensive Database of Liquid Phase Diffusion Coefficients of Some Frequently Used Test Molecules in Reversed-Phase Liquid Chromatography and Hydrophilic Interaction Liquid Chromatography

This chapter has been published in:

- **Huiying Song,** Yoachim Vanderheyden, Erwin Adams, Gert Desmet, Deirdre Cabooter, Extensive database of liquid phase diffusion coefficients of some frequently used test molecules in reversed-phase liquid chromatography and hydrophilic interaction liquid chromatography, *Journal of Chromatography A*, 1455 (2016) 102-112.

**Abstract**

Diffusion plays an important role in all aspects of band broadening in chromatography. An accurate knowledge of molecular diffusion coefficients in different mobile phases is therefore crucial in fundamental column performance studies. Correlations available in literature, such as the Wilke-Chang equation, can provide good approximations of molecular diffusion under reversed-phase conditions. However, these correlations have been demonstrated to be less accurate for mobile phases containing a large percentage of acetonitrile, as is the case in hydrophilic interaction liquid chromatography.

A database of experimentally measured molecular diffusion coefficients of some of 45 polar and apolar compounds that are frequently used as test molecules under hydrophilic interaction liquid chromatography and reversed-phase conditions is therefore presented. Special attention is given to diffusion coefficients of polar compounds obtained in large percentages of acetonitrile (> 90%). The effect of the buffer concentration (5-10 mM ammonium acetate) on the obtained diffusion coefficients is investigated and is demonstrated to mainly influence the molecular diffusion of charged molecules.

Diffusion coefficients are measured using the Taylor-Aris method and hence deduced from the peak broadening of a solute when flowing through a long open tube. The validity of the set-up employed for the measurement of the diffusion coefficients is demonstrated by ruling out the occurrence of longitudinal diffusion, secondary flow interactions and extra-column effects, while it is also shown that radial equilibration in the 15 m long capillary is effective.

**Keywords:** Molecular diffusion coefficients; RPLC; HILIC; Taylor-Aris; Curve Fitting

## 5.1. Introduction

With new developments in materials and column packing technologies, an ever increasing number of HPLC columns, such as monolithic columns, ultra-high pressure resistant sub-2 µm columns and highly efficient core-shell columns, are nowadays commercially available [1-3]. Reduced plate height models are often used to compare the intrinsic efficiency of columns packed with different particle sizes or packing morphologies, operated under different mobile phase conditions, since they allow normalizing these differences to a large extent [4-6]. Mass transfer phenomena in packed particle columns can generally be described by the general plate height model [4, 7-11]:

$$h = h_{inhom} + \frac{2}{\nu_i}\frac{D_{eff}}{D_m}(1 + k") + \frac{2}{\alpha}\frac{k"^2}{(1+k")^2}\frac{\varepsilon_e}{1-\varepsilon_e}\frac{\nu_i}{Sh_m} + \frac{2}{\alpha}\frac{k"}{(1+k")^2}\frac{\nu_i}{Sh_{part}\frac{D_{part}}{D_m}} \quad (5.1)$$

In this equation, h is the reduced plate height, $\nu_i$ the reduced velocity (defined as $\nu_i = u_i \times d_p/D_m$), $D_{eff}$, $D_{part}$ and $D_m$ the effective, intra-particle and bulk molecular diffusion coefficients, respectively, k" the zone retention factor, $\varepsilon_e$ the external porosity, $\alpha$ a geometrical constant ($\alpha$= 6 for spherical particles) and $Sh_m$ and $Sh_{part}$ the Sherwood numbers relating to the mobile and the intra-particle zone, respectively. From Eq. (5.1), it is clear that diffusion affects all aspects of band broadening in chromatography. Therefore, an accurate knowledge of the molecular diffusion coefficient ($D_m$) of the employed test solutes is critical when investigating fundamental mass transfer properties of chromatographic columns. Molecular diffusion coefficients are frequently estimated using literature correlations, such as the Wilke-Chang [12], the Scheibel [13], or the Hayduk-Laudie equation [14], of which the former is probably the most popular and most frequently used one. The accuracy of the diffusion coefficients estimated using these correlations is, however, often questionable [15]. Such inaccuracies can obviously influence the interpretation of chromatographic data, by directly affecting the obtained values of the b- and c-term coefficients.

Almost twenty years ago, Li and Carr compared the accuracy of diffusion coefficients estimated via empirical correlations to those obtained via the Taylor-Aris open tube method for typical reversed-phase liquid chromatography (RPLC) conditions [16]. They demonstrated that the absolute percentage errors in the $D_m$-values obtained from the Wilke-Chang correlation was generally less than 20% for methanol/water mixtures, whereas the absolute errors varied from 10% to 30% in mixtures of acetonitrile and water.

They also showed that these errors increased as the volume fraction of ACN exceeded 50%, indicating that the Wilke-Chang correlation does not work well under ACN-rich conditions. In this case, the Scheibel correlation was demonstrated to yield more accurate diffusion coefficients than the Wilke-Chang correlation, but errors still amounted up to 20%.

Since a number of years there is an increasing interest in hydrophilic interaction liquid chromatography (HILIC) for the separation of polar and ionizable analytes [17-20]. This has recently also resulted in a growing number of fundamental studies wherein the intrinsic performance of HILIC columns is evaluated [21-23]. This type of work necessitates an accurate knowledge of the diffusion coefficients of polar molecules, measured in large percentages of organic solvents, such as acetonitrile. As discussed above, the popular Wilke-Chang equation breaks down in such conditions, whereas the accuracy of other, more precise correlations still remains questionable [15].

Rather than estimating them from (imprecise) correlations, it is much more accurate to measure diffusion coefficients under the actual experimental conditions since diffusion coefficients vary significantly with the nature of the solute molecule, the solvent and the temperature. Although the practical procedures required for the experimental measurement of $D_m$-values can be tedious and time-consuming, these values are of great importance for precise fundamental research. Several methods exist for the measurement of the diffusion coefficients, such as the diaphragm-cell method [24], optical methods (such as the light scattering method) [25] and spectroscopic methods (nuclear magnetic resonance) [26].

Although these methods are effective and accurate, they require expensive and elaborate analytical instruments and complex procedures which are costly and lengthy to develop. It is therefore far more convenient for chromatographers to measure accurate diffusion coefficients on an HPLC apparatus. For this purpose, both the Taylor-Aris method [27] and the peak parking method [28] can be used. Since the peak parking method is time-consuming (it requires calibrating a non-porous column using molecules with a known molecular diffusion coefficient in order to deduce the column's obstruction factor) and the occurrence of retention effects cannot be excluded, the much simpler and more straightforward Taylor-Aris open tube method was selected in this study to determine $D_m$-values [27,29]. This method is based on the peak broadening of a solute when flowing through a long open tube or capillary under conditions wherein longitudinal diffusion is absent and can therefore be ignored.

If performed under conditions where the long-time plate height limit ($H_\infty$) for radial diffusion is reached, the diffusion coefficient can be calculated from the peak variance $\sigma^2_t$ and the residence time t of the peak in the tube as follows:

$$D_m = \frac{d_t^2 \cdot t}{96 \cdot \sigma_t^2} \quad (5.2)$$

In this equation, $d_t$ refers to the inner diameter of the open tube. In case the long-time plate height limit for radial diffusion is not reached, e.g. when the tube is too short and/or too wide, and/or when the flow rate is too high, the peak variance in Eq. (5.2) should be replaced by the following expression:

$$\sigma_t^2 = \frac{H \cdot L}{u^2} \quad (5.3)$$

with u the average linear velocity and [30]:

$$H = H_\infty \cdot [1 - \frac{1}{aL}(1 - e^{(-\tau L)})] \quad (5.4)$$

$$H_\infty = \frac{F}{24 \cdot \pi \cdot D_m} \quad (5.5)$$

$$\tau = 15\pi \frac{D_m}{F} \quad (5.6)$$

wherein F is the flow rate, L the tubing length. It can be seen that when $\tau$L $\rightarrow \infty$, the expression between square brackets in Eq. (5.4) turns to unity and H $\rightarrow$ $H_\infty$. Replacing H in Eq. (5.3) by the $H_\infty$-expression in Eq. (5.5) then returns Eq. (5.2).

In the first part of this chapter, the accuracy of the set-up we used to measure $D_m$ will be validated by evaluating the radial equilibration of the sample plug, the absence of longitudinal diffusion, the influence of extra-column contributions and secondary flow interactions. The accuracy of the measurements will also be compared to previously obtained values in literature.

In the second part of the chapter, an extensive database of molecular diffusion coefficients is presented for a wide selection of apolar and polar test molecules frequently used in fundamental column performance studies under RPLC and HILIC conditions, covering a broad range of mobile phase compositions for each molecule. Since buffered mobile phases are commonly used in HILIC applications, the influence of the buffer concentration on the obtained $D_m$-values is assessed as well.

Finally, a set of correlations is presented, allowing to calculate the desired molecular diffusion coefficients for each of the evaluated test compounds over a large range of mobile phase compositions. With this work, we hope to serve the chromatographic community with a large number of accurate $D_m$-values that can be used in future fundamental chromatographic investigations.

## 5.2. Experimental

### 5.2.1. Apparatus

$D_m$-measurements were carried out on a Perkin Elmer 275 UHPLC system (Perkin Elmer, Massachusetts, USA) equipped with a binary high pressure pump (maximum pressure: 690 bar), an autosampler and a variable wavelength detector with a flow cell of 2.6 µL. A stainless steel piece of tubing with fingertight connections (Viper tubing with an ID of 125 µm) (Thermofisher, Germering, Germany) was used between the injector and the inlet of the capillary. Between the outlet of the capillary and the detector, PEEK tubing with an I.D. of 125 µm was used. The tubing was not altered during the experiments to avoid changing the extra-column volume. Chromera software (Perkin Elmer) was used for system operation and data acquisition. Absorbances were measured at a sample rate of 50 Hz. The temperature of the capillary was kept constant at 30°C using a thermostatted water bath (Julabo, Seelbach, Germany).

### 5.2.2. Chemicals and capillary tubing

Ammonium acetate was obtained from Sigma-Aldrich (Steinheim, Germany). Milli-Q water was prepared in the lab using a Milli-Q gradient water purification system from Millipore (Bedford, MA, USA). HPLC grade acetonitrile (ACN) was purchased from Fisher Chemicals (Erembodegem, Belgium). Acetic acid was obtained from Merck (Darmstadt, Germany). Following molecules were evaluated as apolar test compounds: benzene was from Merck (Darmstadt, Germany), butylbenzene, naphthalene, pyridine, phenol and toluene were from Acros Organics (Geel, Belgium), acetanilide, acetophenone, 3'-methyl acetophenone, propiophenone, butyrophenone, benzophenone, valerophenone, hexanophenone, heptanophenone, octanophenone, methylparaben, ethylparaben, propylparaben, butylparaben and caffeine were from Sigma-Aldrich (Steinheim, Germany), phenanthrene was from Carlo Erba (Val-de-Reuil, France), and as polar test compounds: thiourea, diphenhydramine hydrochloride, thymidine, adenosine, procainamide hydrochloride, adenine, *p*-xylene-2-

sulfonic hydrate, atenolol, cytidine, uridine, nortriptyline hydrochloride and 2-naphthalenesulfonic acid were obtained from Sigma-Aldrich (Steinheim, Germany), uracil, thymine, deoxyuridine, guanine and cytosine were from Janssen Chimica (Geel, Belgium), guanosine was from TCI (Zwijndrecht, Belgium), benzylamine and ascorbic acid were from Acros Organics (Geel, Belgium), benzoic acid is from Merck (Darmstadt, Germany), potassium iodide is from VWR (Leuven, Belgium). nicotinic acid is from Ferak (Berlin, Germany). To perform the $D_m$-measurements, PEEK tubing (vendor specifications: 0.020 in × 50 ft) with a measured length of 1532 cm and a calibrated internal diameter ($d_t$) of 0.051709 cm was purchased from GRACE (Columbia, MD, USA). The tubing was coiled into a diameter ($d_{coil}$) of 12 cm for temperature control and calibrated by weighing the amount of water contained within it [16].

### 5.2.3. Methodology

#### 5.2.3.1 Sample preparation

Stock solutions of each test molecule were prepared in $H_2O$ or ACN in concentrations ranging between 0.5 and 5 mg/mL, and then stored in the freezer (-20°C). Fresh test samples were prepared daily in concentrations resulting in signal intensities between 60 mAU and 400 mAU, by diluting stock solutions in their individual sample solvent compositions. UV detection was performed at 210, 215 or 254 nm.

#### 5.2.3.2 Taylor-Aris experiments

The Taylor-Aris experiments were conducted by injecting a very narrow sample plug (1 µL) in the empty capillary PEEK tubing under isocratic mobile phase conditions at a flow rate of 0.1 mL/min. The dispersed sample peak was detected at the end of the tubing and its variance measured (in time coordinates). The diffusion coefficient was subsequently calculated using Eq. (5.2). Each experiment was performed in triplicate and average values are presented.

#### 5.2.3.3 Data processing

Recorded peaks were analyzed with an in-house written Matlab program that determines peak variances using the method of moments. Peak boundaries were selected based on the variance profile analysis method [31]. This method calculates peak variance values for any possible

value of the peak end time ($t_2$) and makes a plot of $\sigma^2$ versus $t_2$. Theoretically, this curve levels off to the true variance.

### 5.3. Results

All diffusion coefficients reported in this study were obtained for peaks displaying a near-Gaussian peak profile. To ensure symmetrical peak shapes, samples were prepared in concentrations that were sufficiently low to avoid solubility issues and where necessary, sample solvent compositions were adapted to obtain symmetrical peak shapes (see 5.3.1.6). Overall, tailing factors (TF) between 0.95 and 1.05 were obtained for all reported molecules under all experimental conditions (some example chromatograms are shown in Figure 5.1).

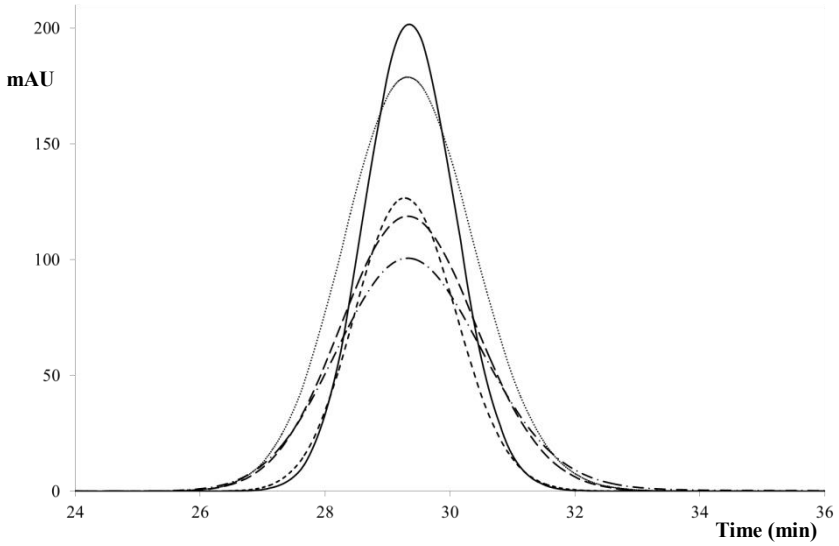


**Figure 5.1:** Symmetrical peak profiles obtained for a number of representative compounds and conditions: acetanilide (mobile phase: pure water; dashed-dotted line, tailing factor: 1.05), uracil (mobile phase: 60/40 (v/v) $H_2O$/ACN; dashed line, tailing factor: 1.03), benzoic acid (mobile phase: 10mM $NH_4Ac$ pH 6.0 in 80% ACN; dotted line, tailing factor: 1.03), thymine (mobile phase: 5mM $NH_4Ac$ pH 6.0 in 95% ACN; long dashes, tailing factor: 1.03), acetanilide (mobile phase: pure ACN; full line, tailing factor: 1.02).

### 5.3.1 Verification of the validity of the employed set-up

To verify the validity of the set-up we used to measure $D_m$, it was first investigated whether the conditions below were met.

#### 5.3.1.1 Axial diffusion negligible

As a first condition, the contribution of axial molecular diffusion to the total variance should be negligible. The contribution to the peak variance from Taylor-Aris dispersion is given in Eq. (5.2), while the contribution from axial diffusion is defined by [16,29]:

$$\sigma_{t,diff}^2 = \frac{2 \cdot D_m \cdot t_R}{u^2} \quad (5.7)$$

With $t_R$ the residence time of the solute. Under all investigated experimental conditions, $\sigma^2_{t,diff} << 10^{-4} \times \sigma^2_{t,Taylor\text{-}Aris}$, indicating that the contribution of axial diffusion to the total measured variance could be ignored.

#### 5.3.1.2 Effective radial equilibration of the sample concentration

To deduce the molecular diffusion coefficient from the measured peak profiles according to Eq. (5.2), the sample concentration should be completely radially equilibrated along the tubing length. As mentioned in the introduction, this condition is met when $a$L >> 1 in Eq. (5.4), or, equivalently:

$$L \gg \frac{d_t^2 \cdot u}{60 \cdot D_m} \quad (5.8)$$

The expression in Eq. (5.8) corresponds to the original expression for the radial equilibration time of Taylor [27]. Even for the smallest encountered diffusion coefficients, the expression on the right-hand side of Eq. (5.8) always returned values that were well below the length of the employed capillary (max. encountered values on the right hand side of Eq. (5.8) were 0.07-0.08 m versus 15.32 m for the length of the capillary). This indicates that radial equilibration of the sample was established under all considered circumstances.

#### 5.3.1.3 Extra column variance negligible

The contribution of extra-column effects to the total variance should be negligible. The extra-column volume variance ($\sigma^2_v$) was calculated as the sum of the variances of the injector ($\sigma^2_{v,i}$), the detector ($\sigma^2_{v,d}$) and the tubing ($\sigma^2_{v,t}$) connecting the capillary to the system. In the ideal case, the injection and detection signal can be treated as rectangular signals, whose variances ($\sigma^2_v$) are calculated as [32]:

$$\sigma_v^2 = \frac{V^2}{12} \quad (5.9)$$

With V the injection or detection volume, respectively. In practice, however, it has been shown in [34] that the value of the denominator can vary between 1 and 12 (a value of 1 corresponding to an ideal mixer). This would bring the variance of the injection and detection volume contributions to a maximum value of $\sigma^2_{v,i}$= 1 µL² and $\sigma^2_{v,d}$= 6.8 µL², respectively.

The contribution to the extra-column volume variance originating from the connection tubing can be calculated according to Eqs. (5.3-5.6) using the flow rate to relate volumetric to time units ($\sigma^2_V = F^2 \times \sigma^2_t$). To connect the capillary to the instrument, two pieces of tubing with an I.D. of 125 µm and lengths of 75 cm and 25 cm, respectively, were used. This resulted in a total variance of $\sigma^2_{V,t} = 6.4\ \mu L^2$, bringing the total extra-column variance to $\sigma^2_V = 14.2\ \mu L^2$. Even for the compounds with the highest molecular diffusion coefficients (with volumetric variances of $\sigma^2_V \sim 4000\ \mu L^2$), the extra-column variance represented less than 0.4% of the total volume variance measured, making the extra-column variance negligible.

#### 5.3.1.4 No secondary flow circulation

The derivation of the molecular diffusion coefficient from Eq. (5.2) assumes that the capillary tube wherein the experiments are performed is straight. For practical reasons (temperature control and available laboratory space) it was, however, necessary to coil the capillary tube. Under these conditions, secondary flow circulation can occur in the tube as a result of centrifugal forces, which will obviously affect the dispersion of the solute. According to Atwood and Goldstein, the effects of secondary flow in the coiled tube are avoided when the applied flow rate is less than the transition flow rate ($F_{trans}$) [34]:

$$F < F_{transition} = \sqrt{\frac{518 \cdot R_{coil} \cdot r_t \cdot D_m \cdot \eta}{\rho}} \tag{5.10}$$

where $R_{coil}$ is the radius of the coiled tube, ρ is the density of the solvent, η is the viscosity of the solvent and $r_t$ is the radius of the PEEK tube ($=d_t/2$). When the flow rate F is divided by the expression for the transition flow rate $F_{transition}$, the ratio between F and $F_{transition}$ can be normalized and expressed in terms of the dimensionless Dean (Dn) and Schmidt (Sc) numbers [34,35]:

$$\frac{F}{F_{transition}} = \frac{\pi}{2 \cdot (518)^2} \cdot Dn \cdot \sqrt{Sc} \tag{5.11}$$

$$Dn = \frac{2\rho u r_t}{\eta} \sqrt{\frac{r_t}{R_{coil}}} \tag{5.12}$$

$$Sc = \frac{\eta}{\rho D_m} \tag{5.13}$$

Janssen demonstrated that there is no significant difference in molecular diffusion coefficient measured in a straight tube versus a coiled tube when the product of the Dean number squared and the Schmidt number is smaller than 100 [36]. In terms of the transition flow rate (Eqs. 5.10-5.11) this means that the employed flow rate should be lower than ~ 0.7 × $F_{transition}$ to avoid secondary flow.

For all reported compounds under all considered mobile phase conditions, the applied flow rate (F= 0.1 mL/min) was always lower than ~ 0.7 × $F_{transition}$. At the same time, the product of $Dn^2$ × Sc was always lower than 100 for all reported compounds (maximum encountered value of $Dn^2$ × Sc was 88, while the values of $Dn^2$ × Sc were on average 40-50). These results confirm that secondary flow was insignificant in the coiled tube for all compounds and conditions investigated in this study.

#### 5.3.1.5 Influence of injection volume

The influence of the injection volume on the obtained $D_m$-values was verified by employing four different injection volumes (0.5 µL, 1 µL, 2 µL and 5 µL) for the $D_m$-determination of thiourea in pure water. Compound concentrations were adapted such that the injected mass was identical in each experiment. The obtained $D_m$-values are shown in Table 5.1 and indicate an excellent agreement in $D_m$-values for the different injection volumes (max. deviation of 0.63% in $D_m$ for different injection volumes). Considering the contribution to the total variance of the largest injection volume (5 µL) according to Eq. (5.9) was only 25 $\mu L^2$, while the volumetric variance of the thiourea plug in pure water was $\sigma^2_v$~ 10000 $\mu L^2$, it is clear that injection volumes below 5 µL will not affect the measured peak broadening. For practical reasons, it was decided to employ a fixed injection volume of 1 µL in all ensuing experiments.

**Table 5.1**: Experimentally determined $D_m$ -values of thiourea in pure water (30°C) and using different injection volumes

| Compound conc. (ppm) | Injection volume (µL) | $D_m$ ($m^2/s$) | RSD |
|---|---|---|---|
| 1000 | 0.5 | $1.450 \times 10^{-9}$ | 0.63% |
| 500 | 1 | $1.468 \times 10^{-9}$ | |
| 250 | 2 | $1.467 \times 10^{-9}$ | |
| 100 | 5 | $1.470 \times 10^{-9}$ | |

### 5.3.1.6 Sample solvent composition

In nearly all experiments, the sample solvent composition was identical to the mobile phase composition. In some cases, however, solubility problems occurred when polar compounds were dissolved in a large percentage of ACN. This was reflected by a steep decrease in diffusion coefficient compared to the $D_m$-values obtained for the same compound in mobile phases containing slightly larger percentages of water (Fig. 5.2 open symbols and dashed line). This solubility problem could not be solved by adapting the compound concentration. Therefore, under circumstances where solubility problems occurred, the sample solvent composition was altered by adding a small percentage of water or buffered mobile phase (Fig. 5.2 full symbols). The percentage of aqueous phase in the sample, however, never deviated more than 20% from the percentage of aqueous phase in the employed mobile phase.

To investigate whether differences in sample solvent composition would affect the value of the obtained diffusion coefficient in a specific mobile phase composition, molecular diffusion coefficients were measured for an apolar compound (benzene) in different sample solvent compositions using a mobile phase containing 100% ACN. Benzene was chosen as the test compound, since it is perfectly soluble in 100% ACN. As can be deduced from Table 5.2, the aqueous component of the mobile phase could easily amount up to 30% without affecting the value of the obtained $D_m$-values (max. deviation of 0.45% in $D_m$ for sample solvent containing 70%, 80%, 90% and 100% of ACN). This is probably attributed to the fact that the employed injection volumes (1 µL) were small enough to ensure a fast mixing of the sample solvent with the surrounding mobile phase (capillary volume was 3216 µL).

**Table 5.2:** Experimentally determined values of $D_m$ for benzene (450 ppm) dissolved in four different sample solvent compositions and for a fixed mobile phase composition of 100% ACN.

| Mobile phase | Sample solvent | $D_m$ ($m^2/s$) | RSD (%) |
|---|---|---|---|
| 100%ACN | 100%ACN | $3.486 \times 10^{-9}$ | 0.45 |
| | 90%ACN | $3.506 \times 10^{-9}$ | |
| | 80%ACN | $3.514 \times 10^{-9}$ | |
| | 70%ACN | $3.524 \times 10^{-9}$ | |

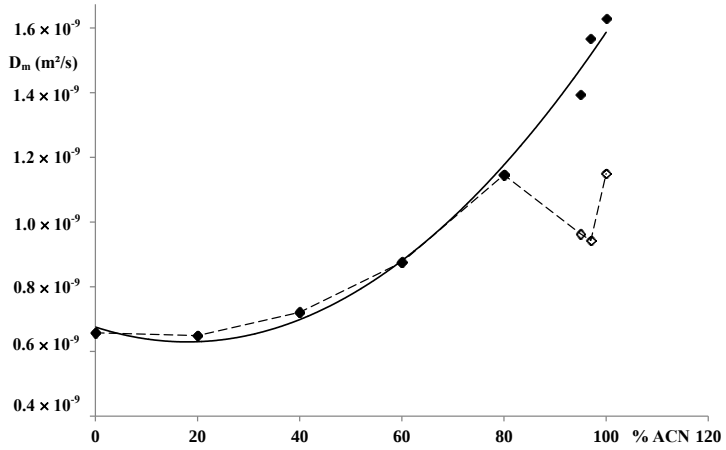


**Figure 5.2:** Experimentally determined values of $D_m$ for procainamide hydrochloride as a function of % ACN in the mobile phase (the aqueous component of the mobile phase was water). The $D_m$-values corresponding with the open symbols (◇) were obtained when the sample solvent had the same composition as the mobile phase. $D_m$-values clearly deviate from the expected trend when the fraction of ACN exceeds 90%. When procainamide hydrochloride is dissolved in a higher percentage of water (80/20 (v/v) $H_2O$/ACN), the obtained $D_m$-values (♦) can be fitted to a second-order polynomial (solid line, $R^2$: 0.992).

### 5.3.1.7 Validation of data with literature results

Finally, the accuracy of the employed methodology was validated by comparing some experimentally obtained $D_m$-values, with values that were previously reported in literature. For this purpose, data reported in four different papers were selected and re-measured using the set-up used in this study [16,35,37,38]. From Table 5.3, it can be deduced that the agreement between our data and values reported in literature is very good, with a maximum relative deviation of 4.0%. This implies that the accuracy of the set-up employed in this work can be considered adequate to construct $D_m$-databases.

**Table 5.3:** Comparison of experimentally measured diffusion coefficients with literature values. The relative deviation is calculated.

| compound | ref. | Experimental conditions (mobile phase; T) | measured $D_m$ ($\times 10^{-9}$ $m^2/s$) | Literature $D_m$ ($\times 10^{-9}$ $m^2/s$) | relative deviation (%) |
|---|---|---|---|---|---|
| thiourea | [34] | $H_2O$; 25°C | 1.34 | 1.33 | 0.5 |
| acetophenone | [13] | ACN/$H_2O$ (30/70 v/v); 40°C | 1.20 | 1.17 | 3.4 |
| toluene | [13] | ACN/$H_2O$ (40/60 v/v); 30°C | 1.19 | 1.17 | 1.7 |
| acetophenone | [31] | ACN/$H_2O$ (75/25 v/v); 23°C | 1.79 | 1.77 | 1.1 |
| thiourea | [31] | ACN/$H_2O$ (75/25 v/v); 23°C | 1.62 | 1.63 | 0.8 |
| valerophenone | [31] | ACN/$H_2O$ (75/25 v/v); 23°C | 1.47 | 1.45 | 1.2 |
| octanophenone | [31] | ACN/$H_2O$ (75/25 v/v); 23°C | 1.26 | 1.24 | 2.0 |
| cytosine | [33] | ACN/5.24 mM ammonium formate pH 3.0 (92.7/7.3 v/v); 30°C | 1.70 | 1.77 | 4.0 |
| nortriptyline | [33] | ACN/5.25 mM ammonium formate pH 3.0 (94.2/5.8 v/v); 30°C | 1.40 | 1.43 | 2.0 |

### 5.3.2 Molecular diffusion coefficients of frequently encountered test compounds under RPLC and HILIC conditions

The methodology described and validated above, was subsequently used to measure the molecular diffusion coefficients of some typical apolar and polar compounds that are frequently encountered in fundamental column performance studies under RPLC and HILIC conditions. Under RPLC and HILIC conditions, diffusion coefficients were measured in water/acetonitrile mixtures wherein the content of acetonitrile varied between 0 and 100% in increments of 20%. Under HILIC conditions, diffusion coefficients were additionally measured in 90%, 95% and 97% acetonitrile, since these reflect realistic HILIC conditions. For the polar compounds (HILIC conditions), the same experiments were also repeated using 5 mM and 10 mM of ammonium acetate buffer (brought to pH= 6.0 using acetic acid) as the aqueous component of the mobile phase. All reported diffusion coefficients were measured at a temperature of 30°C. The obtained data were subsequently fitted to a second-order polynomial:

$$D_m = ax^2 + bx + c \qquad (5.14)$$

Wherein $x$ is the percentage of acetonitrile (% ACN) and a, b and c are the regression coefficients of the second-order polynomial. Figs. 5.3 and 5.4 show some experimentally obtained data points of $D_m$ versus % ACN and the second-order curves fitted to these data points for a number of representative apolar and polar compounds, respectively.

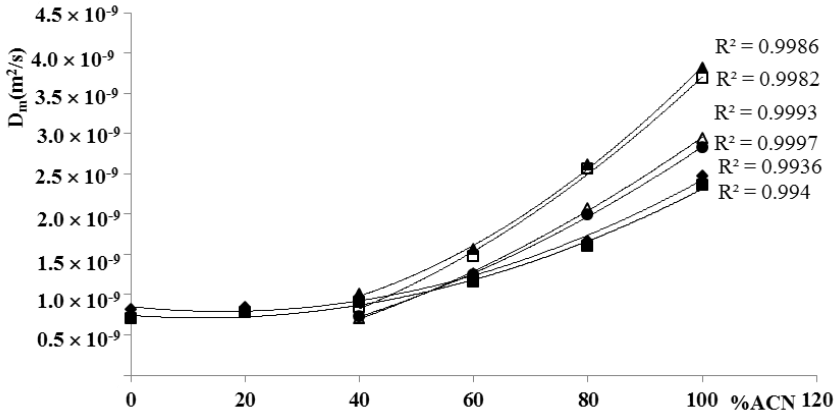


**Figure 5.3:** Examples of second order polynomial curves fitted to experimentally measured $D_m$-data for apolar compounds as a function of the % ACN in the mobile phase at T= 30°C. The aqueous component of the mobile phase was water. Legend: (▲) benzene, (□) toluene, (Δ) butylbenzene, (●) phenanthrene, (♦) methylparaben, (■) ethylparaben. $R^2$-values indicating the goodness of fit are shown.

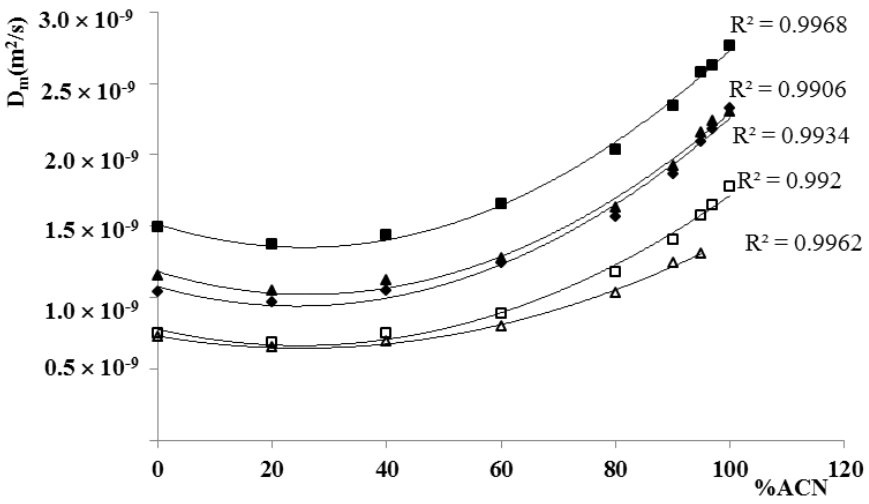


**Figure 5.4:** Examples of second order polynomial curves fitted to experimentally measured $D_m$-data for polar compounds as a function of the % ACN in the mobile phase at T= 30°C. The aqueous component of the mobile phase was water. Legend: (▲) uracil, (□) thymidine, (Δ) guanosine, (♦) thymine, (■) thiourea. $R^2$-values indicating the goodness of fit are shown.

Tables 5.4-5.7 give an overview of all experimentally determined $D_m$-values as a function of the % ACN in the mobile phase (Table 5.4: apolar compounds, Table 5.5: polar compounds using water as the aqueous component of the mobile phase, Table 5.6: polar compounds using 5 mM ammonium acetate and Table 5.7: polar compounds using 10 mM ammonium acetate as the aqueous component of the mobile phase). The values of the a-, b- and c-coefficients are given for each compound, together with the goodness of fit of the second-order polynomial ($R^2$). Note that it was not possible to measure $D_m$-values for each compound over the entire range of acetonitrile compositions. This was due to the fact that under certain mobile phase conditions asymmetrical peaks were obtained (even when the sample solvent composition was adapted as discussed in 5.3.1.6). In this case, the investigated range of mobile phase conditions is clearly specified in Tables 5.4-5.7.

Whereas it was difficult to obtain symmetrical peak shapes for many of the polar compounds at high percentages of ACN (% ACN > 90%) when using pure water as the aqueous component of the mobile phase, peak shapes were significantly improved when adding 5-10 mM ammonium acetate to the mobile phase. This is reflected in the larger range of ACN content that was accessible for $D_m$-measurements in Tables 5.6 and 5.7 and is most likely related to the improved solubility of the compounds in a mobile phase with a somewhat higher ionic strength. Comparing the $D_m$-values obtained when using either 5 mM or 10 mM ammonium acetate as the aqueous component of the mobile phase, a relatively good agreement was found between the obtained $D_m$-values (Tables 5.6-5.7).

The deviation between the values measured in 5 and 10 mM ammonium acetate, calculated as: $deviation\ (\%) = \frac{|D_{m,5\ mM} - D_{m,10\ mM}|}{D_{m,average\ (5-10\ mM)}} \times 100\%$, was generally below 2%, with a few outliers between 2% and maximum 6%. These results indicate that the actual concentration of the buffer does not have a large impact on the measured $D_m$-values.

Comparing the $D_m$-values obtained when using pure water as the aqueous component of the mobile phase (Table 5.5) or ammonium acetate (Tables 5.6-5.7), more pronounced differences in $D_m$ were obtained for several compounds, such as p-xylene-2-sulfonic hydrate, adenosine, potassium iodide, procainamide hydrochloride, benzylamine, nicotinic acid, ascorbic acid, atenolol, benzoic acid and 2-naphthalenesulfonic acid. For these compounds, deviations between the values measured in water on the one hand and 5-10 mM ammonium acetate on the other hand amounted up to 10% and in some cases even 20% or 30% (both positive and negative deviations were observed). These particular compounds were charged at pH= 6.0 (positively or negatively). Differences in $D_m$ for neutral compounds in buffered aqueous phase or pure water were much less pronounced, with differences generally below 5%.

The viscosity of all evaluated mobile phases was measured experimentally [39]. Since only marginal differences in viscosity were observed between purely aqueous and buffered mobile phases, the observed effects cannot be attributed to differences in viscosity and must therefore be related to the ionization of the compounds. These observations suggest that the pH of the buffer could have an effect on the measured diffusion coefficient. A follow-up study will be conducted to investigate the effect of pH and ionization on the obtained diffusion coefficients in more detail. For now, we want to stress that the $D_m$-data presented in this study should only be used for compounds that are evaluated under similar mobile phase conditions (in terms of buffer concentration and pH), at least when ionized compounds are being considered.

**Table 5.4:** Molecular diffusion coefficients ($m^2/s$) of some typical apolar molecules in water-acetonitrile mixtures at 30°C, the regression coefficients and the goodness of fit ($R^2$) of the best fitting second-order polynomial are shown.

| T=30°C | ACN % | | | | | | | | $D_m=ax^2+bx+c$ | | |
|---|---|---|---|---|---|---|---|---|---|---|---|
| Test molecules | 0% | 20% | 40% | 60% | 80% | 100% | Range(%ACN) | $R^2$ | $a\times10^{-9}$ | $b\times10^{-9}$ | $c\times10^{-9}$ |
| acetanilide | 9.56E-10 | 9.18E-10 | 1.04E-09 | 1.31E-09 | 1.8E-09 | 2.64E-09 | 0-100 | 0.997 | 2.605 | -0.986 | 0.982 |
| acetophenone | / | / | 1.19E-09 | 1.57E-09 | 2.24E-09 | 3.15E-09 | 40-100 | 1.000 | 3.396 | -1.477 | 1.238 |
| 3'-methyl acetophenone | / | / | 1.08E-09 | 1.44E-09 | 2.08E-09 | 2.93E-09 | 40-100 | 1.000 | 3.033 | -1.167 | 1.063 |
| propiophenone | / | / | 1.06E-09 | 1.45E-09 | 2.1E-09 | 2.99E-09 | 40-100 | 1.000 | 3.109 | -1.134 | 1.014 |
| butyrophenone | / | / | 9.87E-10 | 1.35E-09 | 1.99E-09 | 2.83E-09 | 40-100 | 1.000 | 2.938 | -1.032 | -0.927 |
| benzophenone | / | / | 9.02E-10 | 1.25E-09 | 1.82E-09 | 2.53E-09 | 40-100 | 1.000 | 2.278 | -0.461 | 0.718 |
| valerophenone | / | / | 9.03E-10 | 1.27E-09 | 1.89E-09 | 2.69E-09 | 40-100 | 1.000 | 2.737 | -0.840 | 0.797 |
| hexanophenone | / | / | 8.56E-10 | 1.18E-09 | 1.8E-09 | 2.54E-09 | 40-100 | 0.999 | 2.603 | -0.804 | 0.753 |
| heptanophenone | / | / | 7.98E-10 | 1.13E-09 | 1.72E-09 | 2.44E-09 | 40-100 | 0.999 | 2.475 | -0.703 | 0.676 |
| octanophenone | / | / | 7.38E-10 | 1.06E-09 | 1.62E-09 | 2.33E-09 | 40-100 | 1.000 | 2.442 | -0.746 | 0.640 |
| methylparaben | 8.12E-10 | 8.42E-10 | 9.62E-10 | 1.22E-09 | 1.67E-09 | 2.47E-09 | 0-100 | 0.994 | 2.315 | -0.741 | 0.850 |
| ethylparaben | 7.01E-10 | 7.81E-10 | 8.99E-10 | 1.16E-09 | 1.6E-09 | 2.35E-09 | 0-100 | 0.994 | 2.081 | -0.511 | 0.742 |
| propylparaben | / | / | 8.55E-10 | 1.1E-09 | 1.55E-09 | 2.25E-09 | 40-100 | 1.000 | 2.851 | -1.670 | 1.070 |
| butylparaben | / | / | 8.11E-10 | 1.06E-09 | 1.48E-09 | 2.17E-09 | 40-100 | 1.000 | 2.804 | -1.670 | 1.036 |
| benzene | / | / | 9.99E-10 | 1.56E-09 | 2.62E-09 | 3.82E-09 | 40-100 | 0.999 | 3.972 | -0.809 | 0.670 |
| butylbenzene | / | / | 7.08E-10 | 1.26E-09 | 2.07E-09 | 2.95E-09 | 40-100 | 0.999 | 1.988 | 0.978 | -0.011 |
| caffeine | 8.84E-10 | 8.38E-10 | 9.38E-10 | 1.16E-09 | 1.55E-09 | 2.32E-09 | 0-100 | 0.993 | 2.346 | -0.982 | 0.912 |
| naphthalene | / | / | 8.21E-10 | 1.4E-09 | 2.26E-09 | 3.23E-09 | 40-100 | 1.000 | 2.457 | 0.598 | 0.180 |
| pyridine | 1.21E-09 | 1.24E-09 | 1.43E-09 | 1.8E-09 | 2.45E-09 | 3.82E-09 | 0-100 | 0.988 | 3.805 | -1.371 | 1.281 |
| phenol | 9.79E-10 | 1.01E-09 | 1.19E-09 | 1.53E-09 | 2.09E-09 | 3.72E-09 | 0-100 | 0.971 | 4.245 | -1.776 | 1.087 |
| toluene | / | / | 8.46E-10 | 1.48E-09 | 2.56E-09 | 3.68E-09 | 40-100 | 0.998 | 3.067 | 0.505 | 0.133 |
| phenanthrene | / | / | 7.32E-10 | 1.25E-09 | 1.99E-09 | 2.83E-09 | 40-100 | 1.000 | 2.033 | 0.672 | 0.131 |

/: asymmetrical peak shape prevented an accurate determination of $D_m$

**Table 5.5:** Molecular diffusion coefficients ($m^2/s$) of some typical polar molecules in water-acetonitrile mixtures at 30°C, the regression coefficients and the goodness of fit ($R^2$) of the best fitting second-order polynomial are shown.

| T=30°C | ACN% | | | | | | | | | | $D_m=ax^2+bx+c$ | | | |
|---|---|---|---|---|---|---|---|---|---|---|---|---|---|---|
| Test molecules | 0% | 20% | 40% | 60% | 80% | 90% | 95% | 97% | 100% | Range (% ACN) | $R^2$ | $a\times10^{-9}$ | $b\times10^{-9}$ | $c\times10^{-9}$ |
| thiourea | 1.50E-09 | 1.37E-09 | 1.43E-09 | 1.66E-09 | 2.04E-09 | 2.34E-09 | 2.58E-09 | 2.63E-09 | 2.77E-09 | 0-100 | 0.997 | 2.489 | -1.271 | 1.514 |
| uracil | 1.16E-09 | 1.05E-09 | 1.12E-09 | 1.28E-09 | 1.63E-09 | 1.92E-09 | 2.16E-09 | 2.24E-09 | 2.30E-09 | 0-100 | 0.993 | 2.333 | -1.222 | 1.183 |
| diphenhydramine hydrochloride | / | / | / | 8.59E-10 | / | / | / | / | / | 60 | / | / | / | / |
| thymine | 1.05E-09 | 9.67E-10 | 1.05E-09 | 1.24E-09 | 1.57E-09 | 1.86E-09 | 2.09E-09 | 2.18E-09 | 2.33E-09 | 0-100 | 0.991 | 2.299 | -1.119 | 1.077 |
| guanosine | 7.26E-10 | 6.51E-10 | 6.97E-10 | 7.98E-10 | 1.03E-09 | 1.24E-09 | 1.31E-09 | / | / | 0-95 | 0.996 | 1.354 | -0.678 | 0.731 |
| thymidine | 7.55E-10 | 6.87E-10 | 7.53E-10 | 8.90E-10 | 1.18E-09 | 1.40E-09 | 1.58E-09 | 1.65E-09 | 1.78E-09 | 0-100 | 0.992 | 1.858 | -0.922 | 0.779 |
| adenosine | 7.35E-10 | 6.62E-10 | 7.19E-10 | 8.44E-10 | 1.11E-09 | 1.33E-09 | 1.50E-09 | 1.54E-09 | / | 0-97 | 0.993 | 1.680 | -0.839 | 0.751 |
| procainamide hydrochloride | 5.97E-10 | 7.01E-10 | 7.97E-10 | 8.94E-10 | / | / | / | / | / | 0-60 | 1.000 | -0.045 | 0.521 | 0.598 |
| benzylamine | / | / | / | 1.13E-09 | / | / | / | / | / | 60 | / | / | / | / |
| adenine | 1.00E-09 | 8.74E-10 | 9.26E-10 | 1.08E-09 | 1.38E-09 | 1.69E-09 | 1.95E-09 | / | / | 0-95 | 0.984 | 2.276 | -1.275 | 1.025 |
| p-xylene-2-sulfonic hydrate | 9.92E-10 | 9.20E-10 | 9.81E-10 | 1.02E-09 | 1.26E-09 | / | / | / | / | 0-80 | 0.966 | 1.085 | -0.543 | 0.993 |
| deoxyuridine | 7.65E-10 | 6.99E-10 | 7.53E-10 | 8.91E-10 | 1.16E-09 | 1.43E-09 | 1.60E-09 | / | / | 0-95 | 0.989 | 1.766 | -0.866 | 0.784 |
| cytosine | 1.11E-09 | 1.00E-09 | 1.04E-09 | 1.15E-09 | 1.39E-09 | 1.71E-09 | 1.84E-09 | / | / | 0-95 | 0.985 | 1.870 | -0.106 | 1.125 |
| nicotinic acid | 1.18E-09 | 1.10E-09 | 1.08E-09 | 1.10E-09 | 1.41E-09 | 1.66E-09 | 1.99E-09 | / | / | 0-95 | 0.939 | 2.236 | -1.463 | 1.234 |
| ascorbic acid | 8.58E-10 | 8.23E-10 | 7.95E-10 | 8.53E-10 | 1.16E-09 | 1.61E-09 | 1.66E-09 | / | / | 0-95 | 0.955 | 2.174 | -1.292 | 0.913 |
| atenolol | 4.89E-10 | 4.87E-10 | 4.77E-10 | 6.27E-10 | 8.53E-10 | 1.08E-09 | 1.23E-09 | / | / | 0-95 | 0.987 | 1.461 | -0.686 | 0.517 |
| cytidine | 7.31E-10 | 6.71E-10 | 7.13E-10 | 8.19E-10 | 1.05E-09 | 1.32E-09 | 1.45E-09 | / | / | 0-95 | 0.986 | 1.603 | -0.826 | 0.752 |
| uridine | 7.37E-10 | 6.79E-10 | 7.28E-10 | 8.52E-10 | 1.11E-09 | 1.38E-09 | 1.54E-09 | / | / | 0-95 | 0.989 | 1.701 | -0.840 | 0.758 |
| nortriptyline hydrochloride | / | / | / | 8.06E-10 | / | / | / | / | / | 60 | / | / | / | / |
| benzoic acid | 8.94E-10 | 9.37E-10 | 9.81E-10 | 1.14E-09 | 1.51E-09 | 1.87E-09 | 2.15E-09 | / | / | 0-95 | 0.973 | 2.211 | -0.942 | 0.954 |
| 2-naphthalene sulfonic acid | 9.47E-10 | 8.61E-10 | 9.18E-10 | 1.06E-09 | 1.31E-09 | 1.58E-09 | 1.84E-09 | 1.96E-09 | 2.01E-09 | 0-100 | 0.979 | 2.197 | -1.211 | 0.986 |
| potassium iodide | 2.12E-09 | 1.83E-09 | 1.76E-09 | 1.81E-09 | 1.97E-09 | 2.21E-09 | 2.26E-09 | / | / | 0-95 | 0.985 | 1.980 | -1.716 | 2.114 |

/: asymmetrical peak shape prevented an accurate determination of $D_m$

**Table 5.6:** Molecular diffusion coefficients ($m^2/s$) of some typical polar molecules in mixtures of 5 mM $NH_4Ac$ (pH 6.0) and acetonitrile at 30°C, the regression coefficients and the goodness of fit ($R^2$) of the best fitting second-order polynomial are shown.

| T=30°C | ACN% | | | | | | | | | | $D_{mol}=ax^2+bx+c$ | | |
|---|---|---|---|---|---|---|---|---|---|---|---|---|---|
| Test molecules | 0% | 20% | 40% | 60% | 80% | 90% | 95% | 97% | Range (% ACN) | $R^2$ | $a\times10^{-9}$ | $b\times10^{-9}$ | $c\times10^{-9}$ |
| thiourea | 1.47E-09 | 1.34E-09 | 1.42E-09 | 1.63E-09 | 2.00E-09 | 2.33E-09 | 2.58E-09 | 2.68E-09 | 0-97 | 0.993 | 2.556 | -1.315 | 1.491 |
| uracil | 1.13E-09 | 1.03E-09 | 1.10E-09 | 1.26E-09 | 1.59E-09 | 1.92E-09 | 2.15E-09 | 2.25E-09 | 0-97 | 0.989 | 2.381 | -1.250 | 1.159 |
| diphenhydramine hydrochloride | / | 4.85E-10 | 6.93E-10 | 9.10E-10 | 1.24E-09 | 1.49E-09 | 1.70E-09 | 1.78E-09 | 20-97 | 0.992 | 1.690 | -0.390 | 0.524 |
| thymine | 1.03E-09 | 9.43E-10 | 1.02E-09 | 1.21E-09 | 1.55E-09 | 1.86E-09 | 2.09E-09 | 2.18E-09 | 0-97 | 0.991 | 2.283 | -1.108 | 1.051 |
| guanosine | 6.97E-10 | 6.31E-10 | 6.77E-10 | 7.81E-10 | 9.92E-10 | 1.22E-09 | 1.34E-09 | / | 0-95 | 0.990 | 1.422 | -0.721 | 0.710 |
| thymidine | 7.22E-10 | 6.67E-10 | 7.31E-10 | 8.71E-10 | 1.14E-09 | 1.40E-09 | 1.58E-09 | 1.64E-09 | 0-97 | 0.991 | 1.785 | -0.847 | 0.745 |
| adenosine | 7.06E-10 | 6.34E-10 | 6.85E-10 | 8.07E-10 | 1.06E-09 | 1.32E-09 | 1.50E-09 | 1.56E-09 | 0-97 | 0.988 | 1.815 | -0.948 | 0.730 |
| procainamide hydrochloride | 6.58E-10 | 6.49E-10 | 7.21E-10 | 8.76E-10 | 1.15E-09 | 1.39E-09 | 1.57E-09 | 1.63E-09 | 0-97 | 0.992 | 1.621 | -0.638 | 0.684 |
| benzylamine | 9.57E-10 | 9.50E-10 | 1.04E-09 | 1.22E-09 | 1.55E-09 | 1.99E-09 | 2.43E-09 | 2.62E-09 | 0-97 | 0.953 | 3.054 | -1.530 | 1.045 |
| adenine | 1.01E-09 | 8.76E-10 | 9.33E-10 | 1.08E-09 | 1.38E-09 | 1.72E-09 | 1.95E-09 | 2.07E-09 | 0-97 | 0.984 | 2.464 | -1.411 | 1.040 |
| p-xylene-2-sulfonic hydrate | 8.97E-10 | 8.37E-10 | 9.04E-10 | 1.05E-09 | 1.24E-09 | 1.53E-09 | 1.77E-09 | 1.91E-09 | 0-97 | 0.964 | 1.984 | -1.034 | 0.935 |
| deoxyuridine | 7.68E-10 | 6.95E-10 | 7.60E-10 | 8.93E-10 | 1.15E-09 | 1.44E-09 | 1.60E-09 | 1.70E-09 | 0-97 | 0.988 | 1.891 | -0.959 | 0.793 |
| cytosine | 1.11E-09 | 1.00E-09 | 1.05E-09 | 1.15E-09 | 1.40E-09 | 1.71E-09 | 1.98E-09 | 2.09E-09 | 0-97 | 0.968 | 2.339 | -1.407 | 1.156 |
| nicotinic acid | 9.72E-10 | 8.72E-10 | 9.04E-10 | 9.76E-10 | 1.15E-09 | 1.44E-09 | 1.72E-09 | 1.75E-09 | 0-97 | 0.950 | 2.046 | -1.291 | 1.015 |
| ascorbic acid | 8.31E-10 | 7.49E-10 | 7.74E-10 | 8.13E-10 | 9.98E-10 | 1.28E-09 | 1.40E-09 | / | 0-95 | 0.962 | 1.592 | -0.987 | 0.859 |
| atenolol | 6.91E-10 | 6.00E-10 | 6.69E-10 | 7.96E-10 | 9.99E-10 | 1.16E-09 | 1.38E-09 | 1.40E-09 | 0-97 | 0.982 | 1.505 | -0.765 | 0.699 |
| cytidine | 7.35E-10 | 6.73E-10 | 7.21E-10 | 8.23E-10 | 1.06E-09 | 1.31E-09 | 1.48E-09 | 1.41E-09 | 0-97 | 0.984 | 1.540 | -0.776 | 0.752 |
| uridine | 7.42E-10 | 6.81E-10 | 7.38E-10 | 8.57E-10 | 1.11E-09 | 1.37E-09 | 1.55E-09 | 1.62E-09 | 0-97 | 0.987 | 1.789 | -0.906 | 0.768 |
| nortriptyline hydrochloride | / | / | / | 8.43E-10 | 1.16E-09 | 1.36E-09 | 1.48E-09 | 1.50E-09 | 60-97 | 1.000 | 1.239 | 2.301 | 0.435 |
| benzoic acid | 9.55E-10 | 8.94E-10 | 9.42E-10 | 1.04E-09 | 1.27E-09 | 1.63E-09 | 2.02E-09 | 2.21E-09 | 0-97 | 0.930 | 2.712 | -1.609 | 1.034 |
| 2-naphthalene sulfonic acid | 8.96E-10 | 8.08E-10 | 8.65E-10 | 1.01E-09 | 1.25E-09 | 1.50E-09 | 1.71E-09 | 1.83E-09 | 0-97 | 0.981 | 1.952 | -1.046 | 0.922 |
| guanine | 9.56E-10 | 8.40E-10 | 8.74E-10 | 9.86E-10 | 1.23E-09 | / | / | / | 0-80 | 0.997 | 1.428 | -0.796 | -0.796 |
| potassium iodide | 2.15E-09 | 1.82E-09 | 1.76E-09 | 1.84E-09 | 2.02E-09 | 2.29E-09 | 2.55E-09 | 2.69E-09 | 0-97 | 0.957 | 2.788 | -2.275 | 2.169 |

/: asymmetrical peak shape prevented an accurate determination of $D_m$

**Table 5.7:** Molecular diffusion coefficients ($m^2/s$) of some typical polar molecules in mixtures of 10 mM $NH_4Ac$ (pH 6.0) and acetonitrile at 30°C, the regression coefficients and the goodness of fit ($R^2$) of the best fitting second-order polynomial are shown.

| T=30°C | ACN% | | | | | | | | | | $D_m=ax^2+bx+c$ | | |
|---|---|---|---|---|---|---|---|---|---|---|---|---|---|
| Test molecules | 0% | 20% | 40% | 60% | 80% | 90% | 95% | 97% | Range (%ACN) | $R^2$ | $a\times10^{-9}$ | $b\times10^{-9}$ | $c\times10^{-9}$ |
| thiourea | 1.47E-09 | 1.32E-09 | 1.42E-09 | 1.61E-09 | 1.98E-09 | 2.32E-09 | 2.56E-09 | 2.67E-09 | 0-97 | 0.992 | 2.584 | -1.346 | 1.484 |
| uracil | 1.13E-09 | 1.03E-09 | 1.09E-09 | 1.25E-09 | 1.58E-09 | 1.90E-09 | 2.14E-09 | 2.25E-09 | 0-97 | 0.987 | 2.380 | -1.257 | 1.158 |
| diphenhydramine hydrochloride | / | 4.97E-10 | 6.80E-10 | 9.02E-10 | 1.20E-09 | 1.45E-09 | 1.66E-09 | 1.76E-09 | 20-97 | 0.990 | 1.731 | -0.500 | 0.556 |
| thymine | 1.03E-09 | 9.40E-10 | 1.02E-09 | 1.20E-09 | 1.53E-09 | 1.85E-09 | 2.07E-09 | 2.18E-09 | 0-97 | 0.990 | 2.283 | -1.120 | 1.053 |
| guanosine | 6.94E-10 | 6.27E-10 | 6.77E-10 | 7.67E-10 | 9.89E-10 | 1.21E-09 | 1.32E-09 | / | 0-95 | 0.991 | 1.411 | -0.719 | 0.707 |
| thymidine | 7.20E-10 | 6.63E-10 | 7.29E-10 | 8.68E-10 | 1.13E-09 | 1.40E-09 | 1.55E-09 | 1.65E-09 | 0-97 | 0.990 | 1.778 | -0.849 | 0.743 |
| adenosine | 7.02E-10 | 6.37E-10 | 6.85E-10 | 7.98E-10 | 1.05E-09 | 1.31E-09 | 1.49E-09 | 1.56E-09 | 0-97 | 0.986 | 1.821 | -0.961 | 0.731 |
| procainamide hydrochloride | 6.44E-10 | 6.35E-10 | 7.12E-10 | 8.58E-10 | 1.13E-09 | 1.36E-09 | 1.54E-09 | 1.62E-09 | 0-97 | 0.991 | 1.602 | -0.630 | 0.670 |
| benzylamine | 9.55E-10 | 9.19E-10 | 1.02E-09 | 1.18E-09 | 1.48E-09 | 1.88E-09 | 2.36E-09 | 2.54E-09 | 0-97 | 0.944 | 3.005 | -1.565 | 1.039 |
| adenine | 9.91E-10 | 8.73E-10 | 9.25E-10 | 1.07E-09 | 1.37E-09 | 1.67E-09 | 1.91E-09 | 2.06E-09 | 0-97 | 0.981 | 2.393 | -1.358 | 1.024 |
| p-xylene-2-sulfonic hydrate | 8.86E-10 | 8.19E-10 | 8.92E-10 | 1.01E-09 | 1.21E-09 | 1.45E-09 | 1.70E-09 | 1.86E-09 | 0-97 | 0.956 | 1.898 | -1.009 | 0.922 |
| deoxyuridine | 7.62E-10 | 6.94E-10 | 7.51E-10 | 8.81E-10 | 1.14E-09 | 1.41E-09 | 1.59E-09 | 1.70E-09 | 0-97 | 0.985 | 1.907 | -0.983 | 0.790 |
| cytosine | 1.10E-09 | 9.91E-10 | 1.03E-09 | 1.13E-09 | 1.36E-09 | 1.66E-09 | 1.92E-09 | 2.04E-09 | 0-97 | 0.964 | 2.249 | -1.362 | 1.142 |
| nicotinic acid | 9.67E-10 | 8.70E-10 | 9.01E-10 | 9.67E-10 | 1.14E-09 | 1.42E-09 | 1.72E-09 | 1.79E-09 | 0-97 | 0.941 | 2.107 | -1.341 | 1.015 |
| ascorbic acid | 8.27E-10 | 7.41E-10 | 7.62E-10 | 8.07E-10 | 1.16E-09 | 1.26E-09 | 1.43E-09 | 1.48E-09 | 0-97 | 0.987 | 1.634 | -0.953 | 0.846 |
| atenolol | 6.74E-10 | 6.09E-10 | 6.48E-10 | 7.90E-10 | 1.01E-09 | 1.21E-09 | 1.38E-09 | 1.48E-09 | 0-97 | 0.985 | 1.630 | -0.835 | 0.694 |
| cytidine | 7.29E-10 | 6.66E-10 | 7.17E-10 | 8.15E-10 | 1.04E-09 | 1.29E-09 | 1.45E-09 | 1.40E-09 | 0-97 | 0.986 | 1.523 | -0.771 | 0.746 |
| uridine | 7.35E-10 | 6.74E-10 | 7.32E-10 | 8.49E-10 | 1.11E-09 | 1.35E-09 | 1.52E-09 | 1.60E-09 | 0-97 | 0.989 | 1.747 | -0.879 | 0.759 |
| nortriptyline hydrochloride | / | / | / | 8.48E-10 | 1.13E-09 | 1.33E-09 | 1.47E-09 | 1.47E-09 | 60-97 | 0.999 | -1.101 | 1.677 | 0.843 |
| benzoic acid | 9.58E-10 | 8.85E-10 | 9.40E-10 | 1.02E-09 | 1.25E-09 | 1.58E-09 | 1.99E-09 | 2.21E-09 | 0-97 | 0.919 | 2.723 | -1.648 | 1.037 |
| 2-naphthalene sulfonic acid | 8.84E-10 | 8.06E-10 | 8.49E-10 | 9.99E-10 | 1.22E-09 | 1.46E-09 | 1.67E-09 | 1.81E-09 | 0-97 | 0.975 | 1.909 | -1.029 | 0.913 |
| guanine | 9.58E-10 | 8.27E-10 | 8.70E-10 | 9.80E-10 | 1.22E-09 | / | / | / | 0-80 | 0.993 | 1.449 | -0.819 | 0.951 |
| potassium iodide | 2.14E-09 | 1.82E-09 | 1.75E-09 | 1.84E-09 | 2.00E-09 | 2.28E-09 | 2.55E-09 | 2.68E-09 | 0-97 | 0.950 | 2.779 | -2.269 | 2.160 |

/: asymmetrical peak shape prevented an accurate determination of $D_m$

## 5.4. Conclusions

The Taylor-Aris methodology is employed to measure molecular diffusion coefficients ($D_m$) of a large number of polar and apolar compounds in a wide range of mobile phase compositions typically used in reversed-phase liquid chromatography (RPLC) and hydrophilic interaction liquid chromatography (HILIC) studies. For this purpose, the peak broadening of a solute is measured when flowing through a long, open tube. The experimental conditions (dimensions of the open tube, flow rate, injection volume) are chosen such that the effects of longitudinal diffusion, secondary flows and extra-column volumes on the observed peak broadening can be excluded. The length of the employed capillary (15.32 m) is moreover demonstrated to be long enough to ensure effective radial equilibration of the sample plug, even for the smallest encountered diffusion coefficients.

In cases where solute solubility problems occur (for polar compounds in large percentages of ACN), it is demonstrated that these solutes can be dissolved in a slightly larger percentage of water with respect to the mobile phase. Measuring the diffusion coefficient of benzene, dissolved in varying percentages of water, in a mobile phase consisting of pure acetonitrile, it is shown that the percentage of water in the sample solvent can deviate with as much as 30% from the mobile phase composition, without affecting the value of the diffusion coefficient.

A database containing molecular diffusion coefficients of some 45 polar and apolar solutes that are frequently used as test molecules in RPLC and HILIC column evaluation studies is subsequently presented using the described methodology. It is shown that diffusion coefficients measured in discrete percentages of ACN can be fitted relatively well to second-order polynomials, enabling to deduce $D_m$-values for any desired composition of the mobile phase. Finally, it is demonstrated that replacing water in the mobile phase by an aqueous solution of a salt such as ammonium acetate, mainly influences the $D_m$-values of charged molecules.

**5.5. References**

[1] D. Guillarme, J. Ruta, S. Rudaz, J. Veuthey, New trends in fast and high-resolution liquid chromatography : a critical comparison of existing approaches, (2010) 1069–1082.

[2] J. Ruta, D. Zurlino, C. Grivel, S. Heinisch, J. Veuthey, D. Guillarme, Evaluation of columns packed with shell particles with compounds of pharmaceutical interest, J. Chromatogr. A. 1228 (2012) 221–231.

[3] S. Fekete, E. Olàh, J. Fekete, Fast liquid chromatography : The domination of core – shell and very fine particles, J. Chromatogr. A. 1228 (2012) 57–71.

[4] C. Giddings, Dynamics of Chromatography: Principles and Theory, New York, 1965.

[5] J.H. Knox, H.P. Scott, B and C terms in the Van Deemter equation for liquid chromatography, J. Chromatogr. A. 282 (1983) 297–313.

[6] G. Desmet, D. Clicq, P. Gzil, Geometry-independent plate height representation methods for the direct comparison of the kinetic performance of LC supports with a different size or morphology, Anal. Chem. 77 (2005) 4058–4070.

[7] G. Desmet, K. Broeckhoven, Equivalence of the different Cm- and Cs- term expressions used in liquid chromatography and a geometrical model uniting them, Anal. Chem. 80 (2008) 8076–8088.

[8] L. Lapidus, N.R. Amundson, Mathematics of Adsorption in Beds. VI. The Effect of Longitudinal Diffusion in Ion Exchange and Chromatographic Columns, J. Phys. Chem. 56 (1952) 984–988.

[9] J. Huber, High Efficiency, High Speed Liquid Chromatography in Columns, J. Chromatogr. Sci. 7 (1969) 85–90.

[10] E. Kucera, Contribution to the theory of chromatography: linear non-equilibrium elution chromatography., J. Chromatogr. 19 (1965) 237–248.

[11] C. Horvath, H.-J. Lin, Movement and band spreading liquid chromatography, J. Chromatogr. 126 (1976) 401–420.

[12] C. Wilke, P. Chang, Correlation of diffusion coefficients in dilute solutions, AIChE J. 1 (1955) 264–270.

[13] E.G. Scheibel, Liquid Diffusivities, Ind. Eng. Chem. 46 (1954) 2007–2008.

[14] W. Hayduk, H. Laudie, Prediction of diffusion coefficients for nonelectrolytes in dilute aqueous solutions, AIChE J. 20 (1974) 611–615.

[15] N. Miložič, M. Lubej, U. Novak, I. Plazl, Evaluation of Diffusion Coefficient Determination using a Microfluidic Device, Chem. Biochem. Eng. Q. 28 (2014) 215–223.

[16] J. Li, P.W. Carr, Accuracy of empirical correlations for estimating diffusion coefficients in aqueous organic mixtures., Anal. Chem. 69 (1997) 2530–2536.

[17] B. Chauve, D. Guillarme, P. Cléon, J.L. Veuthey, Evaluation of various HILIC materials for the fast separation of polar compounds, J. Sep. Sci. 33 (2010) 752–764.

[18] D.V. McCalley, Is hydrophilic interaction chromatography with silica columns a viable alternative to reversed-phase liquid chromatography for the analysis of ionisable compounds?, J. Chromatogr. A. 1171 (2007) 46–55.

[19] L. Nováková, L. Havlíková, H. Vlčková, Hydrophilic interaction chromatography of polar and ionizable compounds by UHPLC, Trends Anal. Chem. 63 (2014) 55–64.

[20] G. Kahsay, H. Song, A. Van Schepdael, D. Cabooter, E. Adams, Hydrophilic interaction chromatography (HILIC) in the analysis of antibiotics, J. Pharm. Biomed. Anal. 87 (2014) 142–154.

[21] J. Heaton, N. Gray, D. a. Cowan, R.S. Plumb, C. Legido-Quigley, N.W. Smith, Comparison of reversed-phase and hydrophilic interaction liquid chromatography for the separation of ephedrines, J. Chromatogr. A. 1228 (2012) 329–337.

[22] F. Gritti, G. Guiochon, Mass transfer mechanism in hydrophilic interaction chromatography, J. Chromatogr. A. 1302 (2013) 55–64.

[23] H. Song, E. Adams, G. Desmet, D. Cabooter, Evaluation and comparison of the kinetic performance of ultra-high performance liquid chromatography and high-performance liquid chromatography columns in hydrophilic interaction and reversed-phase liquid chromatography conditions, J. Chromatogr. A. 1369 (2014) 83–91.

[24] B.R.H. Stokes, An Improved Diaphragm-cell for Diffusion Studies , and Some Tests of the Method, J. Am. Chem. Soc. 72 (1950) 763–767.

[25] W. Krahn, G. Schwelger, K. Lucas, Light scattering measurements of mutual diffusion coefficients in binary liquid mixtures, (1983) 4515–4519.

[26] E.O. Stejskal, J.E. Tanner, Spin Diffusion Measurements : Spin Echoes in the Presence of a Time Dependent Field Gradient, J. Chem. Phys. 42 (1964) 288-292.

[27] G. Taylor, Dispersion of Soluble Matter in Solvent Flowing Slowly through a Tube, Proc. R. Soc. Lond. A. 219 (1953) 186–203.

[28] K. Miyabe, J. Nagai, G. Guiochon, Peak parking-moment analysis : A strategy for the measurement of molecular diffusivity in liquid phase, Chem. Eng. Sci. 65 (2010) 3859–3864.

[29] R. Aris, On the dispersion of a solute in a fluid flowing through a tube, Proc. R. Soc. Lond. A. 235 (1956) 67–77.

[30] K. Broeckhoven, G. Desmet, Numerical and analytical solutions for the column length-dependent band broadening originating from axisymmetrical trans-column velocity gradients, J. Chromatogr. A. 1216 (2009) 1325–1337.

[31] Y. Vanderheyden, K. Broeckhoven, G. Desmet, Comparison and optimization of different peak integration methods to determine the variance of unretained and extra-column peaks, J. Chromatogr. A. 1364 (2014) 140–150.

[32] U.D. Neue, HPLC Columns: Theory, Technology and Practice, Wiley-VCH, New York, 1997.

[33] H. Poppe, Column liquid chromatography, in: E. Heftmann (Ed.), J. Chromatogr. Libr., Elsevier, New York, 1992: pp. A151–225.

[34] J.G. Atwood, J. Goldstein, Measurements of Diffusion Coefficients in Liquids at Atmospheric and Elevated Pressure by the Chromatographic Broadening Technique, J. Phys. Chem. 88 (1984) 1875–1885.

[35] F. Gritti, S.J. Shiner, J.N. Fairchild, G. Guiochon, Evaluation of the kinetic performance of new prototype superficially porous particles, J. Chromatogr. A. 1334 (2014) 30–43.

[36] L.A.M. Janssen, Axial dispersion in laminar flow, Chem. Eng. Sci. 31 (1976) 215–218.

[37] J.C. Heaton, X. Wang, W.E. Barber, S.M.C. Buckenmaier, D. V. McCalley, Practical observations on the performance of bare silica in hydrophilic interaction compared with C18 reversed-phase liquid chromatography, J. Chromatogr. A. 1328 (2014) 7–15.

[38] D.B. Ludlum, R.C. Warner, H.W. Smith, The diffusion of thiourea in water at 25°C, J. Phys. Chem. 66 (1962) 1540–1542.

[39] J. Billen, K. Broeckhoven, A. Liekens, K. Choikhet, G. Rozing, G. Desmet, Influence of pressure and temperature on the physico-chemical properties of mobile phase mixtures commonly used in high-performance liquid chromatography, J. Chromatogr. A. 1210 (2008) 30-44.

# Chapter 6

# General Discussion and Future Prospects

## 6.1. Introduction

High-performance liquid chromatography is a well-established separation technique in the pharmaceutical industry, largely due to its many positive features such as robustness, ease of operation, well-understood separation principles, sensitivity and tunable selectivity. Almost 90% of all separations in HPLC are performed in the reversed phase mode. However, the growing demand for the analysis of various small polar and ionizable compounds has promoted the interest in HILIC in the past years. The large volume fraction of volatile organic solvent (ACN) used in HILIC mobile phases makes it compatible with mass spectrometry, and increases the ESI-MS sensitivity significantly [1].

The main limitation of HPLC is the relatively low efficiency, which is due to the slow diffusion of analytes in the stationary phase. For packed columns, the use of smaller particles to shorten the analytes' diffusion path is currently the most prevalent approach to increase the separation efficiency. UHPLC columns ($d_p$= sub-2 µm) have been introduced on the market for this purpose, however, with a higher backpressure as a logical consequence. In 2004, an ultra-high pressure liquid chromatography (UPLC®) system was developed by Waters, which can deliver pressures up to 1000-1200 bar. Besides from the obvious demands placed on HPLC hardware, the packing quality of UHPLC columns is another issue, as it is more difficult to prepare well-packed beds with small particle diameters (sub-2 µm) compared to large ones (≥ 3.0-3.5 µm).

## 6.2. Evaluation and comparison of the performance of UHPLC and HPLC under HILIC and RPLC conditions

In the first experimental part of this thesis (chapter 3), the kinetic performance of UHPLC and HPLC columns under HILIC and RPLC conditions was compared using commercially available columns. Kinetic plots ($t_i$ versus N) allowed assessing that the gain in analysis time obtained by switching from HPLC to UHPLC columns under HILIC conditions is comparable or even slightly larger than under RPLC conditions, mainly due to the much lower viscosity of the mobile phase used in HILIC. This can potentially lead to a large increase in the transfer of existing HILIC HPLC methods to UHPLC conditions to speed up the analysis, as had been witnessed for RPLC methods in the past decade.

When transferring methods from HPLC to UHPLC conditions, it must, however, be taken into account that ultra-high pressures affect the mobile phase density, viscosity and diffusion coefficients, and also lead to the formation of non-uniform temperature gradients within the column as a result of frictional heating [2-3]. Since ACN-enriched (HILIC conditions) and water-enriched (RPLC conditions) mobile phases have different heat conductivities, it is expected that mobile phases with a higher organic content can potentially lead to larger frictional heating effects than water-rich mobile phases [4], especially when both are considered at the same maximum pressures. This is a topic that needs to be taken into consideration and further needs to be investigated before general conclusions on method transfer from HPLC to UHPLC in HILIC can be made.

### 6.3. Investigation of band broadening phenomena for HILIC and RPLC columns under identical packing conditions

The significantly higher external porosities of HILIC columns compared to that of RPLC columns, observed in chapter 3, point at important differences in packing structure [5]. These packing differences may affect and bias any observed difference in mass transfer properties between HILIC and RPLC. Therefore, the evaluation of column performance under HILIC and RPLC conditions without having to account for differences in packing structure was carried out by developing a completely novel protocol in chapter 4 [6]. The proof-of-principle of this protocol was presented for two 50 × 4.6 mm HPLC columns evaluated for compounds with zone retention factors ranging between k"= 5.5 and 16.5.

To further study the underlying mechanisms of intra-particle diffusivity and accurately assess their effect on mass transfer phenomena observed under HILIC and RPLC conditions, this protocol will now also be applied to 250 × 4.6 mm columns using a set of test compounds displaying a broader range of zone retention factors (k"= 0 to 10) to evaluate band broadening under RPLC and HILIC conditions. Plate height data will be collected for a large range of interstitial velocities to cover the different contributions to band broadening. A larger column volume will be used to adequately rule out any possible influence of extra-column contributions.

### 6.4. Evaluation of differences in intra-particle diffusion under HILIC and RPLC conditions

The longitudinal diffusion (b-term) can be accurately measured by the peak parking method. Once the contribution of the b-term under HILIC and RPLC conditions and under identical packing conditions is accurately known, the contribution of intra-particle diffusivity will be deduced by modeling the b-term to an effective medium theory based expression [7]. This expression relates intra-particle diffusivity to longitudinal diffusivity via a number of geometrical parameters. Since the column being evaluated under HILIC and RPLC conditions will be exactly the same, all geometrical parameters will be maintained and the abstraction of these parameters will allow comparing intra-particle diffusivity under RPLC and HILIC conditions. Once the contribution of the intra-particle diffusivity is known, a similar approach can be followed to relate differences in intra-particle diffusivity to differences in surface diffusion and diffusion in the stagnant mobile phase in the pores. The approach assumes an accurate knowledge of a number of geometrical parameters inside the column that will again be largely simplified by the fact that the same column will be assessed under HILIC and RPLC conditions.

Through this approach, it will be investigated whether analytes with similar retention factors experience differences in intra-particle diffusion through different contributions of diffusion in the stagnant mobile phase in the pores and surface diffusion under HILIC and RPLC conditions. This will lead to important insights in the contribution of retention mechanism, pore geometry and pore size on the observed intra-particle diffusivity. The described approach will allow comparing intra-particle diffusion under HILIC and RPLC conditions with a high accuracy and will therefore lead to unprecedented results, since an accurate knowledge on geometrical column parameters will be largely redundant.

### 6.5. Assessment of different contributions to eddy dispersion under HILIC and RPLC conditions

An accurate knowledge of the intra-particle diffusivity will allow extracting both b- and c-term contributions from the observed plate height data, which will again be simplified by the preservation of the most important geometrical factors within the column under HILIC and RPLC

conditions. This will result in the pure contribution of eddy dispersion, a factor that has a large impact on the overall performance of chromatographic columns. It will then be attempted to extract the different contributions to eddy dispersion, namely trans-channel, short-range inter-channel and trans-column eddy dispersion from the remaining plate height contribution [8]. The trans-channel contribution will be estimated by numerically solving the Navier-Stokes equation and simulating the advection-diffusion process [9]. Such attempt has up-to-date not yet been made for porous particles and will be simplified tremendously by the constant column geometry encountered in this study.

In a similar fashion, the contribution of the short-range inter-channel contribution will be estimated. Subtraction of these two contributions (short-range inter-channel and trans-channel) from the overall observed eddy dispersion will then result in the contribution of the trans-column eddy dispersion, which is affected by the trans-column structural heterogeneity of the packed bed and the inlet and outlet frit and end fitting assemblies of the column. It is expected that these observations will lead to a thorough understanding of the extent to which column end fitting design, sample distribution and collection in the column and wall and border effects influence the overall band spreading in RPLC and HILIC columns. This could potentially lead to the proposition of new column designs and formats, separately optimized for HILIC and RPLC separations.

### 6.6. Development of a novel approach to estimate longitudinal diffusion

As we know from previous sections, the accurate determination of longitudinal diffusion (b-term) is the cornerstone of fundamental mass transfer studies in HILIC and RPLC. Longitudinal diffusion is commonly measured by the peak parking (PP) method [10]. Since in practice this method is very time-consuming, it will be investigated whether a more straightforward protocol can be developed to extract the b-term by fitting experimental plate height data to a plate height model such as the van Deemter or Knox equation [11-12]. The accuracy of the fitted data will be verified by PP experiments. A possible way to do this would be to assign an arbitrary value to the b-term and subtract this value from the overall plate height. A plot of the plate height value minus the b-term contribution as a function of the interstitial velocity should in principle result in a

straight curve through the origin for a restricted number of interstitial velocities in the lower range. This should allow iterating the correct value of the b-term.

### 6.7. Measuring liquid phase diffusion coefficients in HILIC and RPLC

For column developers and producers, a correct knowledge of molecular diffusion coefficients is crucial to investigate each contribution to band broadening in detail. In chapter 5, a database containing molecular diffusion coefficients of some frequently used test molecules in RPLC and HILIC column evaluation studies was presented using the Taylor-Aris methodology. Although this method is easily carried out and gives sufficient accuracy, the measurement is relatively time-consuming, with each analysis taking around 45 min. To speed up the methodology, it will be investigated whether the long PEEK tube (~15 m) that is currently used can be replaced with shorter ones. A risk herein is that the contribution to the plate height from radial diffusion may not be complete in shorter tubing lengths, which will inevitably lead to erroneous values of the obtained diffusion coefficients. Therefore, it will be investigated whether a strategy can be elaborated to correct for this incomplete radial diffusion. This will be based on the work of Broeckhoven and Desmet [13].

**6.8. References**

[1] Grumbach, E. S.; Diehi, D. M., Neue, U. D., J. Sep. Sci. 2008, 31, 1511-1518.

[2] Martin, M.; Guiochon, G., J. Chromatogr. A 2005, 1090, 16-38.

[3] Halasz, I.; Endele, R.; Asshauer, J., J. Chromatogr. 1975, 112, 37-60.

[4] Fallas, M. M.; Neue, U. D.; Hadley, M. R.; McCalley, D. V., J. Chromatogr. A 2010, 1217, 276-284.

[5] Song, H.; Adams, E.; Desmet, G.; Cabooter, D., J. Chromatogr. A 2014, 1369, 83-91.

[6] Song, H.; Desmet, G.; Cabooter, D., Anal. Chem. 2015, 87, 12331-12339.

[7] Desmet, G.; Deridder, S., J. Chromatogr. A 2011, 1218, 32-45.

[8] Giddings, J.C., Dynamics of chromatography, principles and theory. Marcel dekker, INC, New York, 1965.

[9] Khirevich, S.; Daneyko, A.; Höltzel, A.; Seidel-Morgenstern, A.; Tallarek, U., J. Chromatogr. A 2010, 1217, 4713-4722.

[10] Miyabe, K.; Nagai, J.-I.; Guiochon, G., Chem. Eng. Sci. 2010, 65, 3859-3864.

[11] van Deemter, J. J.; Zuiderweg, F. J.; Klinkenberg, A., Chem. Eng. Sci. 1956, 5, 271-289.

[12] Knox, J. H.; Scott, H. P., J. Chromatogr. A 1983, 282, 297-313.

[13] Broeckhoven, K.; Desmet, G., J. Chromatogr. A 2009, 1216, 1325-1337.

# Chapter 7

## Summary

In the present thesis, HILIC and RPLC columns were evaluated and compared to assess the true performance potential of the different supports. This comparison was first carried out for six commercially available columns in **Chapter 3**. The higher external porosity and larger minimum separation impedance ($E_{min}$) of the HILIC columns indicated that HILIC columns have a lower packing quality than their RPLC counterparts. It was also demonstrated that the column dead volume ($t_0$) can be severely under- or overestimated depending on the mobile phase conditions used and this can lead to biased permeability ($K_{v0}$) values. Therefore, to omit errors that might arise from an inaccurate assessment of the column dead volume, all plate height and kinetic plot data were expressed as a function of the interstitial velocity ($u_i$).

Comparing the van Deemter curves obtained for HILIC and RPLC columns, it was found that HILIC columns have lower column efficiencies. However, for the kinetic performance comparison, both stationary phase types performed similar. A slightly larger reduction in analysis time was obtained when switching from HPLC columns to UHPLC formats in HILIC. This theoretical finding was also demonstrated for the practical separation of tetracycline and its main impurities and was attributed to the much lower viscosity of the mobile phase used under HILIC conditions.

Although the selected RPLC and HILIC columns were obtained from the same manufacturer, using the same native silica for their HILIC and RPLC columns, differences in packing quality were unavoidable. Since these packing differences can have a large influence on the observed kinetic performance, a novel protocol was developed in **Chapter 4** to compare HILIC and RPLC columns under conditions of identical packing structure. This was done by developing a stripping procedure for the adequate removal of the stationary phase of RPLC columns. In this way, the same column could first be studied under RPLC conditions and subsequently under HILIC conditions. The complete removal of the stationary phase was confirmed by retention studies and thermogravimetric analyses. Moreover, an unchanged external porosity and pressure drop confirmed that the stripping protocol left the column structure unaffected.

An accurate plate height analysis under both retention mechanisms demonstrated that the reduced c-term is significantly larger under HILIC conditions, while the b-term is significantly lower.

Band broadening originating from eddy diffusion, which is normally ascribed to phenomena occurring outside the particles, was also demonstrated to be higher under HILIC conditions. Since the comparison under HILIC and RPLC conditions was performed under conditions of identical packing quality, it was concluded that both the retention mechanism and the internal structure of the particle have a strong influence on the observed eddy dispersion. This makes the comparison of the packing quality of different particle types almost impossible without appropriate means to correct for the intra-particle effect on the observed eddy diffusion.

Accurate molecular diffusion coefficient ($D_m$) values in different mobile phases are crucial in fundamental studies of column performance. In **Chapter 5**, the Taylor-Aris method was employed to measure the $D_m$-values of 45 polar and apolar compounds in a wide range of mobile phase compositions typically used in RPLC and HILIC studies. These values were fitted relatively well to second-order polynomials, enabling to deduce $D_m$-values for these compounds in any desired composition of the mobile phase. It was also demonstrated that the buffer concentration has an influence on the molecular diffusion of charged molecules.

To conclude, some future prospects were made in **Chapter 6**. A potentially new approach to estimate longitudinal diffusion efficiently was discussed. Further application of the stripping protocol to a set of compounds showing a broader range of zone retention factors (k''= 0 to 10) to study the mechanisms of intra-particle diffusivity and different contributions to eddy dispersion under HILIC and RP conditions was discussed as well.

# Samenvatting

In de huidige thesis werden HILIC en RPLC kolommen geëvalueerd en vergeleken om het echte performantie potentieel van de verschillende kolommen te bepalen. Deze vergelijking werd eerst uitgevoerd voor zes commercieel beschikbare kolommen in **Hoofdstuk 3**. De hogere externe porositeit en minimale scheidingsimpedantie ($E_{min}$) van de HILIC kolommen toonden aan dat de HILIC kolommen een lagere pakkingskwaliteit vertonen in vergelijking met de RPLC kolommen. Er werd ook aangetoond dat de kolom dode tijd ($t_0$) beduidend kan onder- of overschat worden afhankelijk van de mobiele fase condities en dat dit tot verkeerde permeabiliteitswaarden ($K_{v0}$) kan leiden. Om fouten die zouden kunnen voortvloeien uit een inaccurate bepaling van de kolom dode tijd te voorkomen, werden alle plaathoogte en kinetic plot data daarom uitgedrukt in functie van de interstitiële snelheid ($u_i$).

Uit de vergelijking van de van Deemter curven die bekomen werden voor de HILIC en RPLC kolommen werd afgeleid dat HILIC kolommen lagere kolomefficiënties hebben. De kinetische performantie van beide stationaire fase types was echter dezelfde. Een iets grotere reductie in analysetijd werd bekomen wanneer er van HPLC naar UHPLC kolommen werd overgegaan in HILIC. Deze theoretische bevinding werd ook aangetoond voor de praktische scheiding van tetracycline en zijn belangrijkste onzuiverheden. Deze waarneming werd verklaard door de veel lagere viscositeit van de mobiele fase onder HILIC condities.

Alhoewel de geëvalueerde RPLC en HILIC kolommen werden bekomen van dezelfde fabrikant, die hetzelfde silica materiaal gebruikte als uitgangsmateriaal voor zijn HILIC en RPLC kolommen, waren verschillen in pakkingskwaliteit onvermijdelijk. Aangezien deze verschillen in pakking een grote invloed kunnen hebben op de waargenomen kinetische performantie, werd een nieuw protocol ontwikkeld om HILIC en RPLC kolommen te vergelijken onder identieke pakkingscondities in **Hoofdstuk 4**. Dit protocol bestond uit een strippingsprocedure die toeliet de stationaire fase van RPLC kolommen adequaat te verwijderen. Op deze manier kon dezelfde kolom eerst onder RPLC condities bestudeerd worden en vervolgens onder HILIC condities. De volledige verwijdering van de stationaire fase werd bevestigd door retentiestudies en thermogravimetrische analyses. Een onveranderde externe porositeit en drukval bevestigden bovendien dat de kolomstructuur niet werd aangetast door de strippingsprocedure.

Een accurate analyse van de plaathoogte onder beide retentiemechanismen toonde aan dat de gereduceerde c-term veel groter is onder HILIC condities, terwijl de gereduceerde b-term significant kleiner is. Piekverbreding afkomstig van eddy diffusie, die normaal wordt toegekend aan fenomenen die zich afspelen buiten de partikels, was ook groter onder HILIC condities.

Aangezien de vergelijking onder HILIC en RPLC condities werd uitgevoerd voor identieke pakkingsstructuren, werd besloten dat zowel het retentiemechanisme als de interne structuur van het partikel een grote invloed hebben op de waargenomen eddy dispersie. Dit maakt de vergelijking van de pakkingskwaliteit van verschillende partikeltypes quasi onmogelijk wanneer niet adequaat voor het intra-partikel effect op de waargenomen eddy dispersie kan gecorrigeerd worden.

Accurate waarden van moleculaire diffusiecoëfficiënten ($D_m$) in verschillende mobiele fasen zijn cruciaal in fundamentele kolomperformantie studies. In **Hoofdstuk 5** werd de Taylor-Aris methode gebruikt om de $D_m$-waarden van 45 polaire en apolaire componenten te meten in een brede waaier van mobiele fases die typische gebruikt worden in RPLC en HILIC studies. Deze waarden konden redelijk goed gefit worden tegen tweede-orde polynomen, wat toeliet om $D_m$-waarden voor de bestudeerde componenten af te leiden in eender welke samenstelling van de mobiele fase. Er werd ook aangetoond dat de buffer concentratie een invloed heeft op de moleculaire diffusie van geladen componenten.

Om te besluiten, werden enkele toekomstperspectieven belicht in **Hoofdstuk 6**. Een potentieel nieuwe aanpak om longitudinale diffusie te schatten werd besproken. Verdere applicatie van de strippingsprocedure waarbij een set van componenten met een bredere range in zone retentiefactoren (k”= 0 tot 10) zal gebruikt worden om de mechanismen van intra-partikel diffusie en de verschillende bijdragen tot eddy dispersie in HILIC en RPLC condities te bestuderen, werd ook besproken.

# List of Symbols

**Regular symbols**

| | |
|---|---|
| $A'$ | column cross section, [$m^2$] |
| A, B,C | terms in the plate height equation |
| a, b,c | terms in the reduced plate height equation |
| As | asymmetry factor, [/] |
| $C_s$ | concentration of the component in the stationary phase, [$mol/m^3$] |
| $C_m$ | concentration of the component in the mobile phase, [$mol/m^3$] |
| $c_s$ | term of resistance to mass transfer in the stationary zone, [/] |
| $c_m$ | term of resistance to mass transfer in the mobile zone, [/] |
| $d_p$ | particle diameter, [m] |
| $d_f$ | thickness of the stationary film, [m] |
| $d_t$ | internal diameter of the PEEK tube, [cm] |
| $D_s$ | molecular diffusion coefficient in the stationary phase, [$m^2/s$] |
| $D_m$ | bulk molecular diffusion coefficients or molecular diffusivity, [$m^2/s$] |
| $D_{eff}$ | effective molecular diffusion coefficients or molecular diffusivity, [$m^2/s$] |
| $D_{part}$ | intra-particle molecular diffusion coefficients or molecular diffusivity, [$m^2/s$] |
| $E_{min}$ | minimum separation impedance |
| f | factor relating the peak width to its standard deviation, [/] |
| h | reduced plate height, [/] |
| $h_{min}$ | minimum reduced plate height, [/] |
| H | plate height, [m] |
| $H_{min}$ | minimum plate height, [m] |
| L | column length, [m] |
| K | equilibrium constant, [/] |
| $k'$ | phase retention factor, [/] |
| k" | zone retention factor, [/] |
| $K_v$ | permeability, [$m^2$] |
| $K_{vs}$ | superficial velocity based permeability, [$m^2$] |
| $K_{vi}$ | interstitial velocity based permeability, [$m^2$] |
| $K_{v0}$ | $t_0$-marker velocity based permeability, [$m^2$] |
| MW | molecular weight of the solvent, [g/mol] |
| N | column plate count, [/] |
| $N_s$ | numbers of the molecules in the stationary phase, [/] |
| $N_m$ | numbers of the molecules in the mobile phase, [/] |
| $N_{s,zone}$ | numbers of solute molecules in the stationary zone, [/] |
| $N_{m,zone}$ | numbers of solute molecules in the mobile zone, [/] |
| $\Delta P$ | pressure drop, [bar] |
| PP | peak parking method |
| $R_s$ | resolution, [/] |
| $r_t$ | radius of the PEEK tube, [cm] |
| $R_{s,crit}$ | critical pair resolution, [/] |

| | |
|---|---|
| $Sh_m$ | Sherwood number relating to the mobile zone, [/] |
| $Sh_{part\ m}$ | Sherwood number relating to the intra-particle zone, [/] |
| $t_0$ | column dead time, residence time of an unretained marker, [s] |
| $t_s$ | time spent by the molecules in the stationary phase, [s] |
| $t_m$ | time spent by the molecules in the mobile phase, [s] |
| $t_{me}$ | time spent by the molecules in the mobile zone, [s] |
| $t_M$ | elution time of compound M, [s] |
| $t_A$ | elution time of compound A, [s] |
| $t_{park}$ | peak parking time, [s] |
| T | temperature, [K] |
| $u_0$ | linear velocity, [m/s] |
| $u_i$ | interstitial velocity, [m/s] |
| $u_s$ | superficial velocity, [m/s] |
| $V_s$ | volume of the stationary phase, [$m^3$] |
| $V_m$ | volume of the mobile phase, [$m^3$] |
| V | specific volume, [$m^3$/kg] |
| ν | reduced velocity, [/] |
| w | peak width, [s] or [m] |
| *x* | percentage of acetonitrile, [/] |

**Greek symbols**

| | |
|---|---|
| $\alpha_{part}$ | relative particle permeability factor, [/] |
| α | selective factor, [/] |
| β | phase ratio, [/] |
| $\beta_1$ | polarizability constant, [/] |
| $\gamma_B$ | obstruction factor relating the B-term with $D_{mol}$, [/] |
| $\varepsilon_e$ | external porosity, [/] |
| $\varepsilon_{int}$ | internal porosity, [/] |
| $\varepsilon_T$ | total porosity, [/] |
| $\zeta_2$ | a geometrical three-point parameter, [/] |
| η | solvent viscosity, [cP] |
| $\lambda_A$ | factor relating the A-term to the particle size, [/] |
| $\sigma^2$ | variance of a peak, [$s^2$] or [$m^2$] |
| ϕ | flow resistance, [/] |
| φ | solvent-solvent interaction or association factor, [/] |

**Abbreviation**

| | |
|---|---|
| ATC | anhydrotetracycline |
| BEH | bridged ethyl hybrid |
| EATC | 4-epianhydrotetracycline |
| ETC | 4-epitetracycline |
| HETP | height equivalent to a theoretical plate |
| HILIC | hydrophilic interaction liquid chromatography |
| ISEC | inverse size exclusion chromatography |
| I.D. | internal diameter |
| NPLC | normal phase liquid chromatography |
| PP | peak parking method |
| RPLC | reversed phase liquid chromatography |
| SFC | supercritical fluid chromatography |
| SEC | size-exclusion chromatography |
| TC | tetracycline |
| TGA | thermo gravimetric analysis |
| TPB | total pore blocking |
| UHPLC | ultra-high phase liquid chromatography |

**Subscripts**

| | |
|---|---|
| col | column |
| exp | experimental |
| ext | extra-column |
| G | geometrical |
| p | optimal |
| sys | system |

# List of Publications

**Huiying Song**, Erwin Adams, Gert Desmet, Deirdre Cabooter, Evaluation and Comparison of the Kinetic Performance of ultra-high performance chromatography and high-performance liquid chromatography Columns in HILIC and Reversed-phase Conditions, *J. Chromatogr. A*, 1369 (2014) 83-91.

**Huiying Song**, Gert Desmet, Deirdre Cabooter, Evaluation of the kinetic performance differences between reversed phase liquid chromatography and hydrophilic interaction liquid chromatography under conditions of identical packing structure, *Anal. Chem.* 87 (2015)12331-12339.

**Huiying Song**, Yoachim Vanderheyden, Erwin Adams, Gert Desmet, Deirdre Cabooter, Extensive Database of liquid phase diffusion coefficients of some frequently used test molecules in reversed phase liquid chromatography and hydrophilic interaction liquid chromatography, *J. Chromatogr. A*, 1455 (2016) 102-112.

**Huiying Song,** Deirdre Cabooter, Relevance and assessment of molecular diffusion coefficients in liquid chromatography, *Chromatographia*, submitted.

Getu Kahsay, **Huiying Song**, Fran Eerdekens, Yaxin Tie, Danny Hendriks, Ann Van Schepdael, Deirdre Cabooter, Erwin Adams, Development and validation of LC methods for the separation of misoprostol related substances and diastereoisomers, *J. Pharm. Biomed. Anal.*111(2015) 91-99. (**Contributed equally**)

Getu Kahsay, **Huiying Song**, Ann Van Schepdael, Deirdre Cabooter, Erwin Adams, Hydrophilic interaction chromatography in the analysis of antibiotics, *J. Pharm. Biomed. Anal.* 87 (2014) 142-154.

Jonas Hereijgers, Tobias Vandermeersch, Nicolas Van Oeteren, Harry Verelst, **Huiying Song**, Deirdre Cabooter, Tom Breugelmans, Wim De Malsche, Separation of Co(II)/Ni(II) with Cyanex 272 using a flat membrane microcontactor: extraction kinetics study, *J. Membr. Sci.* 499 (2016) 370-378.

**Huiying Song**, Gert Desmet, Deirdre Cabooter, Evaluation of the kinetic performance differences between HILIC and RPLC under conditions of identical packing structure II. Assessment of intra-particle diffusivity, *J. Chromatogr. A*, in preparation.

# Acknowledgements

Now, I am so excited standing on the finishing line to express my thanks to all those people who have contributed to my thesis and supported me during my PhD. The first person is of course Deirdre, my promoter, who introduced me into the world of chromatography. I could not finish my thesis without you, thank you for always being supportive and patient. Your constant and enormous enthusiasm for research is absolutely a perfect role model. You are always available to provide tips or suggestions on experiments, help me out with the theory explanation and paper writing etc. Deirdre, thank you very much!!! It's my pleasure working with you. In addition, I also definitely want to thank Prof. Desmet for his guidance in my project.

Further, I also would like to thank my co-promoter Prof. Erwin Adams, my former promoter, for offering me the opportunity to carry out my doctoral studies in this lab. Very appreciate him for meticulously checking my results and reports of the commercial samples, my papers and thesis.

Many thanks to Prof. Ann Van Schepdael for your kindness, and warm smile throughout the time I had spent in the lab. My cordial gratefulness also goes to all the jury members (Prof. Ann Van Schepdal, Prof. Guy Bormans, Prof. Patrick Augustijns, Prof. Ken Broeckhoven, and Prof. Yvan Vander Heyden) for reviewing my thesis in their busy schedules. Their valuable comments have significantly improve my thesis quality.

In 2015, I had a short visit in the lab of Prof. Desmet to work on the low dispersion system, I want to thank Ken for his kind help during my stay. Special mention goes to Kris, who is very humorous, and an absolute expert in technical aspect of chromatography. I can of course not forget Stephanie always bringing a smile to the lab and the pleasant conversations with her. During my PhD, I supervised four students (Yaxin, Danny, Michiel and Shengyun) for the practical work of their master thesis or postgraduate study. We together have managed to finish some small projects. Thank you for the nice collaborations.

I also would like to extend my appreciation to all my former and the present colleagues in our lab for creating a pleasant environment to work in and for the fruitful academic discussion: Stijn, Niels, Glenn, Stanislav, Pranov, Lynch, Shengyun, Peixi, Marwa, Adissu, Paul, Tam, Lan, Ye, Bart, Getu, Lucia, Shruti, Hui, Xu. Special thanks should go to Dunge for her nice guidance at the beginning of my PhD and her unforgettable humor. I also worked on PED

from time to time, thanks Bart for his guidance on this tricky machine. Very happy to meet Chiara, an Italian girl, she not only gave me the tiramisù recipe but also gave me a coffee maker and a new bottle of coffee as the good bye gift.

In the end, I want to say a few more words about my family. How lucky I am to have such nice parents and siblings, thanks for their never-ending selfless love. They always unconditionally support me and encourage me to explore the future. Thanks very much!!! A very special thanks to my sister Xiaoping and brother-in-law Qiuya for their guidance and constant support, and for providing me a home and relieving my homesickness in Leuven. You have helped me overcome many obstacles. I would have never been here without your support. Much love and thanks to my husband Zhanyao for his support and encouragement through my life and research work, I am so happy to be with you.

I would like to appreciate the China Scholarship Council (CSC) for their financial support over the past four years that allowed me to accomplish my thesis. Finally, thanks to Huiying, myself, for my endeavours!